

# 5 Elasticity/Hyperelasticity

---

## Chapter Outline

5.1	Introduction	210
5.2	Linear Elasticity	211
5.2.1	Isotropic Elasticity	211
5.2.2	Anisotropic Elasticity	215
Orthotropic Elasticity		216
5.2.3	Transversely Isotropic Elasticity	217
5.3	Isotropic Hyperelasticity	218
5.3.1	Continuum Mechanics Foundations	219
5.3.2	Similarity Between Uniaxial Compression and Biaxial Tension	225
5.3.3	Similarity Between Pure Shear and Planar Tension	226
5.3.4	Dependence of Stored Energy on $I_1$ and $I_2$	229
5.3.5	Freely Jointed Chain Model	232
5.3.6	Neo-Hookean Model	236
5.3.7	Mooney-Rivlin Model	243
5.3.8	Yeoh Model	245
5.3.9	Polynomial in $I_1$ and $I_2$ Model	250
5.3.10	Eight-Chain Model	250
5.3.11	Ogden Model	259
5.3.12	Gent Model	263
5.3.13	Horgan and Saccomandi Model	265
5.3.14	Knowles Model	268
5.3.15	Response Function Hyperelasticity	270
5.3.16	Extended Tube Model	273
5.3.17	BAM Model	275
5.4	Summary of Predictive Capabilities of Isotropic Hyperelastic Models	277
5.5	Anisotropic Hyperelasticity	281
5.5.1	Generalized Fung Model	282
5.5.2	Invariant Based Anisotropy	282

5.5.3 Bischoff Anisotropic Eight-Chain Model	283
5.5.4 Bergstrom Anisotropic Eight-Chain Model	285
5.5.5 Holzapfel-Gasser-Ogden Model	285
5.6 Hyperelastic Foam Models	287
5.6.1 Blatz-Ko Foam Model	289
5.6.2 Hyperfoam Model	290
5.7 Mullins Effect Models	292
5.7.1 Ogden-Roxburgh Mullins Effect Model	293
5.7.2 Qi-Boyce Mullins Effect Model	295
5.8 Use of Hyperelasticity in Polymer Modeling	295
5.8.1 Experimental Testing	296
5.8.2 Drucker Stability	297
5.8.3 Determination of Material Parameters	298
5.8.4 Limitations of Hyperelasticity	298
5.9 Hyperelastic Code Examples	299
5.10 Exercises	303
References	304

## 5.1 Introduction

Linear elasticity and hyperelasticity are two classes of constitutive models that are both easy to use and computationally efficient. Here, a constitutive model is considered to be easy to use if it requires little effort to calibrate and if it provides robust predictions for other loading conditions than what was used for the calibration. Both of these classes of models can provide useful predictions of the mechanical behavior of different polymers. The following sections discuss the theory behind these two classes of models, and how and when they can be applied to solve polymer mechanics problems.

Note that although the hyperelastic models that are discussed in this chapter are most useful for rubber-like material, they are also a critical component/building block for both linear and non-linear viscoelastic and viscoplastic models that will be discussed in detail in the following chapters. Hence, the theory of hyperelasticity is of significant importance and will be discussed in detail in this chapter.

The last few sections of this chapter introduce extensions of traditional hyperelastic models that allow for predictions of anisotropic non-linear hyperelastic behaviors, and predictions of the Mullins [1–3] effect that is commonly observed for elastomers, thermo-plastic elastomers (TPE), and other elastomer-like materials.

## 5.2 Linear Elasticity

Linear elasticity is the most direct way to represent the small strain mechanical behavior of solid polymers. The theory of linear elasticity is covered in numerous introductory textbooks [4–6] and in advanced textbooks [7–12]. The advanced theory of elasticity is very elegant but requires more sophisticated mathematics than what is covered in this introductory text. For our purposes it is sufficient to consider simple forms of isotropic and anisotropic elasticity, which are discussed in the following two sections.

### 5.2.1 Isotropic Elasticity

The most elementary form of the theory of elasticity is *isotropic* elasticity. In this form of the theory the stress is proportional to the applied strain and independent of the orientation of the material body. The constitutive equation for an elastic material is often called *Hooke's law* and can be written in different equivalent but alternative forms. One common representation is given by the following set of equations that determine the strain for a given stress state:

$$\varepsilon_{11} = \frac{1}{E} [\sigma_{11} - \nu (\sigma_{22} + \sigma_{33})], \quad (5.1)$$

$$\varepsilon_{22} = \frac{1}{E} [\sigma_{22} - \nu (\sigma_{33} + \sigma_{11})], \quad (5.2)$$

$$\varepsilon_{33} = \frac{1}{E} [\sigma_{33} - \nu (\sigma_{11} + \sigma_{22})], \quad (5.3)$$

$$\varepsilon_{12} = \frac{\sigma_{12}}{2\mu}, \quad (5.4)$$

$$\varepsilon_{23} = \frac{\sigma_{23}}{2\mu}, \quad (5.5)$$

$$\varepsilon_{31} = \frac{\sigma_{31}}{2\mu}. \quad (5.6)$$

In these equations,  $E$  is the Young's modulus (also called the modulus of elasticity),  $\mu$  is the shear modulus, and  $\nu$  is the Poisson's ratio. This set of equations can also be written in a more condensed form as follows:

$$\varepsilon_{ij} = \frac{1+\nu}{E}\sigma_{ij} - \frac{\nu}{E}\sigma_{kk}\delta_{ij}, \quad (5.7)$$

where the indices  $i$  and  $j$  take the values 1, 2, and 3, and  $\delta_{ij}$  is the Kronecker delta function defined by:

$$\delta_{ij} = \begin{cases} 1, & \text{if } i = j, \\ 0, & \text{if } i \neq j. \end{cases} \quad (5.8)$$

Another common and useful way to write Hooke's law is to instead solve for the stresses in terms of the applied strains:

$$\sigma_{ij} = 2\mu\varepsilon_{ij} + \lambda\varepsilon_{kk}\delta_{ij}, \quad (5.9)$$

where  $\mu$  is the shear modulus and  $\lambda$  is Lame's constant.

The constitutive theory for linear elasticity requires two material parameters that need to be specified from experimental data. There are different, equally valid, pairs of material parameters that can be chosen. The most common material parameters and conversion formulas between the different parameters are summarized in [Table 5.1](#). This table shows that if we know two of the elastic constants then we can calculate any of the other constants, e.g. if we know the shear modulus ( $\mu$ ) and the bulk modulus ( $\kappa$ ), then the Poisson's ratio can be calculated from:

$$\nu = \frac{3\kappa - 2\mu}{6\kappa + 2\mu}. \quad (5.10)$$

The typical approach to calibrate a linear elasticity model involves a uniaxial tension experiment where the stress-strain response determines the Young's modulus, and the Poisson's ratio is obtained from the transverse contraction in the tension experiment. After the two material parameters have been determined,

**Table 5.1** Conversion Equations Between Different Common Linear Elastic Material Parameters

Known Elastic Constants	$E$	$\nu$	$\mu$	$\kappa$	$\lambda$
Shear modulus $\mu$ , Bulk modulus $\kappa$	$\frac{9\kappa\mu}{3\kappa+\mu}$	$\frac{3\kappa-2\mu}{6\kappa+2\mu}$	$\mu$	$\kappa$	$\frac{3\kappa-2\mu}{3}$
Young's modulus $E$ , Poisson's ratio $\nu$	$E$	$\nu$	$\frac{E}{2(1+\nu)}$	$\frac{E}{3(1-2\nu)}$	$\frac{E\nu}{(1+\nu)(1-2\nu)}$
Young's modulus $E$ , Shear modulus $\mu$	$E$	$\frac{E-2\mu}{2\mu}$	$\mu$	$\frac{E\mu}{3(3\mu-E)}$	$\frac{\mu(E-2\mu)}{3\mu-E}$
Young's modulus $E$ , Bulk modulus $\kappa$	$E$	$\frac{3\kappa-E}{6\kappa}$	$\frac{3\kappa E}{9\kappa-E}$	$\kappa$	$\frac{3\kappa(3\kappa-E)}{9\kappa-E}$
Shear modulus $\mu$ , Lame's constant $\lambda$	$\frac{\mu(3\lambda+2\mu)}{\lambda+\mu}$	$\frac{\lambda}{2(\lambda+\mu)}$	$\mu$	$\frac{3\lambda+2\mu}{3}$	$\lambda$

the calibrated linear elasticity model can be used to predict the behavior of the material in any deformation state in a finite element (FE) analysis (as long as the material behavior is linear elastic).

The main limitation of using a linear elastic model for predicting the mechanical behavior of polymer materials is that polymers behave linearly only for very small strains<sup>1</sup> and a restricted range of strain-rates and temperatures. When performing FE simulations it is sometimes possible to capture the response at different temperatures by specifying the temperature dependence of the elastic constants.

One example illustrating the use and limitations of linear elasticity is shown in Figure 5.1. This figure compares experimental data for ultra high molecular weight polyethylene (UHMWPE) at three different strain rates and two temperatures with predictions from linear elasticity theory. It is clear that the linear elasticity model predictions are only accurate at one temperature and for

<sup>1</sup>Note that some polymers, for example low density polyethylene, often do not exhibit a linear elastic response for any strains at room temperature.

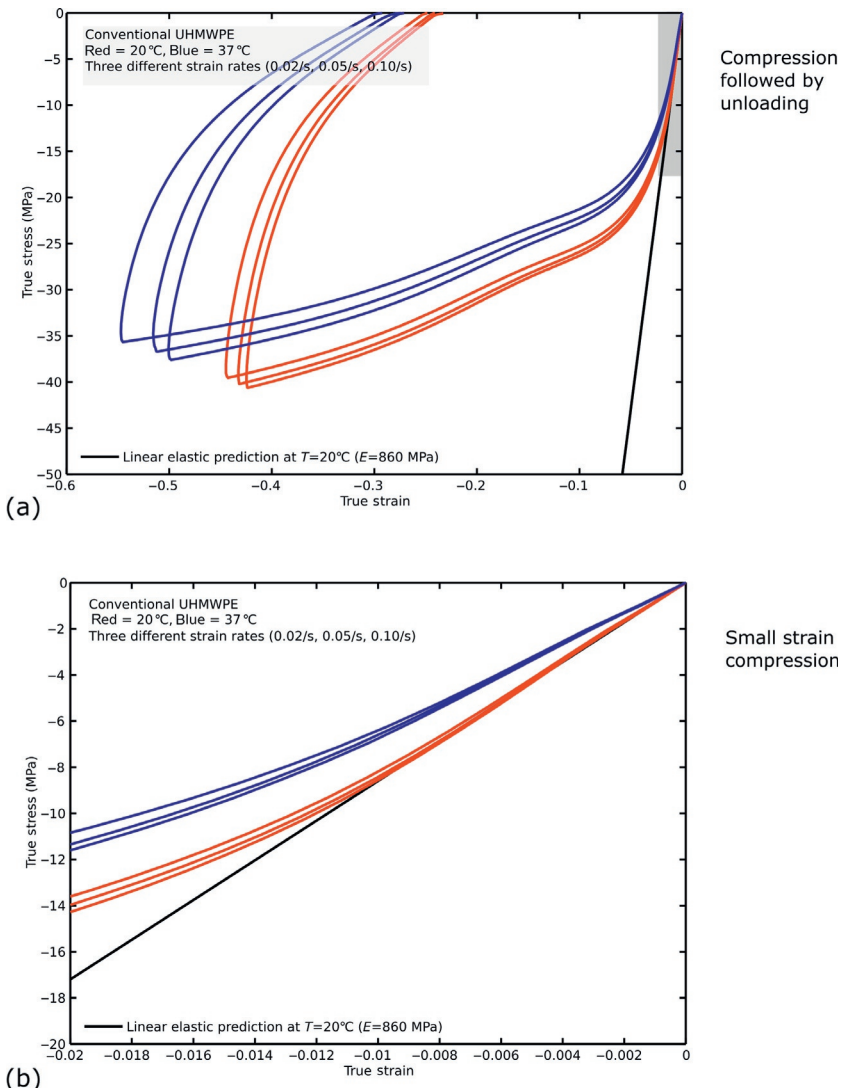


**Figure 5.1** Comparison between experimental data for UHMWPE and predictions from linear elasticity. (a) Stress-strain response from a compression followed by an unloading cycle. (b) Small strain response.

strains smaller than about 1%. The figure also shows that the strain range within the response is linear elastic decreases with increasing temperature.

Linear elasticity is mostly useful for predicting the small-strain behavior of thermoplastics below the glass transition

temperature, and for thermosets. For elastomer-like materials it is recommended to use a hyperelastic model or one of the more advanced models discussed in later chapters.

### 5.2.2 Anisotropic Elasticity

The theory for linear elasticity can be extended to include anisotropic behavior. Many polymers, e.g. fiber reinforced composites, drawn polymer films, or other polymers with a preferred molecular orientation, including many biopolymers, are anisotropic to various degrees. For these materials it is sometimes useful to represent their behavior using anisotropic elasticity.

For an anisotropic elastic material the Hooke's law can be written:

$$\varepsilon_{ij} = S_{ijkl}\sigma_{kl}, \quad (5.11)$$

or when expressed as a function of the strain state

$$\sigma_{ij} = C_{ijkl}\varepsilon_{kl}. \quad (5.12)$$

In these equations  $S_{ijkl}$  is the compliance tensor, and  $C_{ijkl}$  is the stiffness tensor. These equations show that the stress and strain tensors are linearly dependent on each other by a linear stiffness or compliance tensor.<sup>2</sup>

The theory for anisotropic elasticity is covered in detail in numerous textbooks [4–6], here we will simply summarize some of the more important and useful results for engineering analysis. As is shown in Equations (5.11) and (5.12), the stiffness and compliance tensors have  $3 \times 3 \times 3 \times 3 = 81$  components. Fortunately, since both the strain and stress tensors are symmetric, the number of independent components of  $S$  and  $C$  can be reduced to 36 by using symmetry arguments. Hence, it is common to arrange the stiffness and compliance tensors into  $6 \times 6$  tensors as shown in the following equations:

---

<sup>2</sup>The stiffness and compliance tensors are forth-order tensors that are discussed in more detail in various textbooks [4–6, 12].

$$\begin{bmatrix} \varepsilon_{11} \\ \varepsilon_{22} \\ \varepsilon_{33} \\ \varepsilon_{12} \\ \varepsilon_{13} \\ \varepsilon_{23} \end{bmatrix} = \begin{bmatrix} S_{11} & S_{12} & S_{13} & S_{14} & S_{15} & S_{16} \\ S_{21} & S_{22} & S_{23} & S_{24} & S_{25} & S_{26} \\ S_{31} & S_{32} & S_{33} & S_{34} & S_{35} & S_{36} \\ S_{41} & S_{42} & S_{43} & S_{44} & S_{45} & S_{46} \\ S_{51} & S_{52} & S_{53} & S_{54} & S_{55} & S_{56} \\ S_{61} & S_{62} & S_{63} & S_{64} & S_{65} & S_{66} \end{bmatrix} \times \begin{bmatrix} \sigma_{11} \\ \sigma_{22} \\ \sigma_{33} \\ \sigma_{12} \\ \sigma_{13} \\ \sigma_{23} \end{bmatrix}, \quad (5.13)$$

and

$$\begin{bmatrix} \sigma_{11} \\ \sigma_{22} \\ \sigma_{33} \\ \sigma_{12} \\ \sigma_{13} \\ \sigma_{23} \end{bmatrix} = \begin{bmatrix} C_{11} & C_{12} & C_{13} & C_{14} & C_{15} & C_{16} \\ C_{21} & C_{22} & C_{23} & C_{24} & C_{25} & C_{26} \\ C_{31} & C_{32} & C_{33} & C_{34} & C_{35} & C_{36} \\ C_{41} & C_{42} & C_{43} & C_{44} & C_{45} & C_{46} \\ C_{51} & C_{52} & C_{53} & C_{54} & C_{55} & C_{56} \\ C_{61} & C_{62} & C_{63} & C_{64} & C_{65} & C_{66} \end{bmatrix} \times \begin{bmatrix} \varepsilon_{11} \\ \varepsilon_{22} \\ \varepsilon_{33} \\ \varepsilon_{12} \\ \varepsilon_{13} \\ \varepsilon_{23} \end{bmatrix}. \quad (5.14)$$

Depending on the degree of anisotropy these  $6 \times 6$  matrices can often be simplified further. The following subsections present common special cases.

### Orthotropic Elasticity

If the mechanical response of a material contain three orthogonal symmetry planes, as illustrated in the example in [Figure 5.2](#), then the material is said to be orthotropic.

One common case of an orthotropic material is a material which contains fibers in three orthogonal directions. In this case the material contains three-fold symmetry and the constitutive equations are given by:

$$\begin{bmatrix} \varepsilon_{11} \\ \varepsilon_{22} \\ \varepsilon_{33} \\ \varepsilon_{12} \\ \varepsilon_{13} \\ \varepsilon_{23} \end{bmatrix} = \begin{bmatrix} 1/E_1 & -\nu_{21}/E_2 & -\nu_{31}/E_3 & 0 & 0 & 0 \\ -\nu_{12}/E_1 & 1/E_2 & -\nu_{32}/E_3 & 0 & 0 & 0 \\ -\nu_{13}/E_1 & -\nu_{23}/E_2 & 1/E_3 & 0 & 0 & 0 \\ 0 & 0 & 0 & 1/(2G_{12}) & 0 & 0 \\ 0 & 0 & 0 & 0 & 1/(2G_{13}) & 0 \\ 0 & 0 & 0 & 0 & 0 & 1/(2G_{23}) \end{bmatrix} \times \begin{bmatrix} \sigma_{11} \\ \sigma_{22} \\ \sigma_{33} \\ \sigma_{12} \\ \sigma_{13} \\ \sigma_{23} \end{bmatrix}, \quad (5.15)$$

where  $E_1$ ,  $E_2$ ,  $E_3$ ,  $G_{12}$ ,  $G_{13}$ ,  $G_{23}$ ,  $\nu_{12}$ ,  $\nu_{13}$ ,  $\nu_{21}$ ,  $\nu_{23}$ ,  $\nu_{31}$ , and  $\nu_{32}$  are material parameters. Here, the Poisson's ratios  $\nu_{ij}$  is defined



**Figure 5.2** The microstructure of wood is typically orthotropic.

by the transverse strain in the  $j$ -direction when the material is stressed in the  $i$ -direction. In general, the Poisson's ratio terms are not symmetric, i.e.  $\nu_{ij} \neq \nu_{ji}$ .

### 5.2.3 Transversely Isotropic Elasticity

A special case of orthotropic materials are those that have isotropic properties in one plane (here taken to be the 1-2 plane), and different properties in the direction normal to this plane. This type of material symmetry is called transverse isotropic and is described by 5 material parameters ( $E_p$ ,  $E_t$ ,  $G_t$ ,  $\nu_p$ ,  $\nu_{tp}$ , and  $\nu_{pt} = \nu_{tp}E_p/E_t$ ) as shown in the following equations

$$\begin{bmatrix} \varepsilon_{11} \\ \varepsilon_{22} \\ \varepsilon_{33} \\ \varepsilon_{12} \\ \varepsilon_{13} \\ \varepsilon_{23} \end{bmatrix} = \begin{bmatrix} 1/E_p & -\nu_p/E_p & -\nu_{tp}/E_t & 0 & 0 & 0 \\ -\nu_p/E_p & 1/E_p & -\nu_{tp}/E_t & 0 & 0 & 0 \\ -\nu_{pt}/E_p & -\nu_{pt}/E_p & 1/E_t & 0 & 0 & 0 \\ 0 & 0 & 0 & (1 + \nu_p)/E_p & 0 & 0 \\ 0 & 0 & 0 & 0 & 1/G_t & 0 \\ 0 & 0 & 0 & 0 & 0 & 1/G_t \end{bmatrix} \times \begin{bmatrix} \sigma_{11} \\ \sigma_{22} \\ \sigma_{33} \\ \sigma_{12} \\ \sigma_{13} \\ \sigma_{23} \end{bmatrix}. \quad (5.16)$$

An example of material that is transversely isotropic is a fiber-reinforced composite with all fibers oriented in one direction, see Figure 5.3.

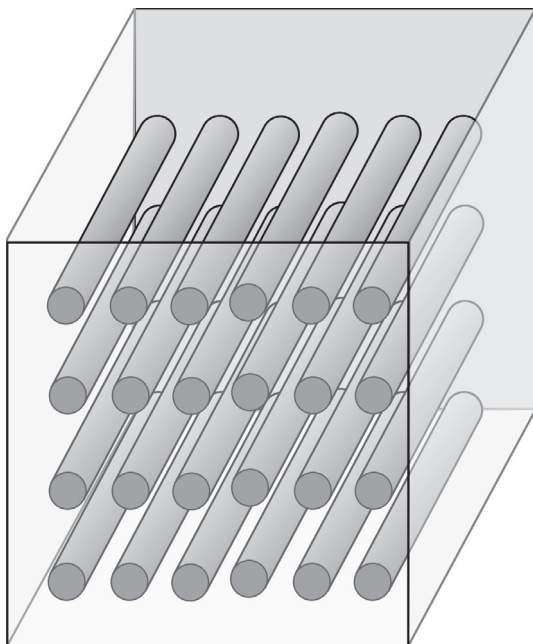


**Figure 5.3** Fiber-reinforced composite having a transverse isotropic behavior.

**Note.** *The number of experimental tests required to fully determine the material parameters for these anisotropic elastic material models can be large. The exact number and type of required tests depends on the type of anisotropic response, typically a combination of tension (or compression) tests and shear tests are required.*

### 5.3 Isotropic Hyperelasticity

Hyperelasticity is a generalization of linear elasticity that is non-linear and suitable for large strain predictions. Throughout the years there have been an extensive amount of work done developing different hyperelasticity theories, and many of these models are available in commercial FE software. One of the most important and interesting aspects of hyperelasticity is that it is the simplest model representation that in some cases can be connected to the micromechanisms that drive the deformation

behavior of polymers. In the following sections we will present some of the most common and useful theories of hyperelasticity.

The continuum mechanics foundation of the hyperelastic theories was derived in Section 4.11.1. In the next section we will extend the general expressions for the stress in terms of the Helmholtz free energy into different and easily applied representations. This section focuses on the different theories, and the strengths and limitations of the different theories to predict the behavior of different polymeric materials.

### 5.3.1 Continuum Mechanics Foundations

As was shown in Section 4.11.1, the Helmholtz free energy per unit reference volume<sup>3</sup>  $\Psi(\cdot)$ , the first Piola-Kirchhoff stress  $\mathbf{P}(\cdot)$ , the entropy per unit reference volume  $\eta_0(\cdot)$ , and the heat flux per unit reference surface area  $\mathbf{Q}(\cdot)$  of a *thermoelastic material* only depend on the deformation gradient  $\mathbf{F}$ , the temperature  $\theta_0$ , and the gradient of temperature  $\text{Grad } \theta_0$ .

To satisfy the Clausius-Duhem inequality Cauchy stress for a thermoelastic material has to be given by:

$$\boldsymbol{\sigma}(\mathbf{F}, \theta_0) = \frac{1}{J} \frac{\partial \Psi(\mathbf{F}, \theta_0)}{\partial \mathbf{F}} \mathbf{F}^\top. \quad (4.235\text{-repeat})$$

To satisfy objectivity (see Section 4.12), a change of observer implies that the stress and the Helmholtz free energy have to have the following functional forms<sup>4</sup>:

$$\boldsymbol{\sigma}(\mathbf{F}) = \mathbf{R}\boldsymbol{\sigma}(\mathbf{U})\mathbf{R}^\top = \mathbf{R}\boldsymbol{\sigma}(\mathbf{C})\mathbf{R}^\top, \quad (5.17)$$

$$\Psi(\mathbf{F}, \theta_0) = \Psi(\mathbf{U}, \theta_0) = \Psi(\mathbf{C}, \theta_0), \quad (5.18)$$

which when inserted into (4.235) gives

$$\boldsymbol{\sigma}(\mathbf{U}, \theta_0) = \mathbf{R} \left[ \frac{1}{J} \frac{\partial \Psi(\mathbf{U}, \theta_0)}{\partial \mathbf{U}} \mathbf{U}^\top \right] \mathbf{R}^\top. \quad (5.19)$$

---

<sup>3</sup>The notation  $\Psi(\cdot)$ ,  $\mathbf{P}(\cdot)$ , etc. indicates that these quantities are functions of arguments that are not listed for notational simplicity.

<sup>4</sup>Here, and in the following, the tensorial functionals are not explicitly showing the inherent arguments. That is, instead of writing  $\hat{\boldsymbol{\sigma}}(\mathbf{F}) = \mathbf{R}\tilde{\boldsymbol{\sigma}}(\mathbf{U})\mathbf{R}^\top = \mathbf{R}\tilde{\boldsymbol{\sigma}}(\mathbf{C})\mathbf{R}^\top$ , we have for notational simplicity skipped the superscripts giving:  $\boldsymbol{\sigma}(\mathbf{F}) = \mathbf{R}\boldsymbol{\sigma}(\mathbf{U})\mathbf{R}^\top = \mathbf{R}\boldsymbol{\sigma}(\mathbf{C})\mathbf{R}^\top$ .

The partial derivative of the Helmholtz free energy with respect to the right stretch tensor ( $\mathbf{U}$ ) can be converted to a derivative with respect to the right Cauchy-Green tensor ( $\mathbf{C}$ ) by the following theorem.

**Theorem.** *The partial derivative  $\partial\Psi/\partial\mathbf{U}$  can be written as follows:*

$$\frac{\partial\Psi(\mathbf{U})}{\partial\mathbf{U}} = 2\mathbf{U}\frac{\partial\Psi(\mathbf{C})}{\partial\mathbf{C}}. \quad (5.20)$$

*Proof.* This theorem can be proven in different ways. Here, we will start by converting the left-hand-side of Equation (5.20) to index notation:

$$\left(\frac{\partial\Psi}{\partial\mathbf{U}}\right)_{ij} = \frac{\partial\Psi}{\partial U_{ij}} \quad (5.21)$$

$$= \frac{\partial\Psi}{\partial C_{kl}} \frac{\partial C_{kl}}{\partial U_{ij}} \quad (5.22)$$

$$= \frac{\partial\Psi}{\partial C_{kl}} \frac{\partial(U_{km}U_{ml})}{\partial U_{ij}}. \quad (5.23)$$

Then by expanding terms and taking the partial derivative, this expression becomes:

$$\left(\frac{\partial\Psi}{\partial\mathbf{U}}\right)_{ij} = 2U_{ik}\frac{\partial\Psi}{\partial C_{kj}} \quad (5.24)$$

$$= \left(2\mathbf{U}\frac{\partial\Psi(\mathbf{C})}{\partial\mathbf{C}}\right)_{ij}, \quad (5.25)$$

which completes the proof.  $\square$

By inserting (5.20) into (5.19), the expression for the Cauchy stress automatically satisfies objectivity if:

$$\boldsymbol{\sigma}(\mathbf{C}, \theta_0) = \frac{2}{J} \mathbf{F} \frac{\partial\Psi(\mathbf{C}, \theta_0)}{\partial\mathbf{C}} \mathbf{F}^\top. \quad (5.26)$$

When working with isotropic hyperelastic models it is often convenient to express the Helmholtz free energy in terms of invariants of the right Cauchy-Green tensor instead of the actual tensor ( $\mathbf{C}$ ). It is common to use the invariants from (4.65) to (4.67):  $I_1(\mathbf{C})$ ,  $I_2(\mathbf{C})$ , and  $I_3(\mathbf{C})$ :

$$I_1(\mathbf{C}) = \lambda_1^2 + \lambda_2^2 + \lambda_3^2, \quad (5.27)$$

$$I_2(\mathbf{C}) = \lambda_1^2 \lambda_2^2 + \lambda_2^2 \lambda_3^2 + \lambda_3^2 \lambda_1^2, \quad (5.28)$$

$$I_3(\mathbf{C}) = \lambda_1^2 \lambda_2^2 \lambda_3^2. \quad (5.29)$$

With these invariants the Helmholtz free energy can be written  $\Psi(I_1, I_2, I_3, \theta_0)$  which when inserted in (5.26) gives:

$$\boldsymbol{\sigma}(I_1, I_2, I_3, \theta_0) = \frac{2}{J} \mathbf{F} \left[ \frac{\partial \Psi}{\partial I_1} \frac{\partial I_1}{\partial \mathbf{C}} + \frac{\partial \Psi}{\partial I_2} \frac{\partial I_2}{\partial \mathbf{C}} + \frac{\partial \Psi}{\partial I_3} \frac{\partial I_3}{\partial \mathbf{C}} \right] \mathbf{F}^\top. \quad (5.30)$$

This equation can be simplified further by the following theorem.

**Theorem.** *The partial derivative of  $I_1$ ,  $I_2$ , and  $I_3$  with respect to  $\mathbf{C}$  can be written:*

$$\frac{\partial I_1(\mathbf{C})}{\partial \mathbf{C}} = \mathbf{I}, \quad (5.31)$$

$$\frac{\partial I_2(\mathbf{C})}{\partial \mathbf{C}} = I_1 \mathbf{I} - \mathbf{C}, \quad (5.32)$$

$$\frac{\partial I_3(\mathbf{C})}{\partial \mathbf{C}} = I_3 \mathbf{C}^{-1} = I_3 \mathbf{F}^{-1} \mathbf{F}^{-\top}. \quad (5.33)$$

*Proof.* The proof of this theorem can be obtained through tensor manipulations as discussed in [13, 14]. Since the proof is somewhat lengthy it is here left as an exercise.  $\square$

Inserting the partial derivatives of  $I_1$ ,  $I_2$ , and  $I_3$  into (5.30) give the following expression for the Cauchy stress:

$$\boldsymbol{\sigma}(I_1, I_2, I_3, \theta_0) = \frac{2}{J} \left( \frac{\partial \Psi}{\partial I_1} + I_1 \frac{\partial \Psi}{\partial I_2} \right) \mathbf{b} - \frac{2}{J} \frac{\partial \Psi}{\partial I_2} \mathbf{b}^2 + \frac{2}{J} I_3 \frac{\partial \Psi}{\partial I_3} \mathbf{I}. \quad (5.34)$$

It is often more common to use the invariant  $I_3(\mathbf{F}) = J$  instead of  $I_3(\mathbf{C}) = J^2$ . By inserting this substitution into Equation (5.34) and using the chain rule we get:

$$\boldsymbol{\sigma}(I_1, I_2, J, \theta_0) = \frac{2}{J} \left( \frac{\partial \Psi}{\partial I_1} + I_1 \frac{\partial \Psi}{\partial I_2} \right) \mathbf{b} - \frac{2}{J} \frac{\partial \Psi}{\partial I_2} \mathbf{b}^2 + \frac{\partial \Psi}{\partial J} \mathbf{I}. \quad (5.35)$$

The hyperelasticity models that are available in most FE programs are based on a decomposition of the deformation gradient into dilatational (volume change) and distortional<sup>5</sup> (no volume change) components (see Equations (4.38)–(4.40)):

$$\mathbf{F} = J^{1/3} \mathbf{F}^*, \quad (5.36)$$

$$\mathbf{C} = \mathbf{F}^\top \mathbf{F} = J^{2/3} \mathbf{C}^*. \quad (5.37)$$

Similarly, the invariants can also be divided into dilatational and distortional parts:

$$I_1(\mathbf{C}) = \text{tr}(\mathbf{C}) = \text{tr}(J^{2/3} \mathbf{C}^*) = J^{2/3} \text{tr}(\mathbf{C}^*) = J^{2/3} I_1^*, \quad (5.38)$$

$$I_2(\mathbf{C}) = \frac{1}{2} \left[ (\text{tr} \mathbf{C})^2 - \text{tr}(\mathbf{C}^2) \right] = J^{4/3} I_2^*. \quad (5.39)$$

Using these invariants, the Helmholtz free energy can be written  $\Psi(I_1^*(I_1, J), I_2^*(I_2, J), J)$ . Inserting this functional form into Equation (5.35) and using the chain rule gives:

$$\begin{aligned} \boldsymbol{\sigma}(I_1^*, I_2^*, J, \theta_0) &= \frac{J}{2} \left( \frac{\partial \Psi}{\partial I_1^*} \frac{\partial I_1^*}{\partial I_1} + J^{2/3} I_1^* \frac{\partial \Psi}{\partial I_2^*} \frac{\partial I_2^*}{\partial I_2} \right) \mathbf{b} - \frac{2}{J} \frac{\partial \Psi}{\partial I_2^*} \frac{\partial I_2^*}{\partial I_2} \mathbf{b}^2 \\ &\quad + \left( \frac{\partial \Psi}{\partial I_1^*} \frac{\partial I_1^*}{\partial J} + \frac{\partial \Psi}{\partial I_2^*} \frac{\partial I_2^*}{\partial J} + \frac{\partial \Psi}{\partial J} \right) \mathbf{I}. \end{aligned} \quad (5.40)$$

This equation can be simplified by inserting the invariants from Equations (5.38) and (5.39) giving the Cauchy stress as:

$$\boldsymbol{\sigma} = \frac{2}{J} \left[ \frac{\partial \Psi}{\partial I_1^*} + \frac{\partial \Psi}{\partial I_2^*} I_1^* \right] \mathbf{b}^* - \frac{2}{J} \frac{\partial \Psi}{\partial I_2^*} (\mathbf{b}^*)^2 + \left[ \frac{\partial \Psi}{\partial J} - \frac{2I_1^*}{3J} \frac{\partial \Psi}{\partial I_1^*} - \frac{4I_2^*}{3J} \frac{\partial \Psi}{\partial I_2^*} \right] \mathbf{I}. \quad (5.41)$$

If there is no dependence on  $I_2^*$ , then the Cauchy stress can be written

$$\boldsymbol{\sigma} = \frac{2}{J} \frac{\partial \Psi}{\partial I_1^*} \text{dev}[\mathbf{b}^*] + \frac{\partial \Psi}{\partial J} \mathbf{I}. \quad (5.42)$$

Equations (5.41) and (5.42) are very useful and will be used extensively in the remainder of this chapter.

---

<sup>5</sup>Here, and in the following, distortional scalars and tensors are denoted by a superscript \*.

### Example

For an incompressible material, Equation (5.41) be simplified to:

$$\sigma = 2 \left[ \frac{\partial \Psi}{\partial I_1} + \frac{\partial \Psi}{\partial I_2} I_1 \right] \mathbf{b} - 2 \frac{\partial \Psi}{\partial I_2} (\mathbf{b})^2 + p \mathbf{I}, \quad (5.43)$$

where  $p$  is a pressure term that is determined from the boundary conditions. Hence, if an incompressible hyperelastic material is exposed to uniaxial loading, then the Cauchy stresses in the loading and transverse directions are given by:

$$\sigma_{\text{uniax}} = 2 \left[ \frac{\partial \Psi}{\partial I_1} + \frac{\partial \Psi}{\partial I_2} I_1 \right] \lambda^2 - 2 \frac{\partial \Psi}{\partial I_2} \lambda^2 + p, \quad (5.44)$$

$$\sigma_{\text{transverse}} = 2 \left[ \frac{\partial \Psi}{\partial I_1} + \frac{\partial \Psi}{\partial I_2} I_1 \right] \frac{1}{\lambda} - 2 \frac{\partial \Psi}{\partial I_2} \frac{1}{\lambda^2} + p \equiv 0 \quad (5.45)$$

giving

$$\sigma_{\text{uniax}} = 2 \left[ \frac{\partial \Psi}{\partial I_1} + \frac{\partial \Psi}{\partial I_2} I_1 \right] \left( \lambda^2 - \frac{1}{\lambda} \right) - 2 \frac{\partial \Psi}{\partial I_2} \left( \lambda^4 - \frac{1}{\lambda^2} \right). \quad (5.46)$$

Furthermore, if the material has no dependence on  $I_2$ , and is exposed to incompressible uniaxial loading, then the Cauchy stress is given by

$$\sigma_{\text{uniax}} = 2 \frac{\partial \Psi}{\partial I_1} \left( \lambda^2 - \frac{1}{\lambda} \right). \quad (5.47)$$

If the hyperelastic material has no dependence on  $I_2$ , the Cauchy stress in incompressible planar loading is given by

$$\sigma_{\text{planar}} = 2 \frac{\partial \Psi}{\partial I_1} \left( \lambda^2 - \frac{1}{\lambda^2} \right), \quad (5.48)$$

and if exposed to incompressible biaxial loading, the Cauchy stress is given by

$$\sigma_{\text{biaxial}} = 2 \frac{\partial \Psi}{\partial I_1} \left( \lambda^2 - \frac{1}{\lambda^4} \right). \quad (5.49)$$

Instead of using the invariants  $I_1$ ,  $I_2$ , and  $I_3$ , it is sometimes useful to express the Helmholtz free energy in terms of the

principal stretches  $\lambda_1$ ,  $\lambda_2$ , and  $\lambda_3$ :  $\Psi(\lambda_1, \lambda_2, \lambda_3, \theta_0)$ . In this case the principal Cauchy stresses can be obtained from Equation (5.26) as follows:

$$\sigma_i(\lambda_1, \lambda_2, \lambda_3, \theta_0) = \sum_{j=1}^3 \frac{2}{J} \lambda_i^2 \frac{\partial \Psi}{\partial \lambda_j} \frac{\partial \lambda_j}{\partial C_{ii}}. \quad (5.50)$$

From the definition of  $\mathbf{C}$  we get that  $\partial \lambda_i / \partial C_{ii} = 1/(2\lambda_i)$ , which when inserted in Equation (5.50) gives:

$$\sigma_i(\lambda_1, \lambda_2, \lambda_3, \theta_0) = \frac{\lambda_i}{J} \frac{\partial \Psi}{\partial \lambda_i} \quad (\text{no summation}). \quad (5.51)$$

The complete Cauchy stress tensor can then be obtained from:

$$\boldsymbol{\sigma} = \sum_{i=1}^3 \frac{\lambda_i}{J} \frac{\partial \Psi(\lambda_1, \lambda_2, \lambda_3, \theta)}{\partial \lambda_i} \hat{\mathbf{n}}_i \otimes \hat{\mathbf{n}}_i, \quad (5.52)$$

where  $\hat{\mathbf{n}}_i$  are the principal directions of the left Cauchy-Green tensor  $\mathbf{b} = \mathbf{F}\mathbf{F}^\top$ , see (4.106). Using the same approach we can similarly show that the principal values of the first Piola-Kirchhoff stress can be obtained from:

$$P_i(\lambda_1, \lambda_2, \lambda_3, \theta_0) = \frac{\partial \Psi}{\partial \lambda_i}, \quad (5.53)$$

giving the Piola-Kirchhoff stress tensor

$$\mathbf{P} = \sum_{i=1}^3 \frac{\partial \Psi(\lambda_1, \lambda_2, \lambda_3, \theta_0)}{\partial \lambda_i} \hat{\mathbf{n}}_i \otimes \hat{\mathbf{N}}_i. \quad (5.54)$$

Similarly, if the Helmholtz free energy is expressed in terms of the distortional stretches:  $\lambda_i^* = J^{-1/3} \lambda_i$ , then the Cauchy stress is given by:

$$\boldsymbol{\sigma} = \sum_{i=1}^3 \frac{\lambda_i^*}{J} \frac{\partial \Psi}{\partial \lambda_i^*} \hat{\mathbf{n}}_i \otimes \hat{\mathbf{n}}_i + \frac{\partial \Psi}{\partial J} \mathbf{I}. \quad (5.55)$$

### 5.3.2 Similarity Between Uniaxial Compression and Biaxial Tension

The deformation gradient in incompressible uniaxial compression is

$$\mathbf{F} = \begin{bmatrix} \lambda & 0 & 0 \\ 0 & 1/\sqrt{\lambda} & 0 \\ 0 & 0 & 1/\sqrt{\lambda} \end{bmatrix}, \quad (5.56)$$

and the deformation gradient in incompressible biaxial tension is given by

$$\mathbf{F} = \begin{bmatrix} 1/\lambda^2 & 0 & 0 \\ 0 & \lambda & 0 \\ 0 & 0 & \lambda \end{bmatrix}. \quad (5.57)$$

At first sight these two deformation gradients look quite different but if we select  $\lambda = 0.5$  in uniaxial compression, and  $\lambda = 2$  in biaxial tension, then the deformation gradient in both cases becomes

$$\mathbf{F} = \begin{bmatrix} 0.5 & 0 & 0 \\ 0 & 2 & 0 \\ 0 & 0 & 2 \end{bmatrix}. \quad (5.58)$$

This means that for an incompressible material uniaxial compression and biaxial tension impose the same deformation state on the material, and hence are equivalent. The two loading modes, however, give different stresses due to the difference in required pressure to satisfy the stress boundary conditions.

Since no real material is fully incompressible, this similarity between uniaxial compression and biaxial tension is not strictly valid. To explore the difference in the predicted stresses due to the material compressibility consider a compressible Neo-Hookean (NH) material model with a shear modulus of  $\mu = 1 \text{ MPa}$ , and different values for the bulk modulus  $\kappa$ . To get concrete stress values consider a compressible stretch state of  $\lambda = 0.5$ , and a biaxial tensile stretch of  $1/\sqrt{0.5}$ . Under these conditions the calculated true stress values are listed in [Table 5.2](#).

**Table 5.2 Summary of Calculated Stress Values in Uniaxial Compression and the Corresponding Biaxial Tension Deformation State**

$\kappa$	$\nu$	Stress Uniaxial	Stress Biaxial	Error
500	0.499	-1.7511 MPa	1.7421 MPa	0.5%
100	0.495	-1.7554 MPa	1.7116 MPa	2.6%
50	0.49	-1.7610 MPa	1.6761 MPa	5.1%
10	0.45	-1.8097 MPa	1.4570 MPa	24.2%

The shear modulus was  $\mu = 1 \text{ MPa}$ . The applied uniaxial stretch was  $\lambda = 0.5$ , and the applied biaxial stretch was  $\lambda = 1/\sqrt{0.5}$ .

The table shows that the bulk modulus needs to be very high compared to the shear modulus in order for there to be a similarity between the predicted stress in uniaxial compression and biaxial tension.

### 5.3.3 Similarity Between Pure Shear and Planar Tension

The results from a planar tension test can under certain conditions be converted to equivalent pure shear data.<sup>6</sup> On occasion, this can be useful if shear data is required, but the experimental equipment for performing shear tests is not available.

To show this similarity between pure shear and planar tension, start with the deformation gradient of an incompressible material in pure shear:

$$\mathbf{F} = \begin{bmatrix} 1/(1 - \alpha^2) & 0 & 0 \\ 0 & 1 & \alpha \\ 0 & \alpha & 1 \end{bmatrix}, \quad (5.59)$$

where  $\alpha$  is the shear displacement. The term  $F_{11}$  is taken to be  $1/(1 - \alpha^2)$  in order to conserve volume, that is to get  $\det(\mathbf{F}) = 1$ . Figure 5.4 shows how a square is deformed in pure shear for different  $\alpha$  values.

<sup>6</sup>Note that pure shear does not impose the same deformation as simple shear. Both loading modes apply shear, but in different ways.

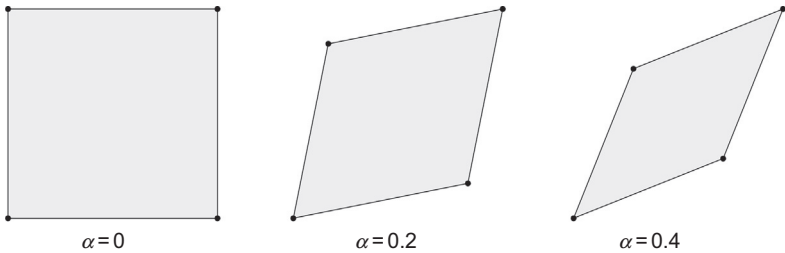


**Figure 5.4** Deformation of a square in pure shear with different  $\alpha$  values. Note that the deformation of a square becomes a rhombus (with all equal sides). This is different than simple shear of a square that becomes a parallelogram.

Now consider the deformation gradient in incompressible plane strain tension:

$$\mathbf{F} = \begin{bmatrix} 1 & 0 & 0 \\ 0 & 1 + \alpha & 0 \\ 0 & 0 & 1/(1 + \alpha) \end{bmatrix}, \quad (5.60)$$

where  $\alpha$  is the same displacement value as in (5.59). With this deformation gradient the stretching is in the 2-direction, and the 1-direction has no strain.

If we rotate this deformation state by 45% around the 1-direction then the rotation matrix becomes:

$$\mathbf{Q} = \begin{bmatrix} 1 & 0 & 0 \\ 0 & \cos 45\% & \sin 45\% \\ 0 & -\sin 45\% & \cos 45\% \end{bmatrix} = \frac{1}{\sqrt{2}} \begin{bmatrix} \sqrt{2} & 0 & 0 \\ 0 & 1 & 1 \\ 0 & -1 & 1 \end{bmatrix}, \quad (5.61)$$

and the rotated deformation gradient becomes:

$$\mathbf{F} = \mathbf{Q}^\top \cdot \begin{bmatrix} 1 & 0 & 0 \\ 0 & 1 + \alpha & 0 \\ 0 & 0 & 1/(1 + \alpha) \end{bmatrix} \cdot \mathbf{Q}. \quad (5.62)$$

For small applied strains this equation can be simplified to:

$$\mathbf{F} = \begin{bmatrix} 1 + \Delta & 0 & 0 \\ 0 & (1 + \alpha^2/2 + \mathcal{O}(\alpha^3)) & (\alpha - \alpha^2/2 + \mathcal{O}(\alpha^3)) \\ 0 & (\alpha - \alpha^2/2 + \mathcal{O}(\alpha^3)) & (1 + \alpha^2/2 + \mathcal{O}(\alpha^3)) \end{bmatrix}, \quad (5.63)$$

where  $\Delta$  is a small value that is needed in order to enforce incompressibility,  $\mathcal{O}(\alpha^3)$  is big O notation indicating the term is of order  $\alpha^3$ . If  $\alpha \ll 1$  then  $\alpha^2$  and higher terms can be ignored giving

$$\mathbf{F} = \begin{bmatrix} 1 + \Delta & 0 & 0 \\ 0 & 1 & \alpha \\ 0 & \alpha & 1 \end{bmatrix}, \quad (5.64)$$

which is the same deformation gradient as in pure shear. This shows that for incompressible materials, at small strains the pure shear and planar tension behaviors are the same.

The difference between pure shear and planar tension increases with the applied deformation. [Figure 5.5](#) shows the true stress as a function of the deformation  $\alpha$  for the idealized case of incompressible loading.<sup>7</sup> In this figure the stress is  $\sigma_{23}$  for pure shear and  $\sigma_{22}$  for planar tension. The stress was calculated using a Neo-Hookean (NH) material model with a shear modulus of 1 MPa. The figure shows that the two deformation modes start to diverge significantly for deformations  $\alpha > 0.5$ .

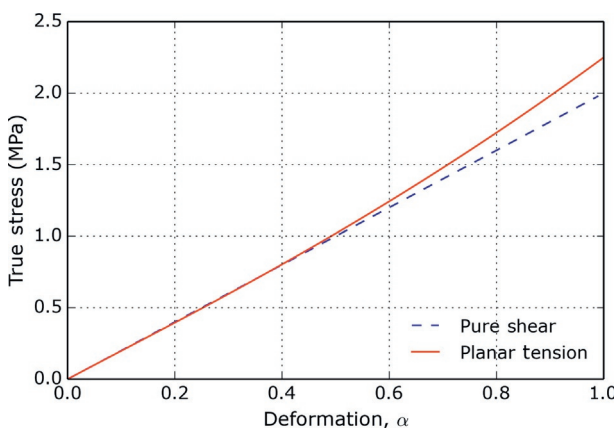


**Figure 5.5** Comparison between predicted stress in pure shear and the corresponding planar tension for different applied deformations.

<sup>7</sup>The difference between the two loading modes will be even larger if the material is compressible.

### 5.3.4 Dependence of Stored Energy on $I_1$ and $I_2$

The Helmholtz free energy that is stored in a solid polymer<sup>8</sup> as it is being deformed depends on the applied deformation invariants  $I_1$ ,  $I_2$ , and  $J$ . That is, a hyperelastic theory is uniquely defined by how the stored energy depends on these invariants.

To better illustrate these dependencies it is useful to consider real experimental data for an elastomer. Figure 5.6 shows experimental data from Treloar [15, 16] for a natural rubber tested in uniaxial tension, biaxial tension, and pure shear.

In this case the rubber material was deformed to very large engineering strains in excess of 300%, and for each applied strain value the equilibrium stress was measured after the material was allowed to relax. This figure shows, as expected, that the stress-

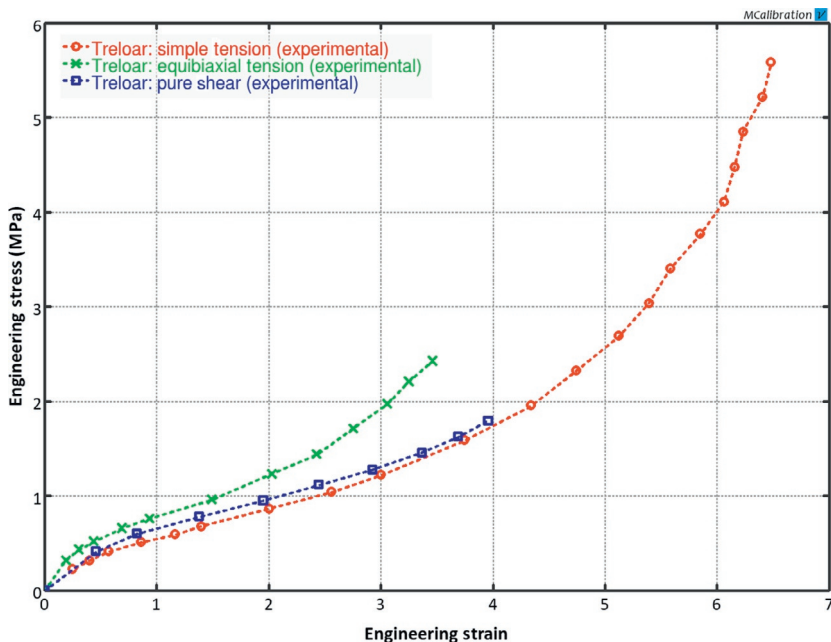


**Figure 5.6** Experimental data in uniaxial tension, biaxial tension, and pure shear [15, 16].

<sup>8</sup>This is only true for materials that are non-linear elastic and follow the theory of hyperelasticity. In other cases some of the applied energy is dissipated and some is stored.

strain response for all three loading modes is non-linear, and that the biaxial stress is the highest and that the uniaxial stress is the lowest.

From this data it is straightforward to calculate the stored energy in the material as a function of the applied deformation in each loading mode. Figure 5.7 shows how the free energy depends on the first invariant  $I_1$ . As mentioned, in general the internal energy does not only depend on the first invariant  $I_1$  but also on  $I_2$  and  $J$ . This is clearly shown in the figure since the energy curves for the three loading modes do not perfectly overlap.

The influence of  $I_1$  and  $I_2$  on the free energy can be studied by calculating how  $I_1$  and  $I_2$  depend on the applied stretch in different loading modes. For example, directly inserting the deformation gradients from Equations (5.78)–(5.80) into the definitions for  $I_1$  and  $I_2$  (see Equations (4.65) and (4.66)) gives the results shown in Figures 5.8 and 5.9. The figures show that of the three loading modes, biaxial loading exposes the material to much higher  $I_2$  values than in uniaxial loading or plane strain loading.

Another way to plot the data is look at the ratio  $I_2/I_1$  as a function of the applied stretch  $\lambda$ , see Figure 5.10. For any arbitrary deformation state there are three invariants, and if the material is

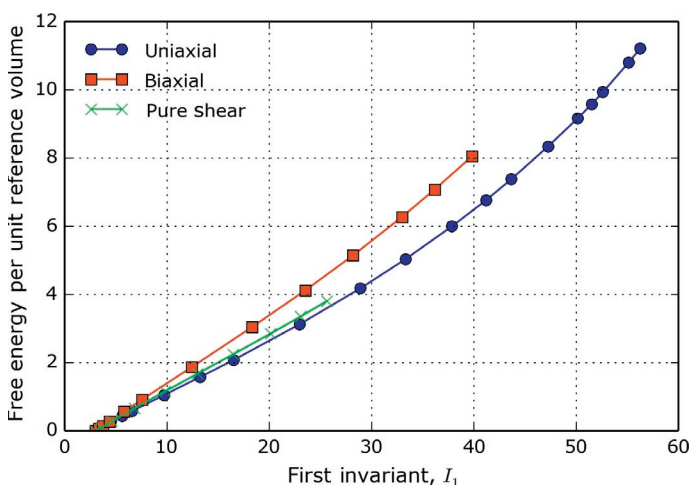


**Figure 5.7** Calculated Helmholtz free energy as a function of the first invariant  $I_1$  for data from Treloar [15, 16].

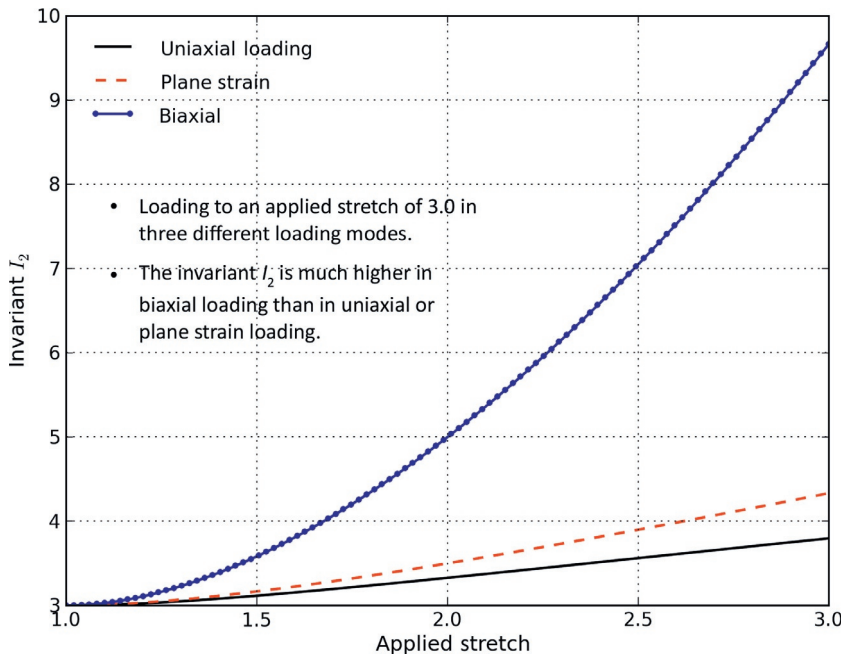


**Figure 5.8** Comparison between the  $I_2$  value in uniaxial, plane strain, and biaxial loading, as a function of the applied stretch  $\lambda_1$ .

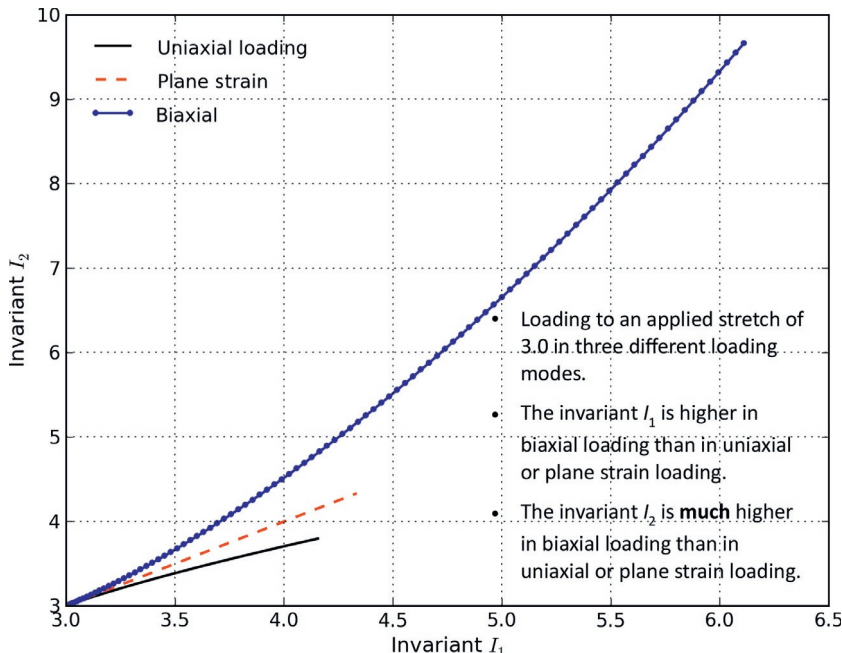


**Figure 5.9** Comparison between the  $I_2$  value in uniaxial, plane strain, and biaxial loading, as a function of the applied  $I_1$ .

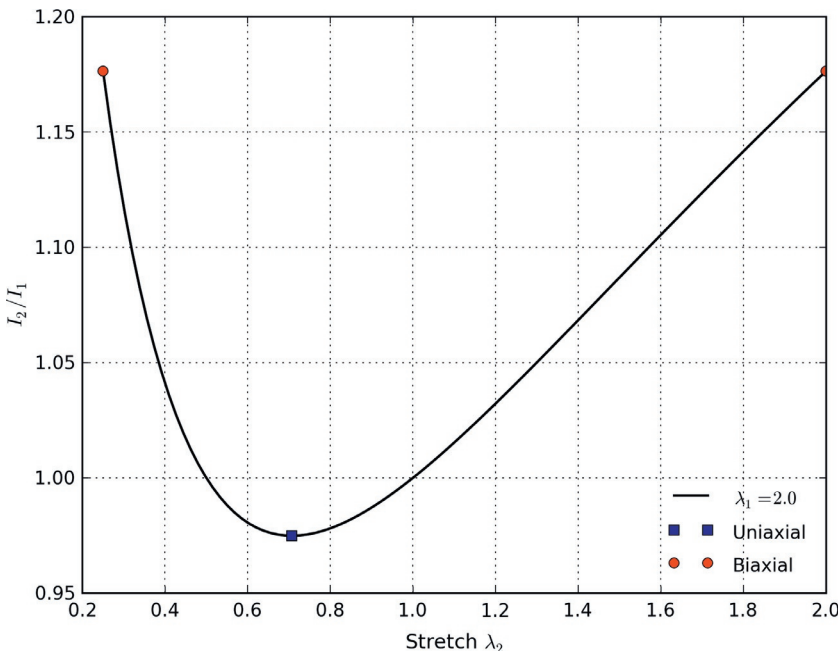


**Figure 5.10** Normalized  $I_2/I_1$  value for all loading modes for isotropic materials.

incompressible there are only two:  $I_1$  and  $I_2$ . To make the example concrete consider a deformation state where  $\lambda_1 = 2$ , and then vary  $\lambda_2$ . The  $I_1$  and  $I_2$  values can be directly calculated from the  $\lambda_1$  and  $\lambda_2$  values, and the ratio  $I_2/I_1$  established. The results from that calculation is shown in Figure 5.10.

Figure 5.10 shows that  $I_2$  is the lowest in uniaxial loading, and the highest in biaxial loading.

These results help understand the experimental Helmholtz energy that was shown in Figure 5.7. In that case the free energy in biaxial loading was higher than the energies in uniaxial loading or pure shear. One of the reasons for this is likely that the value of  $I_2$  is higher in biaxial loading, and hence plotting the energy only as a function of  $I_1$  will underestimate the free energy.

### 5.3.5 Freely Jointed Chain Model

The presentation in this chapter has so far focused on deriving suitable continuum mechanics expressions for the stress response

for a given deformation history. Specifically, it has been shown that the stress can be directly calculated if the expression for the Helmholtz free energy is known. The Helmholtz free energy can either be taken from a phenomenological (often parametrized) expression for  $\Psi(\cdot)$ , or from a micromechanism inspired representation based on the deformation behavior of the microstructure.

This subsection presents a simple micromechanism inspired molecular chain model called the *Freely Jointed Chain* (FJC) model. Other micromechanical chain models, like the Kratky-Porod chain model [17] and the worm-like chain mode [18, 19] have been developed in the literature. These models are not discussed in this text.

In the FJC model the macromolecules in the polymer microstructure are represented as  $n$  “rigid links” (called Kuhn segments), each of length  $l$ , for a total chain contour length of  $L = nl$ , see Figure 5.11. This model is also called the random walk model since the molecular chains are assumed to not interact and to have a distribution that corresponds to a random walk.

The Helmholtz free energy of this molecular chain model is given by the sum of the entropies of the individual molecular

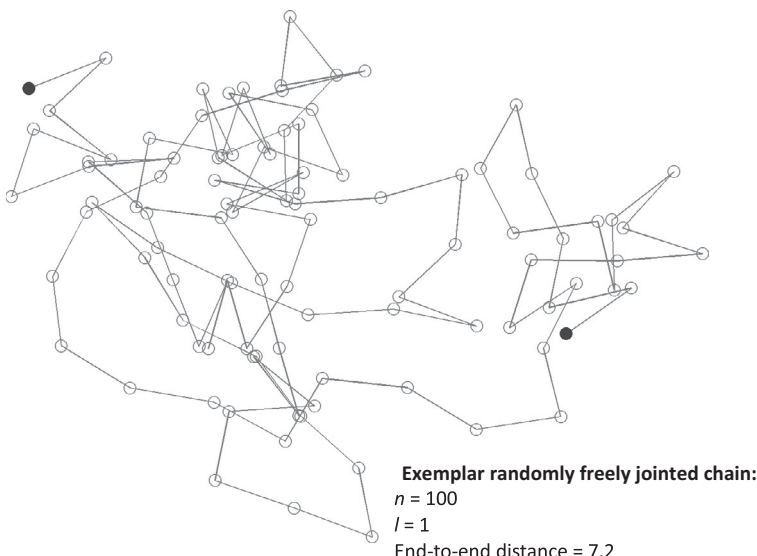


**Figure 5.11** Randomly generated freely jointed chain with  $n = 100$ , and  $l = 1$ .

chains, which can be obtained from a statistical survey of the possible molecular configurations using statistical mechanics.

As a macromolecule is stretched, the number of available configurations which can accommodate the extended chain end-to-end distance decrease, thus giving a decrease in configurational entropy,  $\Delta\eta$ . By assuming the molecules to be freely jointed with a fixed bond length, the entropy can be determined from the statistical mechanics relation [20]:

$$\eta_0 = Nk_B \ln \Omega(r) + c, \quad (5.65)$$

where  $\Omega(r)$  is the probability distribution of the end-to-end distance of the molecular chain,  $N$  is the number of chains per reference unit volume, and  $k_B = 1.38 \times 10^{-23}$  J/K is Boltzmann's constant. Flory [21] showed that the probability distribution under these conditions can be written:

$$\Omega(r) = \frac{1}{2\pi^2 r} \int_0^\infty q \sin(qr) \left[ \frac{\sin ql}{ql} \right]^n dq. \quad (5.66)$$

One approximation of the integral (5.66) that is good for  $n \gg 1$  and  $r \approx n$  is the Langevin expression attributed to Kuhn and Grün [22]:

$$\Omega(r) = \frac{A'}{l^3} \left[ \frac{\sinh \beta}{\beta} \right]^n \exp \left[ \frac{-\beta r}{l} \right], \quad (5.67)$$

where  $\beta = \mathcal{L}^{-1}(r/(nl))$  and  $\mathcal{L}(x) = \coth(x) - 1/x$  is the Langevin function. The inverse Langevin function  $\mathcal{L}^{-1}(x)$  cannot be expressed in elementary functions but can be approximated from the following expression [23] that has a max relative error of  $6.4 \times 10^{-4}$ :

$$\mathcal{L}^{-1}(x) \approx \begin{cases} 1.31446 \tan(1.58986x) + 0.91209x, & \text{if } |x| < 0.84136, \\ 1/(\text{sign}(x) - x), & \text{if } 0.84136 \leq |x| < 1. \end{cases} \quad (5.68)$$

The inverse Langevin function is plotted in Figure 5.12.

Note that in the limit as  $n \rightarrow \infty$ , Equation (5.67) becomes a Gaussian distribution:

$$\Omega(r) = \left[ \frac{3}{2\pi nl^3} \right]^{3/2} \exp \left[ \frac{-3r^2}{2nl^2} \right]. \quad (5.69)$$

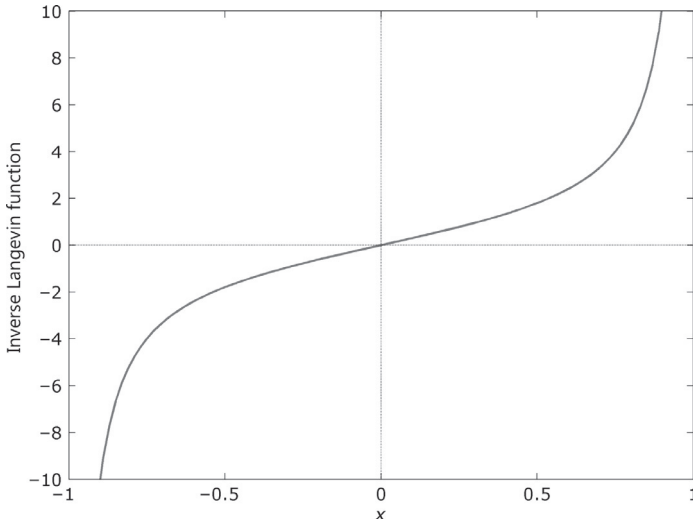


**Figure 5.12** Inverse Langevin function  $\mathcal{L}(x)$ . The value of the function is only defined for  $x$ -values between  $-1$  and  $+1$ .

The change in entropy with chain length for the Langevin expression therefore can be written:

$$\frac{\partial \eta_0}{\partial r} = \frac{\partial [Nk_B \ln \Omega(r)]}{\partial r} = \frac{-Nk_B}{l} \mathcal{L}^{-1} \left( \frac{r}{nl} \right), \quad (5.70)$$

and that the corresponding expression for Gaussian chains becomes:

$$\frac{\partial \eta_0}{\partial r} = \frac{\partial [Nk_B \ln \Omega(r)]}{\partial r} = -\frac{3Nk_B r}{nl^2}, \quad (5.71)$$

where  $N$  is the number of chains per reference unit volume,  $k_B$  is Boltzmann's constant, and  $r$  is the end-to-end distance of the molecular chains.

The definition of Helmholtz free energy per unit reference volume:

$$\Psi = e_0 - \theta_0 \eta_0, \quad (4.219\text{-repeat})$$

together with the lack of storage of internal energy ( $e_0 \equiv 0$ ) since each link in the molecular chain model is rigid, allows us to directly obtain the force required to stretch a molecular chain to a given end-to-end distance:

$$f_c = \frac{\partial \Psi}{\partial r} = \frac{Nk_B\theta_0}{l} \mathcal{L}^{-1} \left( \frac{r}{nl} \right). \quad (5.72)$$

This type of micromechanics inspired model can be used to gain a better understanding the behavior of the mechanical response of polymers. This approach is also directly used in some commonly used hyperelastic material models, like the Arruda-Boyce Eight-Chain model (see [Section 5.3.10](#)).

The next few subsections discusses some of the more commonly used hyperelastic models that are available in FE programs. The purpose of this review is to illustrate some of the similarities between these models, how they work, and under what conditions they can provide accurate predictions of real polymer materials.

### 5.3.6 Neo-Hookean Model

The NH model is a simple hyperelastic model that is based on two material parameters: a shear modulus  $\mu$  and a bulk modulus  $\kappa$ . Here, as is often done, the theory for the NH model will be presented both for compressible and incompressible deformations.<sup>9</sup> The incompressible form is often easier to use in theoretical derivations, but for practical studies, including FE simulations, the compressible version is often more useful and will emphasized in the following. Hyperelasticity models, such as the NH model, are mostly used for solid, rubber-like materials. These materials are characterized by an almost incompressible response and the actual value of the bulk modulus therefore typically has very little influence on the response of the rubber-like component. The only exception is in applications where the component is highly confined, e.g. o-rings that are compressed in a confined space (see Chapter 2, Section 2.2.9).

Like all hyperelastic material models, the NH model is specified by the expression for its Helmholtz free energy per unit reference volume. Here, the Helmholtz free energy is assumed to be independent of the temperature, and is hence identical to the

---

<sup>9</sup>The compressible version of the model can be made incompressible by studying the case when  $\kappa \rightarrow \infty$ . The incompressible version of the NH model consequently only contain one material parameter, the shear modulus  $\mu$ .

internal energy per unit reference volume  $e_0$ . For the NH model, the Helmholtz free energy per unit reference volume is given by:

$$\Psi(I_1^*, J) = \frac{\mu}{2}(I_1^* - 3) + \frac{\kappa}{2}(J - 1)^2. \quad (5.73)$$

**Note 1:** The equation for the free energy is linear in  $I_1^*$ , and can therefore not accurately capture the large-strain non-linear response of many elastomers.

**Note 2:** The equation for the free energy is not including any dependence on the second invariant  $I_2^*$ . As shown in the example below, this may cause the stress predictions to be too low in situations where the loading is mainly biaxial.

**Note 3:** The energy from volumetric deformations is quadratic in  $(J - 1)$ , giving a volumetric stress that is linear in  $(J - 1)$ , see Equation (5.74).

By using Equations (5.41), (4.66), and (4.36) it is easy to show that the compressible NH model has the following expression for the Cauchy stress for an arbitrary deformation state:

$$\boldsymbol{\sigma} = \frac{\mu}{J} \operatorname{dev} [\mathbf{b}^*] + \kappa(J - 1)\mathbf{I}, \quad (5.74)$$

where  $\mu$  is the shear modulus, and  $\kappa$  is the bulk modulus.

For the incompressible NH model, the Cauchy stress is given by Equations (5.47)–(5.49) giving the following expressions for uniaxial, planar, and biaxial deformations:

$$\sigma_{\text{uniax}} = \mu \left( \lambda^2 - \frac{1}{\lambda} \right), \quad (5.75)$$

$$\sigma_{\text{planar}} = \mu \left( \lambda^2 - \frac{1}{\lambda^2} \right), \quad (5.76)$$

$$\sigma_{\text{biaxial}} = \mu \left( \lambda^2 - \frac{1}{\lambda^4} \right). \quad (5.77)$$

Here, and in the remainder of this text, incompressible uniaxial deformation is defined by

$$\mathbf{F} = \begin{bmatrix} \lambda & 0 & 0 \\ 0 & 1/\sqrt{\lambda} & 0 \\ 0 & 0 & 1/\sqrt{\lambda} \end{bmatrix}, \quad (5.78)$$

incompressible planar deformation is defined by

$$\mathbf{F} = \begin{bmatrix} \lambda & 0 & 0 \\ 0 & 1 & 0 \\ 0 & 0 & 1/\lambda \end{bmatrix}, \quad (5.79)$$

and incompressible biaxial deformation is defined by

$$\mathbf{F} = \begin{bmatrix} \lambda & 0 & 0 \\ 0 & \lambda & 0 \\ 0 & 0 & 1/\lambda^2 \end{bmatrix}. \quad (5.80)$$

For incompressible uniaxial loading the NH material model can be implemented into Matlab code as follows:

**Matlab Code: NH\_incompressible\_uniaxial.m**

```
function [stress] = NH(time, strain, params)
%NH Neo-Hookean hyperelastic model
%Incompressible uniaxial loading
%This function is using true stress and strain
mu = params(1);
lambda = exp(strain);
stress = mu * (lambda.^2 - 1./lambda);
end
```

And as Python code as follows:

**Python Code: "NH\_incompressible\_uniaxial.py"**

```
from pylab import *
def NH(strain, params):
    """Neo-Hookean hyperelastic model.
    Incompressible uniaxial loading.
    This function is using true stress and strain"""
    mu = params[0]
    lam = exp(strain)
    return mu * (lam*lam - 1/lam)

strain = linspace(0, 0.8)
params = [1.0]
stress = NH(strain, params)
plot(strain, stress, 'r-')
```

The response of the NH model in this case is only controlled by the shear modulus  $\mu$ . A direct comparison between predictions

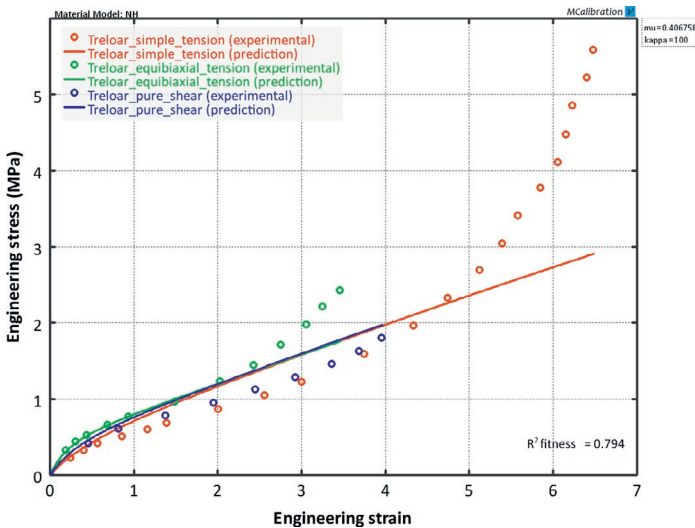


**Figure 5.13** Comparison between experimental data from Treloar [15, 16] and predictions from the Neo-Hookean material model.

from the NH model and classical experimental data for vulcanized natural rubber from Treloar [15, 16] is shown in Figure 5.13. This figure shows experimental data in simple tension, equibiaxial tension, and planar tension. As illustrated in the figure, the NH model does not capture the large strain response very well. This limitation of the model is caused by its inability to capture the limiting molecular chain stretch of the material as it becomes highly deformed.

As shown in the following code and figure, it is also easy to implement the NH model for compressible loading. This code numerically searches for the transverse strain that gives  $\sigma_{22} = 0$  for each value of the applied strain  $\varepsilon_{11}$ .

The value of the NH model lies in its simplicity—if the shear modulus is known, the response in any loading mode can be determined in a robust and computationally efficient way. The main limitation of the NH model is its limited range of conditions that give accurate predictions.

### Example: Shear Modulus in the NH Model.

In this example we will demonstrate that the material parameter  $\mu$  in Equation (5.73) is indeed the shear modulus of the material.

**Python Code: "Polymer\_Mechanics\_Chap05.py"**

```

from pylab import *
import scipy.optimize

def uniaxial_stress(model, trueStrainVec, params):
    """Compressible uniaxial loading. Returns true stress."""
    stress = zeros(len(trueStrainVec))
    for i in range(len(trueStrainVec)):
        lam1 = exp(trueStrainVec[i])
        calcS22Abs = lambda x: abs(model([lam1,x,x],params)[1,1])
        # search for transverse stretch that gives S22=0
        lam2 = scipy.optimize.fmin(calcS22Abs, x0=1/sqrt(lam1),
                                   xtol=1e-9, ftol=1e-9, disp=False)
        stress[i] = model([lam1, lam2, lam2], params)[0,0]
    return stress

def NH_3D(stretch, param):
    """Neo-Hookean. 3D loading specified by stretches.
    param[0]=mu, param[1]=kappa"""
    F = array([[stretch[0],0,0], [0,stretch[1],0], [0,0,stretch[2]]])
    J = det(F)
    Fstar = J**(-1/3) * F
    bstar = dot(Fstar, Fstar.T)
    dev_bstar = bstar - trace(bstar)/3 * eye(3)
    return param[0]/J * dev_bstar + param[1]*(J-1) * eye(3)

```

**Python Code: "NH\_compressible\_uniaxial.py"**

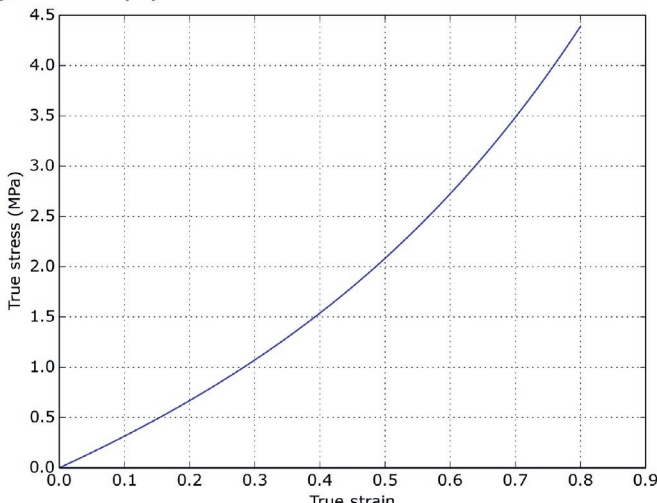
```

from pylab import *
from Polymer_Mechanics_Chap05 import *

trueStrain = linspace(0, 0.8, 100)
trueStress = uniaxial_stress(NH_3D, trueStrain, [1.0, 100])

plot(trueStrain, trueStress, 'b-')
xlabel('True Strain')
ylabel('True Stress (MPa)')
grid('on')
show()

```

**Figure Created by Python Code:**

One way to show this is to consider a case of simple shear defined by:

$$\mathbf{F} = \begin{bmatrix} 1 & \gamma & 0 \\ 0 & 1 & 0 \\ 0 & 0 & 1 \end{bmatrix}. \quad (5.81)$$

Inserting this deformation gradient into Equation (5.74) gives the shear stress  $\sigma_{12} = \mu\gamma$ , which together with Equation (5.4) demonstrates that  $\mu$  is the shear modulus.

Another way to show that  $\mu$  in Equation (5.73) is the shear modulus is to consider the derivative of  $\sigma_{\text{uniax}}$  in Equation (5.75) with respect to  $\lambda$  in the limit when  $\lambda \rightarrow 1$ :

$$\lim_{\lambda \rightarrow 1} \frac{d\sigma_{\text{uniax}}}{d\lambda} = \lim_{\varepsilon \rightarrow 0} \frac{d\sigma_{\text{uniax}}}{d\varepsilon} = 3\mu, \quad (5.82)$$

where  $\varepsilon$  is the uniaxial small strain. The derivative in Equation (5.82) is also, by definition, equal to the Young's modulus, and for an incompressible material the Young's modulus is equal to 3 times the shear modulus, hence  $\mu$  is indeed the shear modulus of the material.

### Example: Bulk Modulus in the NH Model.

This example will demonstrate that the material parameter  $\kappa$  in Equation (5.73) is the bulk modulus of the material. One way to show this is to consider a case of triaxial deformation:

$$\mathbf{F} = \begin{bmatrix} \varepsilon & 0 & 0 \\ 0 & \varepsilon & 0 \\ 0 & 0 & \varepsilon \end{bmatrix}. \quad (5.83)$$

Inserting this into Equation (5.74) gives  $\sigma_{11} = \sigma_{22} = \sigma_{33} = \sigma = \kappa(\lambda^3 - 1)$ . Taking the stretch derivative in the limit of small deformations gives

$$\lim_{\lambda \rightarrow 1} \frac{d\sigma}{d\lambda} = \lim_{\varepsilon \rightarrow 0} \frac{d\sigma}{d\varepsilon} = 3\kappa. \quad (5.84)$$

From Equation (5.9) and Table 5.1 we also know that  $d\sigma/d\varepsilon$  in a triaxial deformation is equal to  $3\kappa$ , hence the parameter  $\kappa$  in Equation (5.73) is the initial bulk modulus of the material.

### Example: Alternative Formulation of the NH Model.

The NH model can also be written using the following alternative equation:

$$\boldsymbol{\sigma} = \frac{\mu}{J} (\mathbf{b} - \mathbf{I}) + \kappa(J - 1)\mathbf{I}. \quad (5.85)$$

That is, the stress is not strictly divided into deviatoric and volumetric parts. For cases when the bulk modulus  $\kappa$  is large the standard NH model and this alternative NH model give similar predictions, but the smaller the bulk modulus the more different the two models become.

Figure 5.14 shows the stress-strain predictions from the standard NH model and the alternative NH model. In this case the shear modulus was taken to be  $\mu = 1 \text{ MPa}$ , and the bulk modulus was taken as  $\kappa = 5 \text{ MPa}$ .

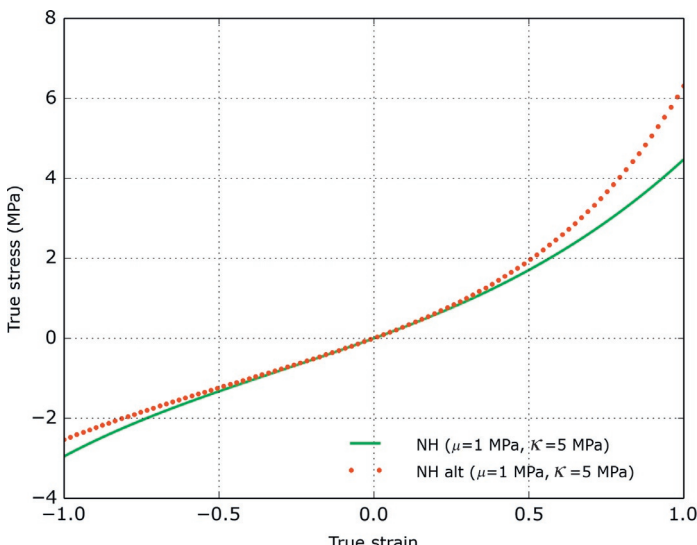


**Figure 5.14** Comparison between predictions from the standard and an alternative NH model formulations.

### 5.3.7 Mooney-Rivlin Model

The Mooney-Rivlin (MR) model is an extension of the NH model that attempts to improve the accuracy by including a linear dependence on  $I_2^*$  in the Helmholtz free energy per unit reference volume:

$$\Psi(C_{10}, C_{01}, \kappa) = C_{10} (I_1^* - 3) + C_{01} (I_2^* - 3) + \frac{\kappa}{2} (J - 1)^2. \quad (5.86)$$

As illustrated in this equation, the compressible version of the MR model requires three material parameters:  $C_{10}$ ,  $C_{01}$ , and  $\kappa$ . Using Equation (5.41) it can be shown that the Cauchy stress for the Mooney-Rivlin model is given by:

$$\boldsymbol{\sigma} = \frac{2}{J} (C_{10} + C_{01} I_1^*) \mathbf{b}^* - \frac{2C_{01}}{J} (\mathbf{b}^*)^2 + \left[ \kappa (J - 1) - \frac{2I_1^* C_{10}}{3J} - \frac{4I_2^* C_{01}}{3J} \right] \mathbf{I}. \quad (5.87)$$

For the incompressible version of the MR model ( $\kappa \rightarrow \infty$ ), the Cauchy stresses in uniaxial, planar, and equibiaxial deformations are given by the following expressions:

$$\sigma_{\text{uniax}} = 2 \left( \lambda^2 - \frac{1}{\lambda} \right) \left[ C_{10} + \frac{C_{01}}{\lambda} \right], \quad (5.88)$$

$$\sigma_{\text{planar}} = 2 \left( \lambda^2 - \frac{1}{\lambda^2} \right) [C_{10} + C_{01}], \quad (5.89)$$

$$\sigma_{\text{biaxial}} = 2C_{10} \left( \lambda^2 - \frac{1}{\lambda^4} \right) + 2C_{01} \left( \lambda^4 - \frac{1}{\lambda^2} \right). \quad (5.90)$$

The accuracy of the Mooney-Rivlin model to predict the behavior of elastomers is demonstrated in Figure 5.15 by comparison to vulcanized natural rubber data of Treloar [16].

This figure shows that the Mooney-Rivlin model can improve the predictions of the NH model. However, the improvements can come with a price—having a negative  $C_{01}$  term, although often improving the predictions in one loading mode, can at the same time make the model unstable at finite deformations in a different

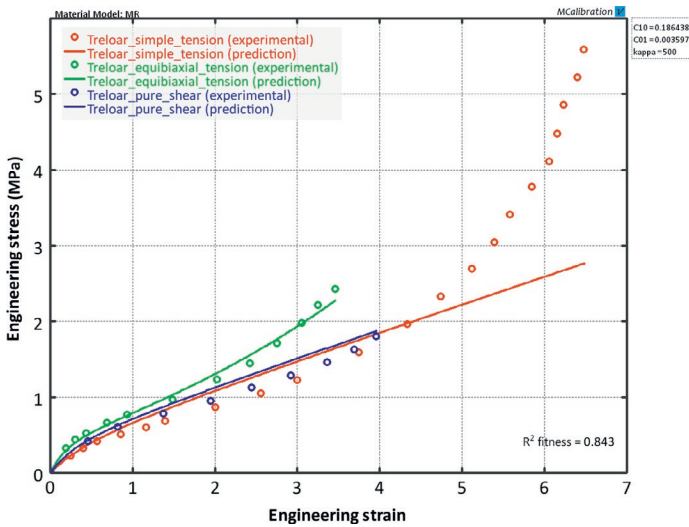


**Figure 5.15** Comparison between experimental data from Treloar [16] and predictions from the incompressible Mooney-Rivlin material model.

loading mode (see [Section 5.8.2](#)). One example of this is shown in [Figure 5.16](#).

For incompressible uniaxial loading the Mooney-Rivlin material model can be implemented in Python using the following code:

Python Code: “MR\_incompressible\_uniaxial.py”

```
from pylab import *

def MR(strain, params):
    """Mooney-Rivlin hyperelastic model.
    Incompressible uniaxial loading.
    This function is using true stress and strain"""
    C10 = params[0]
    C01 = params[1]
    lam = exp(strain)
    return 2 * (lam*lam - 1/lam) * (C10 + C01/lam)

strain = linspace(0, 0.8)
params = [1.0, 0.1]
stress = MR(strain, params)
plot(strain, stress, 'r-')
show()
```

The following code example shows one way to implement the Mooney-Rivlin material model for *compressible* uniaxial loading.

## Additional Python Code to "Polymer\_Mechanics\_Chap05.py"

```
def MR_3D(stretch, param):
    """Mooney-Rivlin. 3D loading specified by stretches.
    param: [C10, C01, kappa]"""
    L1 = stretch[0]
    L2 = stretch[1]
    L3 = stretch[2]
    F = array([[L1, 0, 0], [0, L2, 0], [0, 0, L3]])
    J = det(F)
    bstar = J**(-2.0/3.0) * dot(F, F.T)
    bstar2 = dot(bstar, bstar)
    I1s = trace(bstar)
    I2s = 0.5 * (I1s**2 - trace(bstar2))
    C10 = param[0]
    C01 = param[1]
    kappa = param[2]
    return 2/J*(C10+C01*I1s)*bstar - 2*C01/J*bstar2 + \
        (kappa*(J-1) - 2*I1s*C10/(3*J) - 4*I2s*C01/(3*J))*eye(3)
```

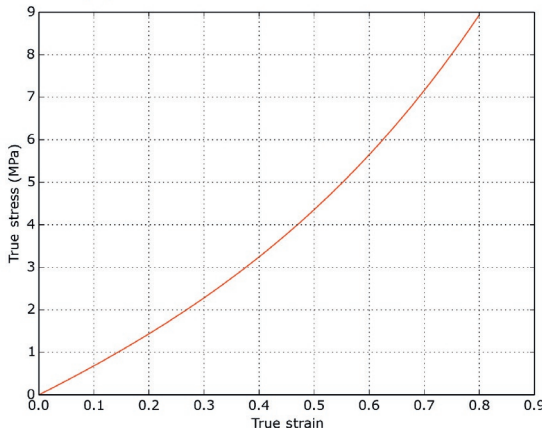
## Python Code: "MR\_compressible\_uniaxial.py"

```
from pylab import *
from Polymer_Mechanics_Chap05 import *

trueStrain = linspace(0, 0.8, 100)
trueStress = uniaxial_stress(MR_3D, trueStrain, [1.0, 0.1, 100])

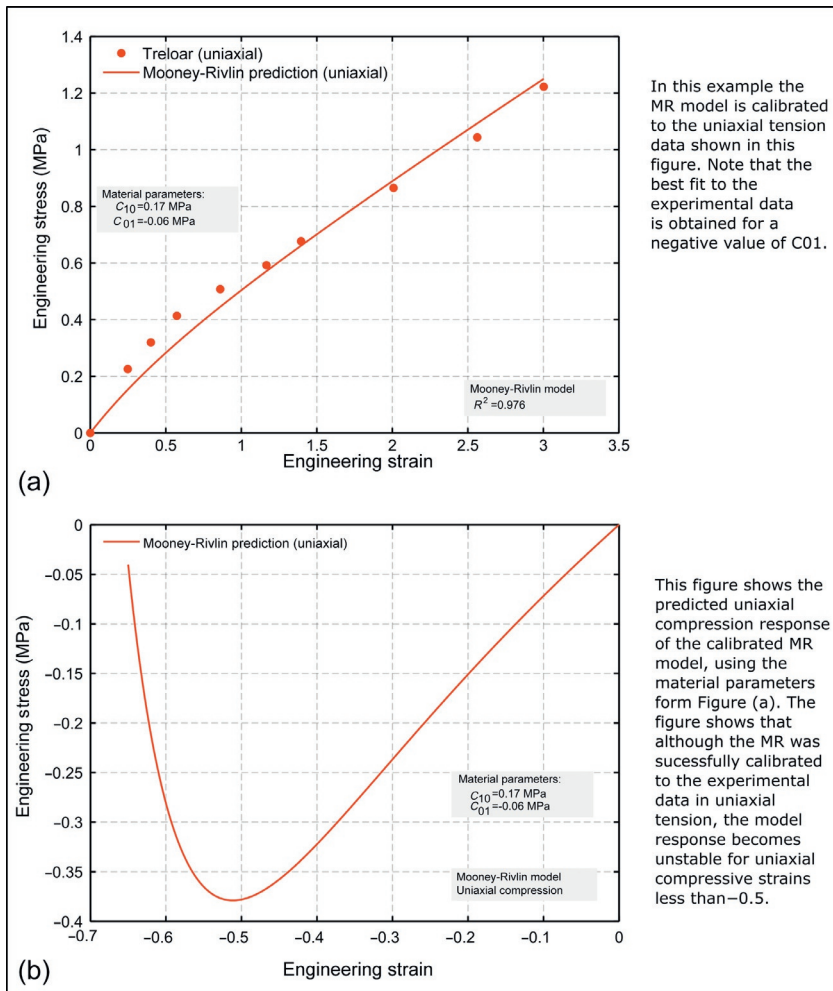
plot(trueStrain, trueStress, 'r-')
xlabel('True Strain')
ylabel('True Stress (MPa)')
grid('on')
show()
```

Figure Created by Python Code:



## 5.3.8 Yeoh Model

The Yeoh model [24] is based on a Helmholtz free energy that is a third-order polynomial in  $I_1^*$ , with no dependence on  $I_2^*$ . Due to the higher order  $I_1^*$  terms, this model will enable more accurate predictions than the NH model, and at the same time potentially



**Figure 5.16** Example illustrating stability problems with the Mooney-Rivlin model.

avoid some of the stability issues of the Mooney-Rivlin model. One convenient way to write the Helmholtz free energy per unit reference volume for a compressible version of the Yeoh model is as follows:

$$\begin{aligned} \Psi(C_{10}, C_{20}, C_{30}, \kappa) = & C_{10} (I_1^* - 3) + C_{20} (I_1^* - 3)^2 \\ & + C_{30} (I_1^* - 3)^3 + \frac{\kappa}{2} (J - 1)^2. \end{aligned} \quad (5.91)$$

The model requires four material parameters:  $C_{10}$ ,  $C_{20}$ ,  $C_{30}$ , and  $\kappa$ . Note that some FE programs also use higher order terms to represent the energy from volumetric deformations. As was discussed in Section 2.2.9, these higher order terms rarely play a role in the accuracy of the model predictions.

One of the main motivations for the Yeoh model is that for most elastomers the Helmholtz free energy is much weaker dependent on the invariant  $I_2^*$  than the first invariant  $I_1^*$  [24–26]. Also, it turns out to be difficult to experimentally determine the dependence of the Helmholtz free energy on the  $I_2^*$  term. Based on these arguments, Yeoh [24] suggested that it is reasonable to neglect the dependence on  $I_2^*$  altogether. It has also been shown that by neglecting the  $I_2^*$  dependence it becomes easier to ensure that a hyperelastic model is Drucker stable [24] (see [Section 5.8.2](#)).

Using Equation [\(5.41\)](#), it can be shown that the Cauchy stress for the compressible Yeoh model is given by:

$$\boldsymbol{\sigma} = \frac{2}{J} \left\{ C_{10} + 2C_{20}(I_1^* - 3) + 3C_{30}(I_1^* - 3)^2 \right\} \text{dev}[\mathbf{b}^*] + \kappa(J - 1)\mathbf{I}. \quad (5.92)$$

For the incompressible version of the Yeoh model, the Cauchy stresses in uniaxial, planar, and equibiaxial deformations are given by the following expressions:

$$\sigma_{\text{uniax}} = 2 \left[ C_{10} + 2C_{20}(I_1 - 3) + 3C_{30}(I_1 - 3)^2 \right] \left( \lambda^2 - \frac{1}{\lambda} \right), \quad (5.93)$$

$$\sigma_{\text{planar}} = 2 \left[ C_{10} + 2C_{20}(I_1 - 3) + 3C_{30}(I_1 - 3)^2 \right] \left( \lambda^2 - \frac{1}{\lambda^2} \right), \quad (5.94)$$

$$\sigma_{\text{biax}} = 2 \left[ C_{10} + 2C_{20}(I_1 - 3) + 3C_{30}(I_1 - 3)^2 \right] \left( \lambda^2 - \frac{1}{\lambda^4} \right). \quad (5.95)$$

The accuracy of the Yeoh model to predict the behavior of elastomers is demonstrated in [Figure 5.17](#).

This figure shows that the Yeoh model can improve the predictions of the NH model for the different loading modes,

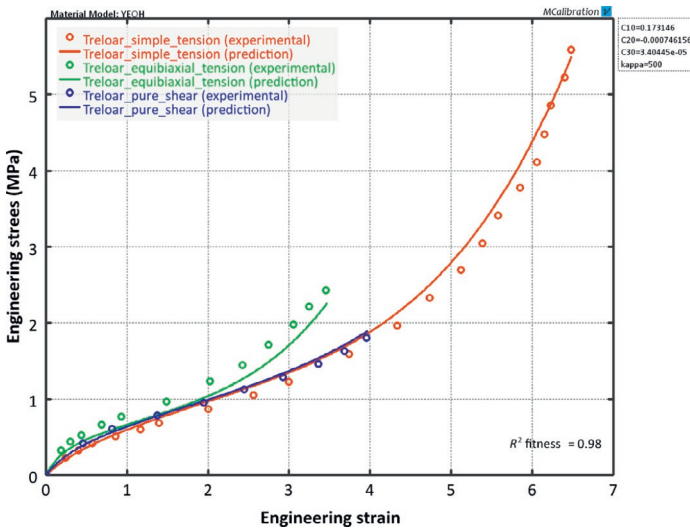


**Figure 5.17** Comparison between experimental data from Treloar [16] and predictions from the incompressible Yeoh material model.

particularly at large deformations. For many elastomeric materials it has been shown [27] that a useful rule-of-thumb rule for the material parameters is to select  $C_{10}$  to be positive and  $C_{20} \approx -0.01C_{10}$ , and  $C_{30} \approx -0.01C_{20}$ .

For incompressible uniaxial loading the Yeoh material model can be implemented in Python using the following code:

Python Code: "Yeoh\_incompressible\_uniaxial.py"

```
from pylab import *
def Yeoh(strain, params):
    """Yeoh hyperelastic model.
    Incompressible uniaxial loading.
    This function is using true stress and strain"""
    C10 = params[0]
    C20 = params[1]
    C30 = params[2]
    lam = exp(strain)
    I1 = lam**2 + 2/lam
    return 2 * (lam*lam - 1/lam) * (C10 + 2*C20*(I1-3) + 3*C30*(I1-3)**2)

strain = linspace(0, 0.8)
params = [1.0, -0.1, 0.01]
stress = Yeoh(strain, params)
plot(strain, stress, 'r-')
show()
```

The following code example shows one way to implement the Yeoh material model for *compressible* uniaxial loading.

**Additional Code to “Polymer\_Mechanics\_Chap05.py”:**

```
def Yeoh_3D(stretch, param):
    """Yeoh. 3D loading specified by stretches.
    param: [C10, C20, C30, kappa]. Returns true stress."""
    L1 = stretch[0]
    L2 = stretch[1]
    L3 = stretch[2]
    F = array([[L1, 0, 0], [0, L2, 0], [0, 0, L3]])
    J = det(F)
    bstar = J**(-2.0/3.0) * dot(F, F.T)
    devbstar = bstar - trace(bstar)/3 * eye(3)
    I1s = trace(bstar)
    return 2/J*(param[0] + 2*param[1]*(I1s-3) + \
                3*param[2]*(I1s-3)**2)*devbstar + param[3]*(J-1) * eye(3)
```

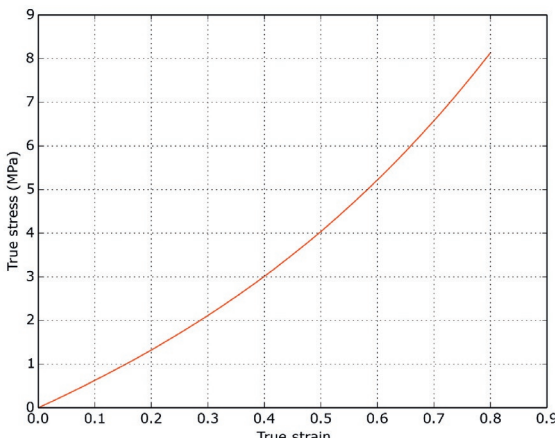
**Python Code: “Yeoh\_compressible\_uniaxial.py”**

```
from pylab import *
from Polymer_Mechanics_Chap05 import *

trueStrain = linspace(0, 0.8, 100)
trueStress = uniaxial_stress(Yeoh_3D, trueStrain, \
    [1.0, -0.01, 1e-4, 100])

plot(trueStrain, trueStress, 'r-')
xlabel('True Strain')
ylabel('True Stress (MPa)')
grid('on')
show()
```

**Figure Created by Python Code:**



### 5.3.9 Polynomial in $I_1$ and $I_2$ Model

A generalization of the NH, Mooney-Rivlin, and the Yeoh models can be obtained by taking the Helmholtz free energy to be a polynomial expansion in terms of  $I_1^*$  and  $I_2^*$ . One common way to express this series expansion is as follows<sup>10</sup>:

$$\Psi(C_{10}, C_{01}, \dots; D_1, D_2, \dots) = \sum_{i+j=1}^N C_{ij} (I_1^* - 3)^i (I_2^* - 3)^j + \sum_{i=1}^N \frac{1}{D_i} (J - 1)^{2i}. \quad (5.96)$$

This expression for the Helmholtz free energy is quite general and encompasses the NH, Mooney-Rivlin, and Yeoh models, but its generality also makes it difficult to determine the best set of material parameters that give accurate and robust predictions in multiaxial loading cases. This polynomial representation is therefore not as commonly used as the simpler models with a fixed number of terms.

### 5.3.10 Eight-Chain Model

The eight-chain (EC) model by Arruda and Boyce [28] is a hyperelasticity model that is motivated by the deformation behavior of the microstructure of elastomers. The basic assumption of the EC model is that the macromolecules (also called chain molecules) on average are located along the diagonals of a unit cell located in principal stretch space as illustrated in Figure 5.18. The side lengths of the unit cell in the reference state are denoted by  $a_0$ , and the undeformed chain length by  $r_0$ . It then directly follows that  $r_0 = a_0\sqrt{3}$ . Further, the macromolecules are taken to be freely jointed with  $n$  rigid links each of length  $l$ . For this FJC model the average end-to-end distance in the absence of an external force field is  $l\sqrt{n}$  [21]. By defining  $\lambda_1^*$ ,  $\lambda_2^*$ , and  $\lambda_3^*$  to be the applied principal distortional stretches, the effective distortional chain length becomes  $r = a_0[(\lambda_1^*)^2 + (\lambda_2^*)^2 + (\lambda_3^*)^2]^{1/2}$ , giving the effective distortional chain stretch

---

<sup>10</sup>This is the expression that is used, for example, by the FE program Abaqus [27].

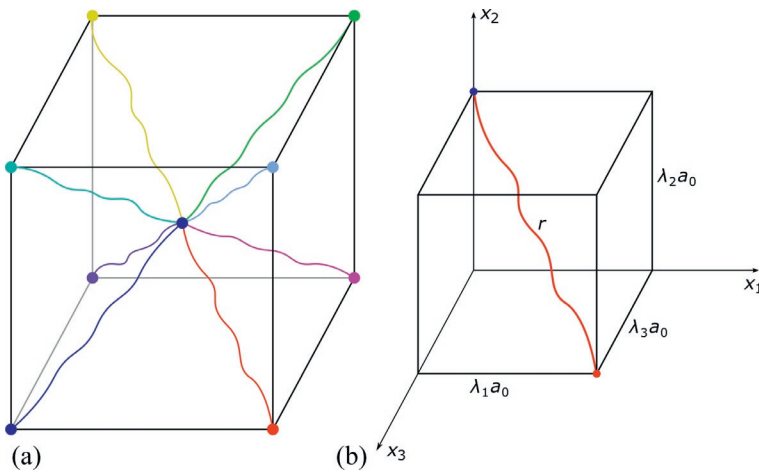


**Figure 5.18** (a) Eight chain molecules are located in the unit cell.  
(b) Volume element for one chain molecule.

$$\overline{\lambda^*} = \left[ \frac{(\lambda_1^*)^2 + (\lambda_2^*)^2 + (\lambda_3^*)^2}{3} \right]^{1/2} = \sqrt{\frac{\text{tr } \mathbf{C}^*}{3}} = \sqrt{\frac{\text{tr } \mathbf{b}^*}{3}} = \sqrt{\frac{I_1^*}{3}}, \quad (5.97)$$

where  $\mathbf{b}^* = (J)^{-2/3} \mathbf{b}$ . This shows that the distortional chain stretch is in fact a function only of the first invariant  $I_1^*$ .

Based on this physically motivated model, an *eight-chain material* is defined as an isotropic thermoelastic material whose Helmholtz free energy per unit reference volume,  $\Psi$ , only depends on the two deformation invariants  $\overline{\lambda^*}(\mathbf{b}^*) = [\text{tr}(\mathbf{b}^*)/3]^{1/2}$  and  $J = \det(\mathbf{F})$ , and the temperature  $\theta_0$ .

By noting that the effective chain stretch is related to the first invariant of  $\mathbf{b}^*$  through  $\overline{\lambda^*} = [I_1(\mathbf{b}^*)/3]^{1/2}$ , it follows that the Helmholtz free energy per unit reference volume can be written  $\Psi(\overline{\lambda^*}, J, \theta)$ , or alternatively  $\Psi(I_1^*, J, \theta_0)$  where  $I_1^* = I_1(\mathbf{b}^*) = \text{tr}(\mathbf{b}^*)$ . The Cauchy stress for an EC material can then be obtained from the continuum mechanics Equation (5.41) which in this case with no dependence on  $I_2^*$  can be simplified to

$$\boldsymbol{\sigma} = \frac{2}{J} \frac{\partial \Psi}{\partial I_1^*} \text{dev}[\mathbf{b}^*] + \frac{\partial \Psi}{\partial J} \mathbf{I}, \quad (5.98)$$

or when expressed in terms of the effective chain stretch  $\bar{\lambda}^*$

$$\boldsymbol{\sigma} = \frac{1}{J} \frac{1}{3\bar{\lambda}^*} \frac{\partial \Psi}{\partial \bar{\lambda}^*} \operatorname{dev}[\mathbf{b}^*] + \frac{\partial \Psi}{\partial J} \mathbf{I}. \quad (5.99)$$

The Helmholtz free energy per unit reference volume ( $\Psi$ ) can be determined by first using the experimental observation that for elastomers the internal energy is typically not a function of the applied distortional stretch [16], i.e.  $e_0(J, \theta_0)$ . Hence, the functional form of the Helmholtz free energy has the form:

$$\Psi(\bar{\lambda}^*, J, \theta_0) = e_0(J) - \theta_0 \eta_0(\bar{\lambda}^*). \quad (5.100)$$

Note that the dependence on  $J$  in  $\eta_0(\bar{\lambda}^*, J)$  has been neglected due to the assumption of small volume change. The assumption of small volumetric deformations also enable the relationship between the pressure component of the Cauchy stress  $\boldsymbol{\sigma}$  and the volumetric deformation  $J$  to be taken as linear:

$$\boldsymbol{\sigma} : \mathbf{I} = \frac{\partial \Psi(\bar{\lambda}^*, J, \theta_0)}{\partial J} = \kappa(J - 1), \quad (5.101)$$

giving the internal energy  $e_0(J) = \kappa J(J/2 - 1)$ . The Cauchy stress can then be calculated from Equation (5.99) giving

$$\boldsymbol{\sigma} = \frac{-\theta_0}{3J\bar{\lambda}^*} \frac{\partial \eta_0(\bar{\lambda}^*)}{\partial \bar{\lambda}^*} \operatorname{dev}[\mathbf{b}^*] + \kappa[J - 1] \mathbf{I}. \quad (5.102)$$

To completely specify the constitutive relationship it now only remains to determine how the entropy depends on the effective chain stretch. From the chain rule we get:

$$\frac{\partial \eta_0(r(\bar{\lambda}^*))}{\partial \bar{\lambda}^*} = \frac{\partial \eta_0}{\partial r} \frac{\partial r}{\partial \bar{\lambda}^*} = \frac{\partial \eta_0}{\partial r} \frac{1}{\frac{\partial}{\partial r} [rl\sqrt{n}]} = l\sqrt{n} \frac{\partial \eta_0}{\partial r}. \quad (5.103)$$

Thus it is sufficient to determine how the entropy of a single macromolecule depends on its end-to-end distance in order to finalize the constitutive equation. This derivation was discussed in detail in [Section 5.3.5](#).

By using Equation (5.70), the equation for the Cauchy stress (5.102) can now be written

$$\boldsymbol{\sigma} = \frac{Nk_B\theta}{3J} \frac{\lambda^{\text{lock}}}{\bar{\lambda}^*} \mathcal{L}^{-1} \left( \frac{\bar{\lambda}^*}{\lambda^{\text{lock}}} \right) \operatorname{dev}[\mathbf{b}^*] + \kappa[J - 1] \mathbf{I}, \quad (5.104)$$

where  $\lambda^{\text{lock}} \equiv nl$  is the maximum (fully extended) stretch that a molecule can be exposed to.

For the special case of incompressible uniaxial deformation Equation (5.104) simplifies to

$$\sigma_{\text{uniax}} = \frac{Nk_B\theta}{3J} \frac{\lambda^{\text{lock}}}{\bar{\lambda}^*} \mathcal{L}^{-1} \left( \frac{\bar{\lambda}^*}{\lambda^{\text{lock}}} \right) \left[ \lambda^2 - \frac{1}{\lambda} \right], \quad (5.105)$$

and for simple shear defined by  $\mathbf{F} = \mathbf{I} + \gamma \mathbf{e}_1 \otimes \mathbf{e}_2$  the shear stress is given by

$$\sigma_{\text{shear}} = \frac{Nk_B\theta_0}{3J} \frac{\lambda^{\text{lock}}}{\bar{\lambda}^*} \mathcal{L}^{-1} \left( \frac{\bar{\lambda}^*}{\lambda^{\text{lock}}} \right) \gamma, \quad (5.106)$$

where  $\bar{\lambda}^* = \sqrt{1 + \gamma^2/3}$ .

The initial shear modulus of the material is given by  $\mu = \left. \frac{\partial \sigma_{12}}{\partial \gamma} \right|_{\gamma=0}$  giving

$$\mu = \frac{Nk_B\theta_0}{3} \lambda^{\text{lock}} \mathcal{L}^{-1} \left( \frac{1}{\lambda^{\text{lock}}} \right), \quad (5.107)$$

which when inserted in (5.104) gives the Cauchy stress for the EC model as

$$\boldsymbol{\sigma} = \frac{\mu}{J \bar{\lambda}^*} \frac{\mathcal{L}^{-1} \left( \frac{\bar{\lambda}^*}{\lambda^{\text{lock}}} \right)}{\mathcal{L}^{-1} \left( \frac{1}{\lambda^{\text{lock}}} \right)} \text{dev}[\mathbf{b}^*] + \kappa [J - 1] \mathbf{I}. \quad (5.108)$$

In this equation  $[\mu, \lambda^{\text{lock}}, \kappa]$  are the material parameters.

For the incompressible version of the EC model, the Cauchy stresses in uniaxial, planar, and equibiaxial deformations are given by the following expressions:

$$\sigma_{\text{uniax}} = \frac{\mu}{\bar{\lambda}^*} \frac{\mathcal{L}^{-1} \left( \frac{\bar{\lambda}^*}{\lambda^{\text{lock}}} \right)}{\mathcal{L}^{-1} \left( \frac{1}{\lambda^{\text{lock}}} \right)} \left[ \lambda^2 - \frac{1}{\lambda} \right], \quad (5.109)$$

$$\sigma_{\text{planar}} = \frac{\mu}{\bar{\lambda}^*} \frac{\mathcal{L}^{-1} \left( \frac{\bar{\lambda}^*}{\lambda^{\text{lock}}} \right)}{\mathcal{L}^{-1} \left( \frac{1}{\lambda^{\text{lock}}} \right)} \left[ \lambda^2 - \frac{1}{\lambda^2} \right], \quad (5.110)$$

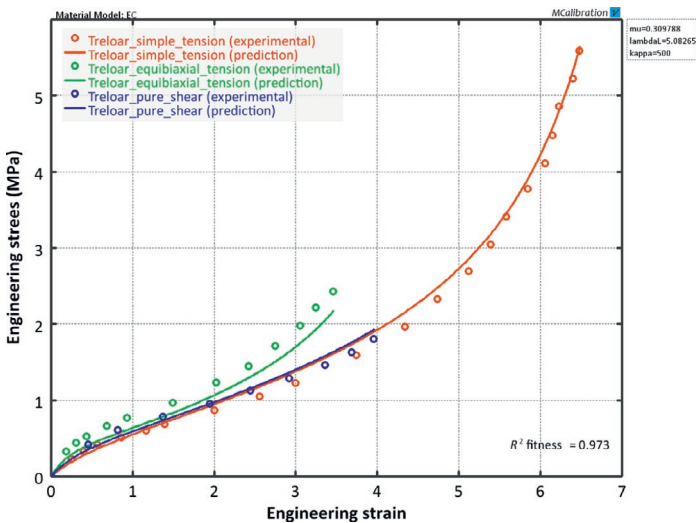


**Figure 5.19** Comparison between experimental data from Treloar [16] and predictions from the eight-chain material model.

$$\sigma_{\text{biax}} = \frac{\mu}{\lambda^*} \frac{\mathcal{L}^{-1}\left(\frac{\lambda^*}{\lambda^{\text{lock}}}\right)}{\mathcal{L}^{-1}\left(\frac{1}{\lambda^{\text{lock}}}\right)} \left[ \lambda^2 - \frac{1}{\lambda^4} \right]. \quad (5.111)$$

The compressible EC model contains three material parameters: a shear modulus  $\mu$ , a limiting chain stretch  $\lambda^{\text{lock}}$ , and a bulk modulus  $\kappa$ . The EC model has no dependence on  $I_2$  and give predictions that are similar in accuracy to the Gent model [29]. The accuracy of the EC model to predict the behavior of elastomers is demonstrated in Figure 5.19 by comparison to vulcanized natural rubber data of Treloar [16].

The figure shows that the EC model in this case is more accurate than the NH model and the Mooney-Rivlin model, and almost as accurate as the Yeoh model. The figure also shows that the EC model slightly underpredicts the biaxial response. This can be expected since the model is  $I_1$ -based, and does not include any dependence on  $I_2$ .

For incompressible uniaxial loading the EC material model can be implemented into Matlab using the following code:

**Matlab Code:**

```

function [stress] = mat_EC(time, strain, params)
%mat_EC Arruda-Boyce Eight-Chain hyperelastic model
%Incompressible uniaxial loading
%This function is using true stress and strain
mu = params(1);
lambdaL = params(2);
lambda = exp(strain);
lambdaChain = sqrt((lambda.^2 + 2./lambda) / 3);
stress = mu./lambdaChain .* invLangevin(lambdaChain/lambdaL) ...
    ./ invLangevin(1/lambdaL) .* (lambda.^2 - 1./lambda);
end

function [res] = invLangevin(x)
%INVLANGEVIN implementation of the inverse langevin function
x(find(x>=1)) = 1-eps;
x(find(x<=-1)) = -1+eps;
res = zeros(size(x));
index = find(abs(x) < 0.839);
res(index) = 1.31435 * tan(1.59*x(index)) + 0.911249*x(index);
index = find(abs(x) >= 0.839);
res(index) = 1 ./ (sign(x(index)) - x(index));
end

```

For incompressible uniaxial loading the NH material model can be implemented in Python using the following code:

**Additional Code to "Polymer\_Mechanics\_Chap05.py":**

```

def invLangevin(x):
    EPS = spacing(1)
    if type(x) == float: # x is a scalar
        if x >= 1-EPS: x = 1 - EPS
        if x <= -1+EPS: x = -1 + EPS
        if abs(x) < 0.839:
            return 1.31435 * tan(1.59*x) + 0.911249*x
        return 1.0 / (sign(x) - x)
    # x is an array
    x[x >= 1-EPS] = 1 - EPS
    x[x <= -1+EPS] = -1 + EPS
    res = zeros(size(x))
    index = abs(x) < 0.839
    res[index] = 1.31435 * tan(1.59*x[index]) + 0.911249*x[index]
    index = abs(x) >= 0.839
    res[index] = 1.0 / (sign(x[index]) - x[index])
    return res

```

**Python Code: "EC\_incompressible\_uniaxial.py"**

```

from pylab import *
from Polymer_Mechanics_Chap05 import *

def EightChain(trueStrain, params):
    """Arruda-Boyce eight-chain model.
       Incompressible uniaxial loading. Returns true stress."""
    mu = params[0]
    lambdaL = params[1]
    lam = exp(trueStrain)
    lamChain = sqrt((lam**2 + 2/lam)/3)
    return mu/lamChain * invLangevin(lamChain/lambdaL)/invLangevin(1/lambdaL) \
        * (lam*lam - 1/lam)

trueStrain = linspace(0, 0.8, 10)
trueStress = EightChain(trueStrain, [1.0, 3.0])

plot(trueStrain, trueStress, 'r-')
xlabel('True Strain')
ylabel('True Stress (MPa)')
grid('on')
show()

```

The following code example shows one way to implement the EC material model for *compressible* uniaxial loading.

Additional Code to "Polymer\_Mechanics\_Chap05.py":

```
def EC_3D(stretch, param):
    """Eight-Chain. 3D loading specified by stretches.
    param: [mu, lambdaL, kappa]. Returns true stress."""
    L1 = stretch[0]
    L2 = stretch[1]
    L3 = stretch[2]
    F = array([[L1, 0, 0], [0, L2, 0], [0, 0, L3]])
    J = det(F)
    bstar = J**(-2.0/3.0) * dot(F, F.T)
    lamChain = sqrt(trace(bstar)/3)
    devbstar = bstar - trace(bstar)/3 * eye(3)
    return param[0]/(J*lamChain) * invLangevin(lamChain/param[1]) / \
        invLangevin(1/param[1]) * devbstar + param[2]*(J-1) * eye(3)
```

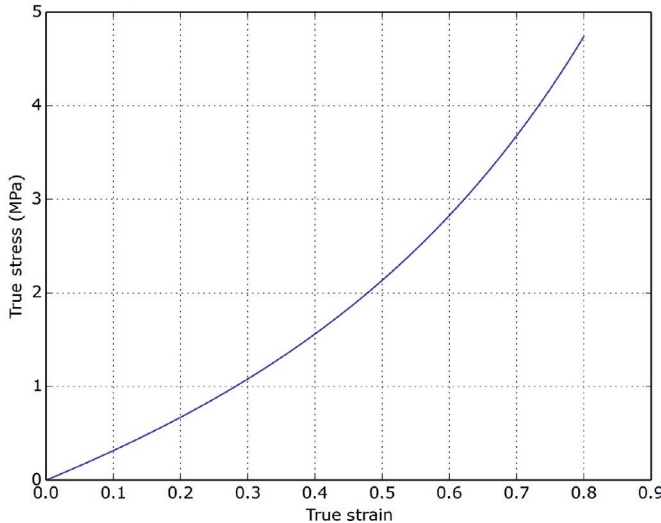
Python Code: "EC\_compressive\_uniaxial.py"

```
from pylab import *
from Polymer_Mechanics_Chap05 import *

trueStrain = linspace(0, 0.8, 100)
trueStress = uniaxial_stress(EC_3D, trueStrain, [1.0, 3.0, 100])

plot(trueStrain, trueStress, 'b-')
xlabel('True Strain')
ylabel('True Stress (MPa)')
grid('on')
show()
```

Figure Created by Python Code:



### Example: Different Implementations for the Inverse Langevin Function.

The Langevin function is defined by:

$$\mathcal{L}(x) = \coth(x) - 1/x. \quad (5.112)$$

The inverse of this function is called the inverse Langevin function  $\mathcal{L}^{-1}(x)$  and cannot be expressed in elementary functions. As shown above, to numerically calculate the stress for the EC model it is necessary to evaluate the inverse Langevin function. This can be done by solving for  $x$  in Equation (5.112) using a numerical equation solver, such as the Newton method. This approach, however, is computationally expensive and multiple alternative faster approximations have been developed.

One method that was developed by Arruda and Boyce [28] is to express the inverse Langevin function as a series expansion:

$$\mathcal{L}(x) \approx 3x + \frac{9}{5}x^3 + \frac{297}{175}x^5 + \frac{1539}{875}x^7. \quad (5.113)$$

The function can also be approximated using a Padé approach [30]:

$$\mathcal{L}(x) \approx \frac{x(3 - x^2)}{1 - x^2}. \quad (5.114)$$

Yet another approach was developed by Bergstrom [23] who derived the functional response into two regions. For small  $x$  values the function was represented using a curve fit based on a tan-function, and for large  $x$  values the function was represented by its asymptotic form:

$$\mathcal{L}^{-1}(x) \approx \begin{cases} 1.31446 \tan(1.58986x) + 0.91209x, & \text{if } |x| < 0.84136, \\ 1/(\text{sign}(x) - x), & \text{if } 0.84136 \leq |x| < 1. \end{cases} \quad (5.115)$$

These different approximations are compared in Figure 5.20, and a comparison between the accuracy of the approximations is given in Table 5.3.

The difference between these numerical approximations may seem more like an academic issue than an important practical concern, but the issue becomes important since different FE codes have decided to implement the inverse Langevin function in different ways. For example, Abaqus uses a series expansion, and the PolyUMod library [31] uses the more accurate Bergstrom solution approach.

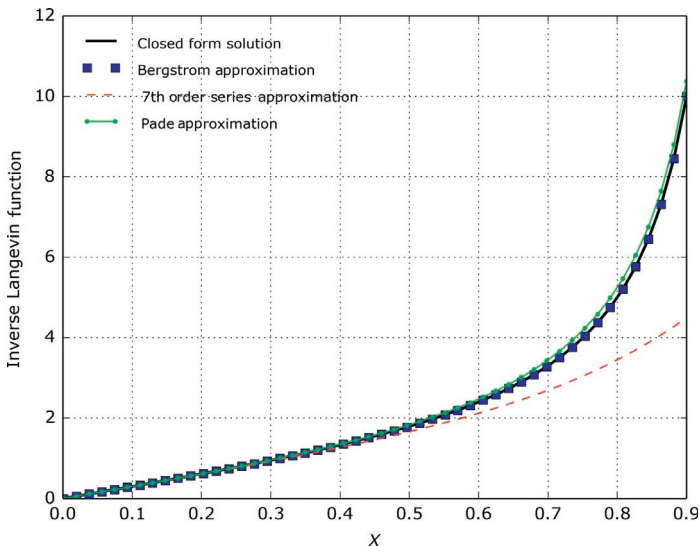


**Figure 5.20** Comparison between different approaches for calculating the inverse Langevin function.

**Table 5.3 Comparison in Errors in the Different Approaches for Calculating the Inverse Langevin Function**

Approximation Method	Relative Error in Prediction at $x = 0.7$
Bergstrom Approximation	0.06%
5-term Series Expansion	18.5%
Padé Approximation	4.3%

In other words, it is difficult to translate the parameters for the EC model from one FE solver to another. It may be necessary to recalibrate the model for each specific FE package.

### Example: Gaussian Chains.

The constitutive relationship for the EC model for the case of Gaussian chains (instead of Langevin chains) can be directly obtained by replacing the inverse Langevin function by the first term in its series expansion:

$$\mathcal{L}^{-1}(x) = 3x + \frac{9}{5}x^3 + \frac{297}{175}x^5 + \mathcal{O}(x^7),$$

giving for uniaxial tension

$$\boldsymbol{\sigma} = \frac{\mu_0}{J} \operatorname{dev}[\mathbf{b}^*] + \kappa[J - 1] \mathbf{I}, \quad (5.116)$$

which is identical to the NH model (Equation (5.74)).

### 5.3.11 Ogden Model

The Ogden model [12] is a very general hyperelasticity model with a Helmholtz free energy per reference volume that is expressed in terms of the applied principal stretches. The Helmholtz free energy for the Ogden model can be written in different ways. One common compressible representation [27] is given in Equation (5.117). In this equation the volumetric response is written in terms of  $D_i$  parameters instead of the bulk modulus terms.

$$\begin{aligned} \Psi(\lambda_1^*, \lambda_2^*, \lambda_3^*) &= \sum_{k=1}^N \frac{2\mu_k}{\alpha_k^2} ((\lambda_1^*)^{\alpha_k} + (\lambda_2^*)^{\alpha_k} + (\lambda_3^*)^{\alpha_k} - 3) \\ &\quad + \sum_{k=1}^N \frac{1}{D_k} (J - 1)^{2k}. \end{aligned} \quad (5.117)$$

This general form of the Helmholtz free energy makes the model powerful but can also complicate the selection of an appropriate set of material parameters that give stable predictions of general deformation states.

The principal stresses  $\sigma_i$ ,  $i \in [1, 2, 3]$ , for the Ogden model, are given by:

$$\begin{aligned} \sigma_i &= \frac{2}{J} \sum_{k=1}^N \frac{\mu_k}{\alpha_k} \left( (\lambda_i^*)^{\alpha_k} - \frac{1}{3} [(\lambda_1^*)^{\alpha_k} + (\lambda_2^*)^{\alpha_k} + (\lambda_3^*)^{\alpha_k}] \right) \\ &\quad + \sum_{k=1}^N \frac{2k}{D_k} (J - 1)^{2k-1}. \end{aligned} \quad (5.118)$$

The stresses from the incompressible Ogden model in uniaxial loading, planar loading, and biaxial loading are given by:

$$\sigma_{\text{uniax}} = \sum_{k=1}^N \frac{2\mu_k}{\alpha_k} \left[ \lambda^{\alpha_k} - \left( \frac{1}{\sqrt{\lambda}} \right)^{\alpha_k} \right], \quad (5.119)$$

$$\sigma_{\text{planar}} = \sum_{k=1}^N \frac{2\mu_k}{\alpha_k} \left[ \lambda^{\alpha_k} - \left( \frac{1}{\lambda} \right)^{\alpha_k} \right], \quad (5.120)$$

$$\sigma_{\text{biax}} = \sum_{k=1}^N \frac{2\mu_k}{\alpha_k} \left[ \lambda^{\alpha_k} - \left( \frac{1}{\lambda^2} \right)^{\alpha_k} \right]. \quad (5.121)$$

It is interesting to note that if  $N = 1$  and  $\alpha_2 = 1$ , then the Ogden model becomes equal to the NH model.

The accuracy of the Ogden model to predict the behavior of elastomers is demonstrated in [Figure 5.21](#) by comparison to

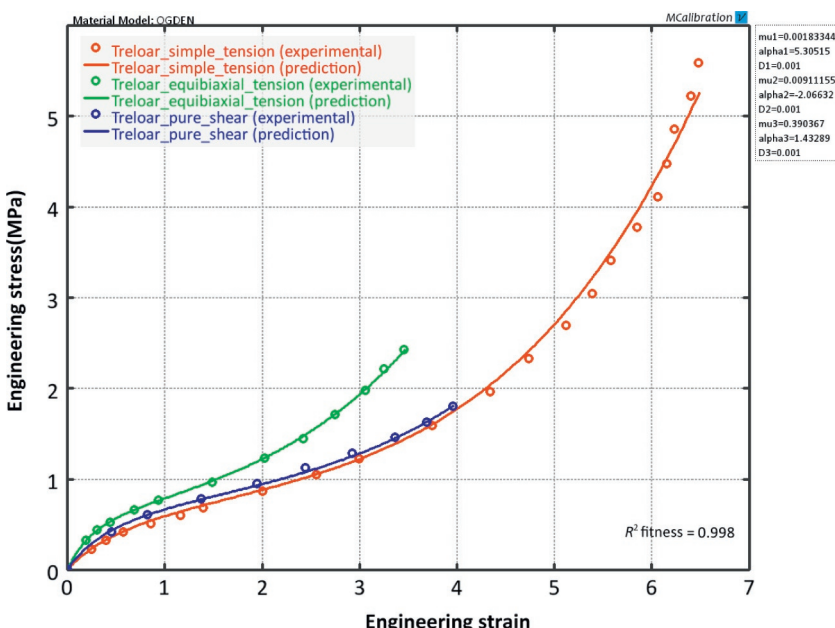


**Figure 5.21** Comparison between experimental data from Treloar [16] and predictions from a three-term Ogden model.

vulcanized natural rubber data of Treloar [16]. The figure shows that a 3-term Ogden model in this case is more accurate than the NH model and the Mooney-Rivlin model, but not as accurate as the Yeoh model or the EC model.

For incompressible uniaxial loading the Ogden material model can be implemented into Matlab using the following code:

**Matlab Code: "Ogden\_incompressible\_uniaxial.m"**

```
function [stress] = mat_Ogden(time, strain, params)
%mat_Ogden Ogden hyperelastic model
%Incompressible uniaxial loading
%This function is using true stress and strain
mu = params(1:2:end);
alpha = params(2:2:end);
lambda = exp(strain);
for i = 1 : length(lambda)
    stress(i) = sum(2*mu./alpha .* (lambda(i).^alpha - ...
        1./(lambda(i).^(alpha/2))));
end
end
```

For incompressible uniaxial loading the Ogden material model can also be implemented in Python using the following code:

**Python Code: "Ogden\_incompressible\_uniaxial.py"**

```
from pylab import *
from Polymer_Mechanics_Chap05 import *

def Ogden(trueStrain, muVec, alphaVec):
    """Ogden model. Incompressible uniaxial loading.
    Returns true stress."""
    lam = exp(trueStrain)
    res = 0
    for i in range(len(muVec)):
        mu = muVec[i]
        alpha = alphaVec[i]
        res = res + 2*mu/alpha * (lam**alpha - (1/sqrt(lam))**alpha)
    return res

trueStrain = linspace(0, 0.8, 100)
trueStress = Ogden(trueStrain, [1.0, 3.0], [3.0, 0.4])

plot(trueStrain, trueStress, 'r-')
xlabel('True Strain')
ylabel('True Stress (MPa)')
grid('on')
show()
```

The following code example shows one way to implement the Ogden material model for *compressible* uniaxial loading.

**Additional Code to “Polymer\_Mechanics\_Chap05.py”:**

```
def Ogden_3D(stretch, param):
    """Ogden model. 3D loading specified by stretches.
    param: [mu1, mu2, ..., alpha1, alpha2, kappa].
    Returns true stress."""
    J = stretch[0] * stretch[1] * stretch[2]
    lam = J**(-1/3) * stretch
    N = round((len(param)-1)/2)
    mu = param[0:N]
    alpha = param[N:2*N]
    kappa = param[-1]
    Stress = kappa*(J-1)*eye(3)
    for i in range(N):
        fac = (2/J) * mu[i] / alpha[i]
        tmp = (lam[0]**alpha[i]+lam[1]**alpha[i]+lam[2]**alpha[i])/3
        Stress[0,0] = Stress[0,0] + fac * (lam[0]**alpha[i] - tmp)
        Stress[1,1] = Stress[1,1] + fac * (lam[1]**alpha[i] - tmp)
        Stress[2,2] = Stress[2,2] + fac * (lam[2]**alpha[i] - tmp)
    return Stress
```

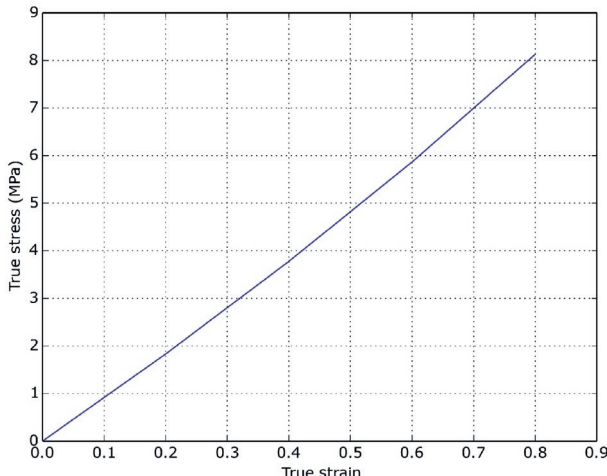
**Python Code: “Ogden\_compressible\_uniaxial.py”**

```
from pylab import *
from Polymer_Mechanics_Chap05 import *

param = [1.0, 2.0, 1.1, 0.4, 100.0]
trueStrain = linspace(0, 0.8, 5)
trueStress = uniaxial_stress(Ogden_3D, trueStrain, param)

plot(trueStrain, trueStress, 'b-')
xlabel('True Strain')
ylabel('True Stress (MPa)')
grid('on')
show()
```

**Figure Created by Python Code:**



### 5.3.12 Gent Model

The Gent model [32] is an extension of the NH model that aims at better characterizing the response of elastomer-like materials at large deformations. The Helmholtz free energy per unit reference volume for the Gent model is given by<sup>11</sup> [32]:

$$\Psi(I_1, J) = -\frac{\mu}{2} J_m \ln \left( 1 - \frac{I_1^* - 3}{J_m} \right) + \frac{\kappa}{2} [J - 1]^2. \quad (5.122)$$

This expression contains three material parameters: the shear modulus  $\mu$ , a dimensionless parameter  $J_m$  that controls the limited chain extensibility at large applied strains, and the bulk modulus  $\kappa$ . The Cauchy stress for the Gent model is given by

$$\boldsymbol{\sigma} = \frac{\mu}{J} \cdot \frac{1}{1 - \frac{I_1^* - 3}{J_m}} \operatorname{dev}[\mathbf{b}^*] + \kappa [J - 1] \mathbf{I}. \quad (5.123)$$

In the Gent model the first invariant  $I_1^*$  is always less than  $J_m + 3$ , and in the limit as  $J_m \rightarrow \infty$ , the model becomes identical to the NH model.

The Cauchy stresses for the incompressible Gent model in uniaxial loading, planar loading, and biaxial loading are given by:

$$\sigma_{\text{uniax}} = \mu \left( \lambda^2 - \frac{1}{\lambda} \right) \frac{J_m}{J_m - (\lambda^2 + 2/\lambda - 3)}, \quad (5.124)$$

$$\sigma_{\text{planar}} = \mu \left( \lambda^2 - \frac{1}{\lambda^2} \right) \frac{J_m}{J_m - (\lambda^2 + 2/\lambda - 3)}, \quad (5.125)$$

$$\sigma_{\text{biax}} = \mu \left( \lambda^2 - \frac{1}{\lambda^4} \right) \frac{J_m}{J_m - (\lambda^2 + 2/\lambda - 3)}. \quad (5.126)$$

The accuracy of the Gent model to predict the behavior of elastomers is demonstrated in Figure 5.22 by comparison to vulcanized natural rubber data of Treloar [16].

For incompressible uniaxial loading the Gent material model can be implemented into Matlab using the following code:

---

<sup>11</sup>The original version of the Gent model was incompressible. Here we have added a simple compressibility term. Other forms of the compressibility can be chosen if desired.

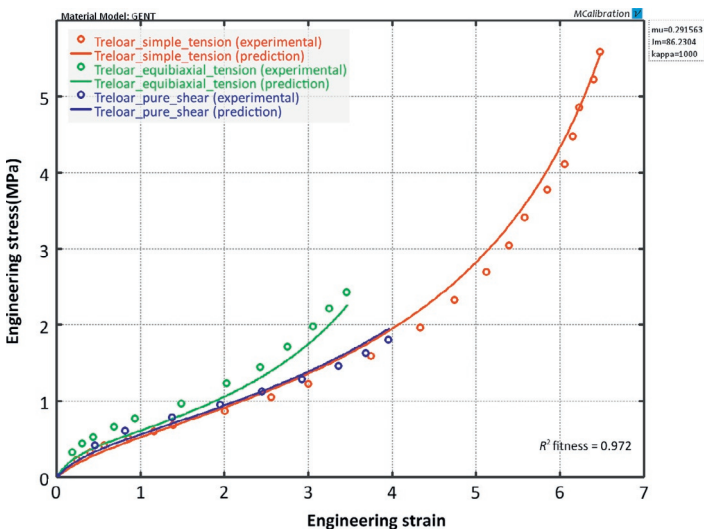


**Figure 5.22** Comparison between experimental data from Treloar [16] and predictions from the Gent model.

Matlab Code: "Gent\_incompressible\_uniaxial.m"

```
function [stress] = mat_Gent(time, strain, params)
%mat_Gent Gent hyperelastic model
%Incompressible uniaxial loading
%This function is using true stress and strain
mu = params(1);
Jm = params(2);
lambda = exp(strain);
stress = Jm*mu * (lambda.^2 - 1./lambda) ./ \
(Jm - (lambda.^2 + 2./lambda - 3));
end
```

For incompressible uniaxial loading the Gent material model can also be implemented in Python using the following code:

Python Code: "Gent\_incompressible\_uniaxial.py"

```
from pylab import *
def Gent(trueStrain, params):
    """Gent model. Incompressible uniaxial loading. Returns true stress."""
    mu = params[0]
    Jm = params[1]
    lam = exp(trueStrain)
    return mu*Jm / (Jm - lam*lam - 2/lam + 3) * (lam*lam - 1/lam)

trueStrain = linspace(0, 0.8, 100)
trueStress = Gent(trueStrain, [0.29, 86.0])

plot(trueStrain, trueStress, 'r-')
xlabel('True Strain')
ylabel('True Stress (MPa)')
grid('on')
show()
```

The following code example shows one way to implement the Gent material model for *compressible* uniaxial loading.

**Additional Code to “Polymer\_Mechanics\_Chap05.py”:**

```
def Gent_3D(stretch, param):
    """Gent. 3D loading specified by stretches.
    param: [mu, Jm, kappa]. Returns true stress."""
    L1 = stretch[0]
    L2 = stretch[1]
    L3 = stretch[2]
    F = array([[L1, 0, 0], [0, L2, 0], [0, 0, L3]])
    J = det(F)
    bstar = J**(-2.0/3.0) * dot(F, F.T)
    I1s = trace(bstar)
    devbstar = bstar - trace(bstar)/3 * eye(3)
    return param[0]/ J / (1 - (I1s-3)/param[1]) * devbstar + \
        param[2]*(J-1) * eye(3)
```

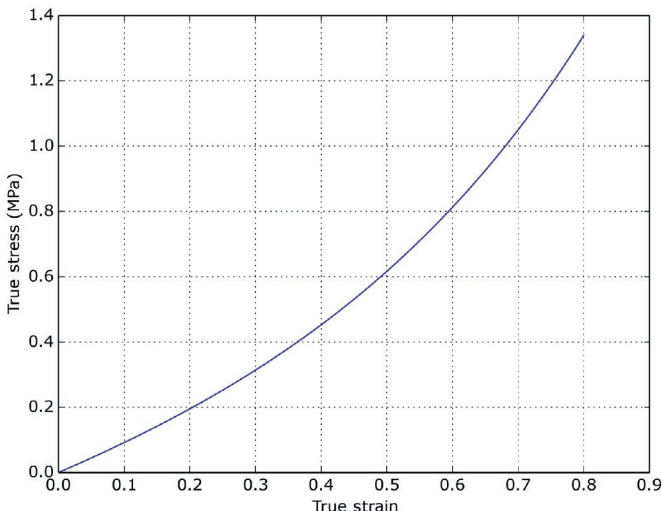
**Python Code: “Gent\_compressible\_uniaxial.py”**

```
from pylab import *
from Polymer_Mechanics_Chap05 import *

trueStrain = linspace(0, 0.8, 100)
trueStress = uniaxial_stress(Gent_3D, trueStrain, [0.29, 86.0, 100])

plot(trueStrain, trueStress, 'b-')
xlabel('True Strain')
ylabel('True Stress (MPa)')
grid('on')
show()
```

**Figure Created by Python Code:**



### 5.3.13 Horgan and Saccoandi Model

Horgan and Saccoandi have developed a model [33, 34] that is an extension of the Gent model. This model, henceforth

called the HS model, also involves three material parameters. The main difference between the Gent and the HS models is that the latter depends on both the first and second strain-invariants and thus might in some cases agree more closely with experimental data. In addition, the limiting chain parameter in the HS model is related directly to the maximum allowable stretch and so is more physically accessible than its counterpart for the Gent model that depends on a maximum value of the first invariant [33]. The Helmholtz free energy per unit reference volume of a compressible version of the HS is given by:

$$\Psi(I_1^*, I_2^*, J) = -\frac{\mu}{2} \lambda_{\max}^2 \ln \left[ \frac{\lambda_{\max}^6 - \lambda_{\max}^4 I_1^* + \lambda_{\max}^2 I_2^* - 1}{(\lambda_{\max}^2 - 1)^3} \right] + \frac{\kappa}{2} [J - 1]^2, \quad (5.127)$$

where  $\mu$  is the shear modulus,  $\lambda_{\max}$  is the limiting chain stretch, and  $\kappa$  is the bulk modulus.

The Cauchy stress for the compressible HS model is given by

$$\sigma = \frac{\mu \lambda_{\max}^4}{J} \frac{[\lambda_{\max}^2 - I_1^*] \mathbf{b}^* + (\mathbf{b}^*)^2 - \frac{1}{3} [\lambda_{\max}^2 I_1^* - 2I_2^*] \mathbf{I}}{\lambda_{\max}^6 - \lambda_{\max}^4 I_1^* + \lambda_{\max}^2 I_2^* - 1} + \kappa [J - 1] \mathbf{I}. \quad (5.128)$$

In this model  $\max(\lambda_1, \lambda_2, \lambda_3) < \lambda_{\max}$ . In the limit as  $\lambda_{\max} \rightarrow \infty$ , the model becomes identical to the NH model. The Cauchy stresses of the incompressible version of the HS model in uniaxial, planar, and equibiaxial deformations are given by the following expressions:

$$\sigma_{\text{uniax}} = \mu \lambda_{\max}^4 \frac{\lambda^3 - 1}{(\lambda \lambda_{\max}^2 - 1)(\lambda_{\max}^2 - \lambda^2)}, \quad (5.129)$$

$$\sigma_{\text{planar}} = \mu \lambda_{\max}^4 \frac{\lambda^4 - 1}{(\lambda^2 \lambda_{\max}^2 - 1)(\lambda_{\max}^2 - \lambda^2)}, \quad (5.130)$$

$$\sigma_{\text{biax}} = \mu \lambda_{\max}^4 \frac{\lambda^6 - 1}{(\lambda^4 \lambda_{\max}^2 - 1)(\lambda_{\max}^2 - \lambda^2)}. \quad (5.131)$$

The accuracy of the HS model to predict the behavior of elastomers is demonstrated in [Figure 5.23](#).

One nice feature of the HS model is that the model is unconditionally stable if  $\mu > 0$  and  $\lambda_{\max} > 1$ .

The following code example shows one way to implement the HS material model for *compressible* uniaxial loading.

Additional Code to "Polymer\_Mechanics\_Chap05.py":

```
def HS_3D(stretch, param):
    """Horgan-Saccomandi. 3D loading specified by stretches.
    param: mu, lamMax, kappa. Returns true stress."""
    L1 = stretch[0]
    L2 = stretch[1]
    L3 = stretch[2]
    F = array([[L1, 0, 0], [0, L2, 0], [0, 0, L3]])
    J = det(F)
    bstar = J*(-2.0/3.0) * dot(F, F.T)
    bstar2 = dot(bstar, bstar)
    I1s = trace(bstar)
    I2s = 0.5 * (I1s**2 - trace(bstar2))
    mu = param[0]
    lamM = param[1]
    kappa = param[2]
    fac = mu * lamM**4 / J
    den = lamM**6 - lamM**4 * I1s + lamM**2 * I2s - 1
    return fac/den * ((lamM**2 - I1s)*bstar + bstar2 - \
        (lamM**2*I1s-2*I2s)/3*eye(3)) + kappa*(J-1) * eye(3)
```

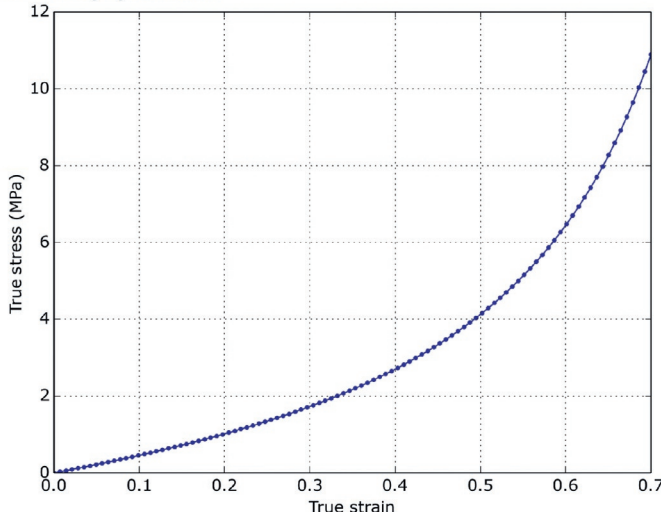
Python Code: "HS\_compressible\_uniaxial.py"

```
from pylab import *
from Polymer_Mechanics_Chap05 import *

trueStrain = linspace(0, 0.7, 100)
trueStress = uniaxial_stress(HS_3D, trueStrain, [1.0, 2.5, 1000])

plot(trueStrain, trueStress, 'b-')
xlabel('True Strain')
ylabel('True Stress (MPa)')
grid('on')
show()
```

Figure Created by Python Code:



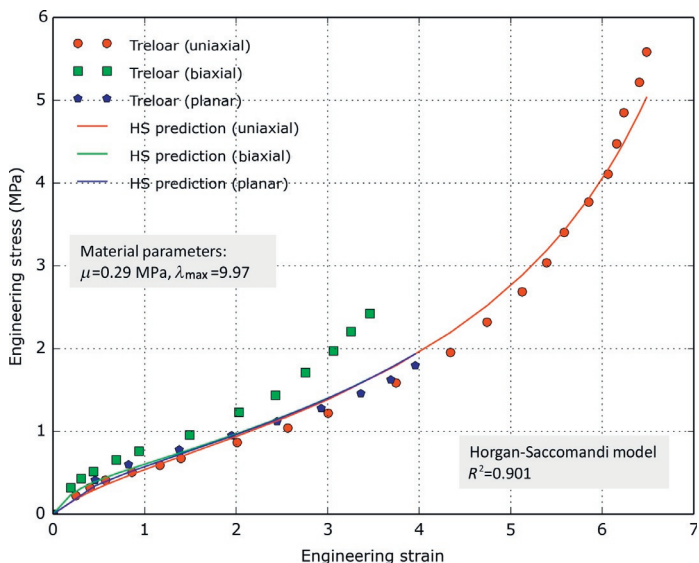


**Figure 5.23** Comparison between experimental data from Treloar [16] and predictions from the Horgan-Saccomandi model.

### 5.3.14 Knowles Model

The Knowles hyperelastic model [35] is a simple and versatile hyperelastic material model that is an extension of the NH model, but is not a built-in native feature of most FE software. The Helmholtz free energy per unit reference volume of a compressible version of the Knowles model [36] is given by:

$$\Psi(I_1^*, J) = -\frac{\mu}{2b} \left[ \left( 1 + \frac{b}{n}(I_1^* - 3) \right)^n - 1 \right] + \frac{\kappa}{2}[J - 1]^2, \quad (5.132)$$

where  $\mu$  is the shear modulus,  $n$  is a hardening parameter,  $b$  is a shape parameter, and  $\kappa$  is the bulk modulus. From this equation it is clear that if  $n = 1$  then the Knowles model becomes equal to the NH model. The Knowles model was originally developed for predicting the crack tip response of incompressible elastic solids [35], but it has recently also been used to study the degradation response of poly-L-lactic acid (PLLA) materials [37].

The Cauchy stress for the compressible Knowles model is:

$$\sigma = \frac{\mu}{J} \left( 1 + \frac{b}{n}(I_1^* - 3) \right)^{n-1} \text{dev}[\mathbf{b}^*] + \kappa(J-1)\mathbf{I}. \quad (5.133)$$

The Cauchy stresses for the incompressible Knowles model in uniaxial loading, planar loading, and biaxial loading are given by:

$$\sigma_{\text{uniax}} = \mu \left( 1 + \frac{b}{n}(\lambda^2 + 2/\lambda - 3) \right)^{n-1} \cdot \left[ \lambda^2 - \frac{1}{\lambda} \right], \quad (5.134)$$

$$\sigma_{\text{planar}} = \mu \left( 1 + \frac{b}{n}(\lambda^2 + 1/\lambda^2 - 2) \right)^{n-1} \cdot \left[ \lambda^2 - \frac{1}{\lambda^2} \right], \quad (5.135)$$

$$\sigma_{\text{biax}} = \mu \left( 1 + \frac{b}{n}(2\lambda^2 + 1/\lambda^4 - 3) \right)^{n-1} \cdot \left[ \lambda^2 - \frac{1}{\lambda^4} \right]. \quad (5.136)$$

The accuracy of the Knowles model to predict the behavior of elastomers is demonstrated in [Figure 5.24](#).

The following code example shows one way to implement the Knowles material model for *compressible* uniaxial loading.

**Additional Code to "Polymer\_Mechanics\_Chap05.py":**

```
def Knowles_3D(stretch, param):
    """Knowles' 3D loading specified by stretches.
    param: mu, n, b, kappa. Returns true stress."""
    L1 = stretch[0]
    L2 = stretch[1]
    L3 = stretch[2]
    F = array([[L1, 0, 0], [0, L2, 0], [0, 0, L3]])
    J = det(F)
    bstar = J**(-2.0/3.0) * dot(F, F.T)
    I1s = trace(bstar)
    devbstar = bstar - trace(bstar)/3 * eye(3)
    return param[0]/J * (1+param[2]/param[1]*(I1s-3))**param[1]-1 \
        * devbstar + param[3]*(J-1) * eye(3)
```

**Python Code: "Knowles\_compressible\_uniaxial.py"**

```
from pylab import *
from Polymer_Mechanics_Chap05 import *

trueStrain = linspace(0, 0.7, 100)
trueStress = uniaxial_stress(Knowles_3D, trueStrain, \
    [1.0, 0.5, 0.5, 100])

plot(trueStrain, trueStress, 'b-')
xlabel('True Strain')
ylabel('True Stress (MPa)')
grid('on')
show()
```

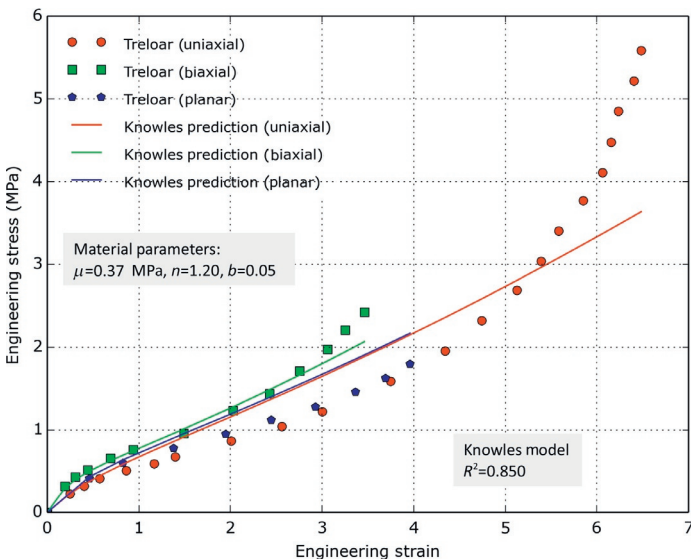


**Figure 5.24** Comparison between experimental data from Treloar [16] and predictions from the incompressible Knowles material model.

The influence of the parameters  $n$  and  $b$  on the predicted stress-strain response of the Knowles model are shown in Figures 5.25 and 5.26. These figures show that the  $n$  and  $b$  parameters strongly influence the predicted stress-strain response.

### 5.3.15 Response Function Hyperelasticity

All hyperelastic models that have been discussed so far in this chapter have been based on specific equations for the Helmholtz free energy per unit reference volume, where the energy equation contains material constants that specify the behavior of a specific material. Another approach is to specify the free energy directly based on experimental data in uniaxial loading [27, 38]. One advantage of this approach is that there are no adjustable material parameters that need to be found, instead the energy function, and as a result the stress calculations, are directly obtained from the provided experimental uniaxial test data.

Most major FE programs have a hyperelastic model of this type, for example, in Abaqus the model is called the

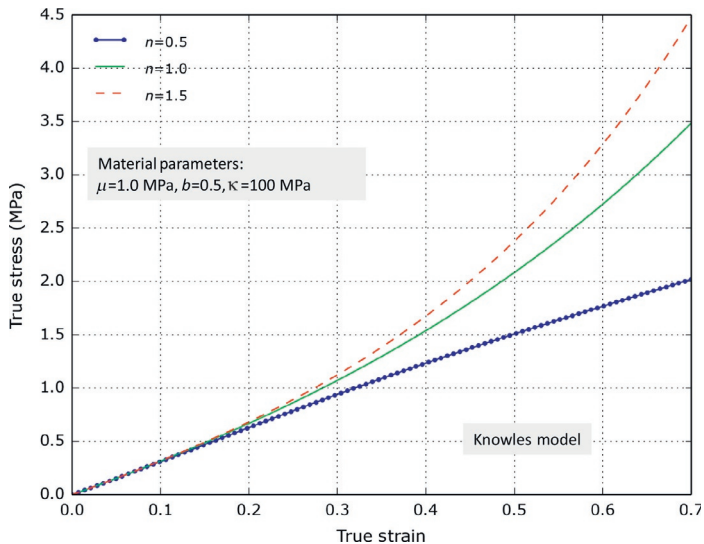


**Figure 5.25** Influence of parameter  $n$  on the stress-strain response for the Knowles model.

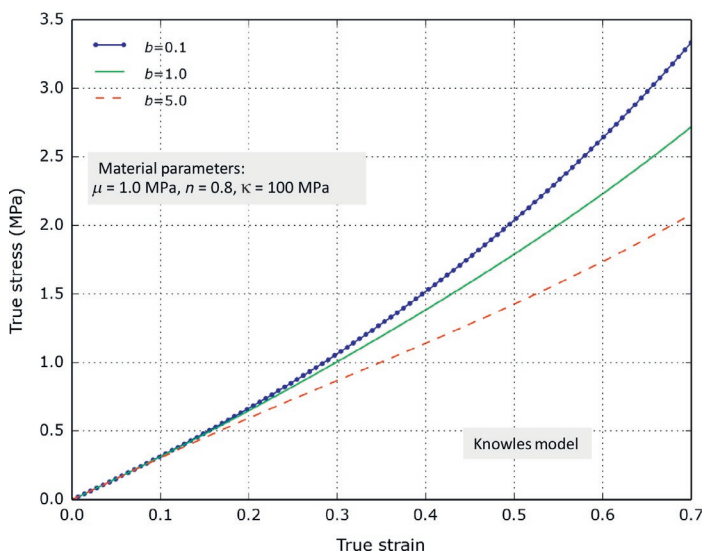


**Figure 5.26** Influence of parameter  $b$  on the stress-strain response for the Knowles model.

Marlow model. This type of model implementation is based on the assumption that the free energy is only dependent on the first invariant  $I_1$ , which is then determined from the experimental data. A consequence of this is that although this model can predict the uniaxial tension data with almost perfect accuracy, the predictions of other loading modes are typically far from perfect.

The accuracy of the response function model to predict the behavior of elastomers is demonstrated in [Figure 5.27](#) by comparison to vulcanized natural rubber data of Treloar [16].

This figure shows that as expected the model predictions agrees with the provided uniaxial tension data, but the predicted stress in biaxial loading is too low. This is typical since accurately predicting the response in biaxial loading often requires an energy function that includes  $I_2$  dependence, which is not the case for response function hyperelasticity.

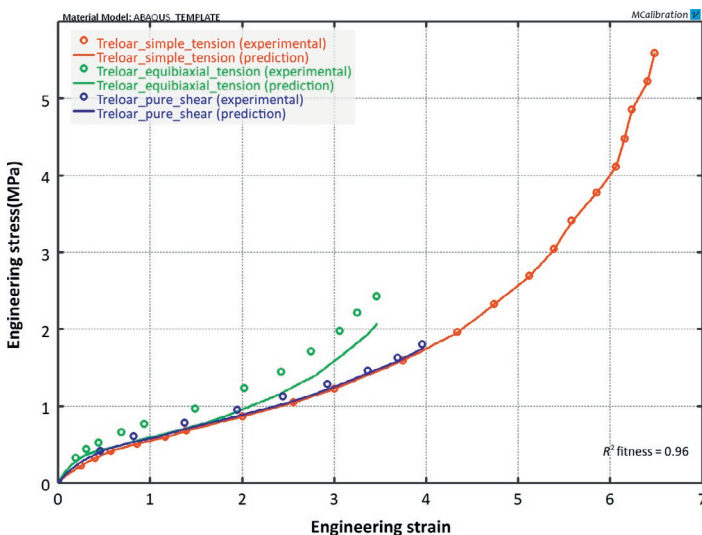


**Figure 5.27** Comparison between experimental data from Treloar [16] and predictions from the response function model as implemented by Abaqus.

### 5.3.16 Extended Tube Model

The Extended Tube (ET) model is a statistical mechanics and micromechanics inspired material model that considers the network constraints from surrounding molecular chains and the limited chain extensibility in the derivation of the Helmholtz free energy expression [39].

The energy function consists of three parts: energy from the cross-linking of the network ( $\Psi_c$ ), energy from confining tube constrains ( $\Psi_e$ ), and energy from volumetric deformations ( $\Psi_v$ ):  $\Psi = \Psi_c + \Psi_e + \Psi_v$ , where:

$$\Psi_c = \frac{G_c}{2} \left[ \frac{(1 - \delta^2)(I_1^* - 3)}{1 - \delta^2(I_1^* - 3)} + \ln(1 - \delta^2(I_1^* - 3)) \right], \quad (5.137)$$

$$\Psi_e = \frac{2G_e}{\beta^2} \sum_{i=1}^3 ((\lambda_i^*)^{-\beta} - 1), \quad (5.138)$$

$$\Psi_v = \kappa(J - 1)^2. \quad (5.139)$$

In this equation  $[G_e, G_c, \delta, \beta, \kappa]$  are material parameters,  $I_1^* = J^{-2/3} \text{tr}[\mathbf{C}]$ ,  $\lambda_i^* = J^{-1/3} \lambda_i$ , and  $J = \det[\mathbf{F}]$ . The energy term  $\Psi_c$  is a simple  $I_1^*$  based expression,  $\Psi_e$  is a one-term Ogden model with a negative exponent, and  $\Psi_v$  gives the volumetric response.

The Cauchy stress for the ET model can be calculated from Equations (5.42) and (5.55) giving:

$$\begin{aligned} \sigma &= \frac{G_c}{J} \left\{ \frac{1 + (1 + (I_1^*)^2 - 4I_1^*) \delta^2 + (5I_1^* - (I_1^*)^2 - 6) \delta^4}{[1 - (I_1^* - 3)\delta^2]^2} \right\} \text{dev}[\mathbf{b}^*] \\ &\quad - \frac{2G_e}{J\beta} \sum_{i=1}^3 \left[ (\lambda_i^*)^{-\beta} - \frac{1}{3} ((\lambda_1^*)^{-\beta} + (\lambda_2^*)^{-\beta} + (\lambda_3^*)^{-\beta}) \right] \hat{\mathbf{n}}_i \otimes \hat{\mathbf{n}}_i + \kappa(J - 1) \mathbf{I}. \end{aligned} \quad (5.140)$$

The Cauchy stresses for the incompressible ET model in uniaxial loading, planar loading, and biaxial loading are given by:

$$\sigma_{\text{uniax}} = G_c \left\{ \frac{1 + (1 + (I_1^*)^2 - 4I_1^*) \delta^2 + (5I_1^* - (I_1^*)^2 - 6) \delta^4}{[1 - (I_1^* - 3)\delta^2]^2} \right\} \cdot \left( \lambda^2 - \frac{1}{\lambda} \right) - \frac{2G_e}{\beta} \left[ \lambda^{-\beta} - \left( \frac{1}{\sqrt{\lambda}} \right)^{-\beta} \right], \quad (5.141)$$

$$\sigma_{\text{planar}} = G_c \left\{ \frac{1 + (1 + (I_1^*)^2 - 4I_1^*) \delta^2 + (5I_1^* - (I_1^*)^2 - 6) \delta^4}{[1 - (I_1^* - 3)\delta^2]^2} \right\} \cdot \left( \lambda^2 - \frac{1}{\lambda^2} \right) - \frac{2G_e}{\beta} \left[ \lambda^{-\beta} - \left( \frac{1}{\lambda} \right)^{-\beta} \right], \quad (5.142)$$

$$\sigma_{\text{biaxial}} = G_c \left\{ \frac{1 + (1 + (I_1^*)^2 - 4I_1^*) \delta^2 + (5I_1^* - (I_1^*)^2 - 6) \delta^4}{[1 - (I_1^* - 3)\delta^2]^2} \right\} \cdot \left( \lambda^2 - \frac{1}{\lambda^4} \right) - \frac{2G_e}{\beta} \left[ \lambda^{-\beta} - \left( \frac{1}{\lambda^2} \right)^{-\beta} \right]. \quad (5.143)$$

The accuracy of the ET model to predict the behavior of elastomers is demonstrated in Figure 5.28 by comparison to vulcanized natural rubber data of Treloar [16]. The figure shows that ET model in this case is more accurate than any of the other hyperelastic models that have been examined so far.

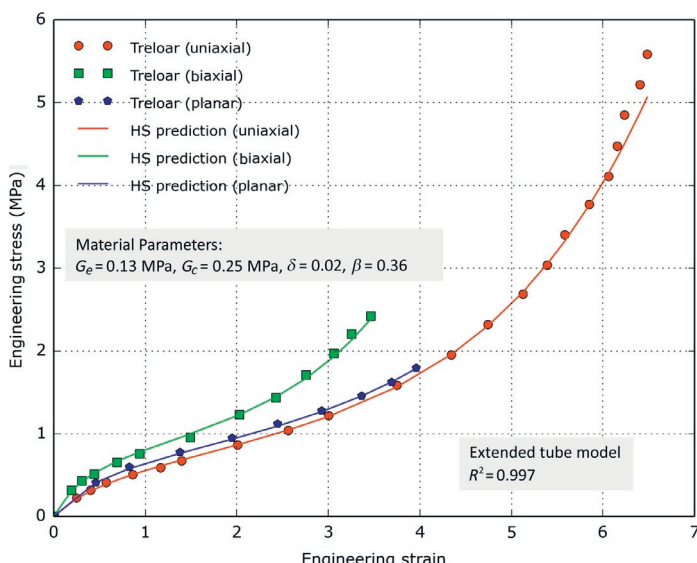


**Figure 5.28** Comparison between experimental data from Treloar [16] and predictions from the Extended Tube model.

The following code example shows one way to implement the ET model for *compressible* uniaxial loading.

Additional Code to "Polymer\_Mechanics\_Chap05.py":

```
def ETube_3D(stretch, param):
    """Extended Tube model. 3D loading specified by stretches.
       Param: Ge, Gc, delta, beta, kappa"""
    Ge = param[0]
    Gc = param[1]
    delta = param[2]
    beta = param[3]
    kappa = param[4]
    L1 = stretch[0]
    L2 = stretch[1]
    L3 = stretch[2]
    F = array([[L1,0,0], [0,L2,0], [0,0,L3]])
    J = det(F)
    bstar = J**(-2.0/3.0) * dot(F, F.T)
    devbstar = bstar - trace(bstar)/3 * eye(3)
    lam = J**(-1/3) * array(stretch)
    I1s = trace(bstar)
    fac1 = (1+(I1s**2-4*I1s)*delta**2 + \
            (*I1s-I1s**2-6)*delta**4) / \
            (1 - (I1s-3)*delta**2)**2
    stressC = Gc/J * fac1 * devbstar
    fac2 = -2*Ge/(J**beta)
    tmp = (lam[0]**(-beta) + lam[1]**(-beta) + lam[2]**(-beta)) / 3
    stressE = zeros((3,3))
    stressE[0,0] = fac2 * (lam[0]**(-beta) - tmp)
    stressE[1,1] = fac2 * (lam[1]**(-beta) - tmp)
    stressE[2,2] = fac2 * (lam[2]**(-beta) - tmp)
    stressV = kappa*(J-1)*eye(3)
    return stressC + stressE + stressV
```

Python Code: "ETube\_compressible\_uniaxial.py"

```
from pylab import *
from Polymer_Mechanics_Chap05 import *

#      [Ge,  Gc,  delta,  beta,  kappa]
param = [1.0, 1.0, 0.1, 0.1, 1000.0]

trueStrain = linspace(0, 0.7, 100)
trueStress = uniaxial_stress(ETube_3D, trueStrain, param)

plot(trueStrain, trueStress, 'b-')
xlabel('True Strain')
ylabel('True Stress (MPa)')
grid('on')
show()
```

The influence of the parameters  $\delta$  and  $\beta$  on the predicted stress-strain response of the ET model are shown in Figures 5.29 and 5.30. These figures show that the  $\delta$  parameter strongly influence the predicted stress-strain response.

### 5.3.17 BAM Model

The BAM model is a new hyperelastic material model that I developed specifically for this book. The purpose of this exercise is to show one way to improve the accuracy of the Arruda-Boyce EC model. The EC model, which was discussed in Section 5.3.10, is an excellent model for predicting the multiaxial response of

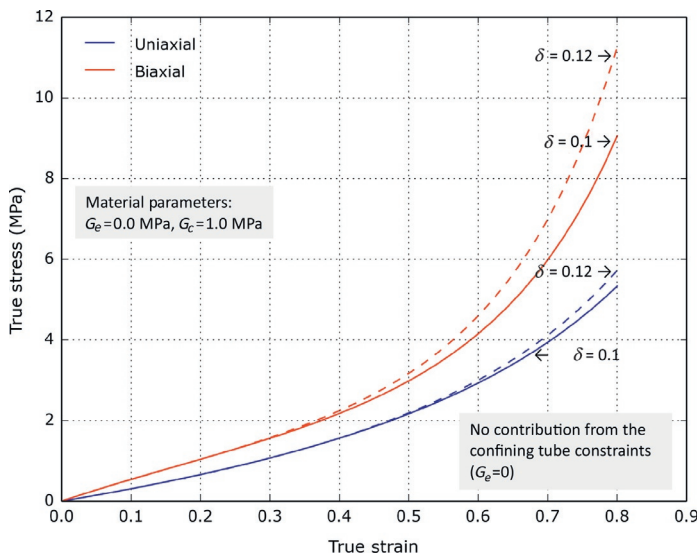


**Figure 5.29** Influence of parameter  $\delta$  on the stress-strain response for the Extended Tube model.

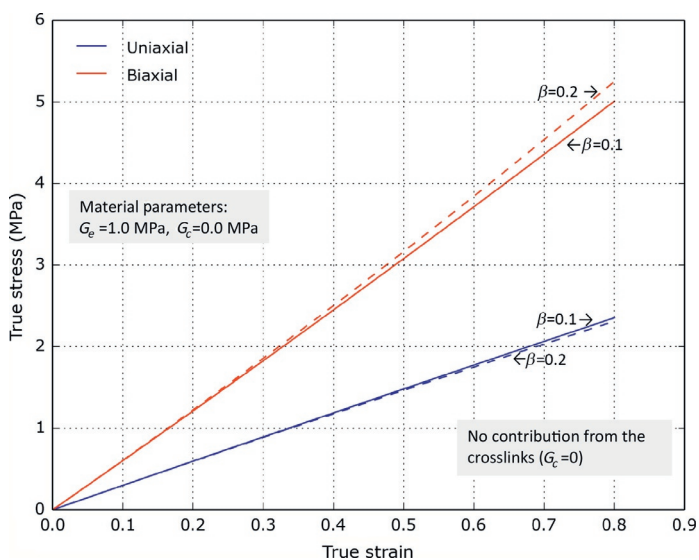


**Figure 5.30** Influence of parameter  $\beta$  on the stress-strain response for the Extended Tube model.

elastomers. One of the main limitations of the EC model is that it underpredicts the stress in biaxial loading since its Helmholtz free energy does not depend on the second invariant. One way to remedy that limitation is to add another contribution to the Helmholtz free energy that specifically helps in biaxial loading. One simple way to do that is to follow the approach developed by the extended tube model, where a first order Ogden model with a negative  $\alpha$  coefficient is used. As was shown in [Figure 5.30](#), a first order Ogden model with a negative  $\alpha$  parameter is exactly what is needed.

The new hyperelastic model can then be obtained by quickly combining the energy functions from the EC model ([Equation \(5.100\)](#)) and the first-order Ogden model ([Equation \(5.117\)](#)), and bam, a new material model is obtained. We will simply call this new model the BAM model.

The predictions from the BAM model when compared to the classical data from Treloar is shown in [Figure 5.31](#). The figure shows that the BAM model is as accurate as the 3-term Ogden model and the extended tube model, which were the most accurate hyperelastic models that have been examined so far for the Treloar data.

## 5.4 Summary of Predictive Capabilities of Isotropic Hyperelastic Models

A summary of the predictive capabilities of the various hyperelastic models discussed in the previous sections are summarized in [Table 5.4](#). In this table the accuracy of the different material models is quantified by the coefficient of determination ( $R^2$ ). The table shows that the Ogden (3-term) model and the ET model are the most accurate. Another way to evaluate the usefulness of the different models is to compare the accuracy of the model predictions to the number of required material parameters, see [Figure 5.32](#). In this case one can argue that a material model with fewer material parameters should be easier to calibrate and therefore should be preferable to a material model with many material parameters. The figure shows that response function

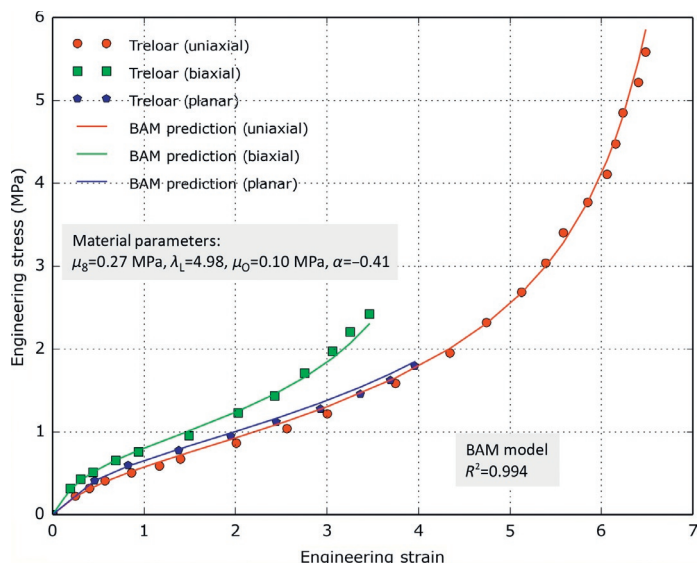


**Figure 5.31** Comparison between experimental data from Treloar [16] and predictions from the BAM model.

**Table 5.4 Comparison Between the Predictive Capabilities of Different Isotropic Hyperelasticity Models**

Hyperelastic Model	$R^2$ -Prediction
Neo-Hookean	0.794
Mooney-Rivlin	0.843
Yeoh	0.980
Eight-Chain	0.973
Ogden (2-term)	0.977
Ogden (3-term)	0.998
Gent	0.972
Horgan-Saccomandi	0.901
Knowles	0.850
Response Function	0.960
Extended Tube	0.997
BAM	0.994

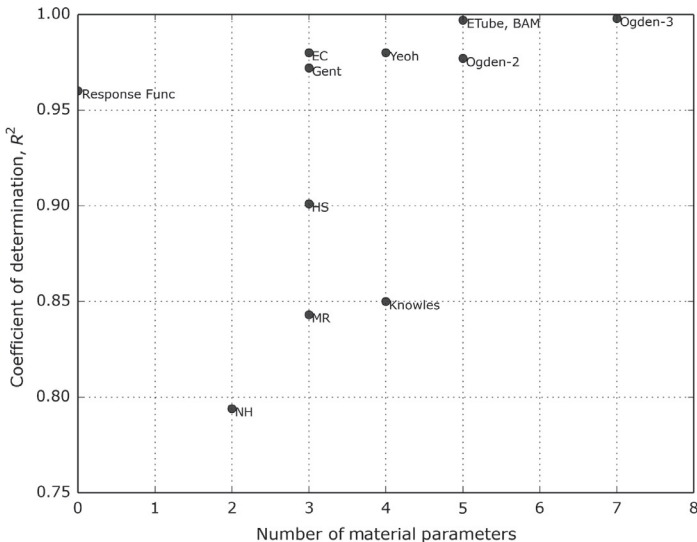


**Figure 5.32** Comparison between the different hyperelastic material model with respect to the accuracy and the number of material parameters.

model, the Arruda-Boyce EC model, the Yeoh model, and the ET model are the most promising from this condition.

Another way to evaluate the usefulness of the different candidate hyperelastic models is to compare the predictive accuracy to the minimum number of experimental tests that are required for the model calibration, see [Figure 5.33](#). In this case, material models that are only based on the first invariant  $I_1$  are assigned a minimum number of experimental tests of one (1), and material model that are based on both the first and second invariants ( $I_1$  and  $I_2$ ) or the principal stretches are assigned a minimum number of experimental tests of two (2). This figure suggests that the Yeoh model, the Arruda-Boyce EC model, the Gent model, and the response function models are most useful since they only require one experimental test.

It is important to note that the results presented in this table were obtained for the classical Treloar [16] data for natural rubber in uniaxial tension, planar tension, and equibiaxial tension. It is possible that the relative ranking of the different models would be different if a different experimental data set was used in the study.

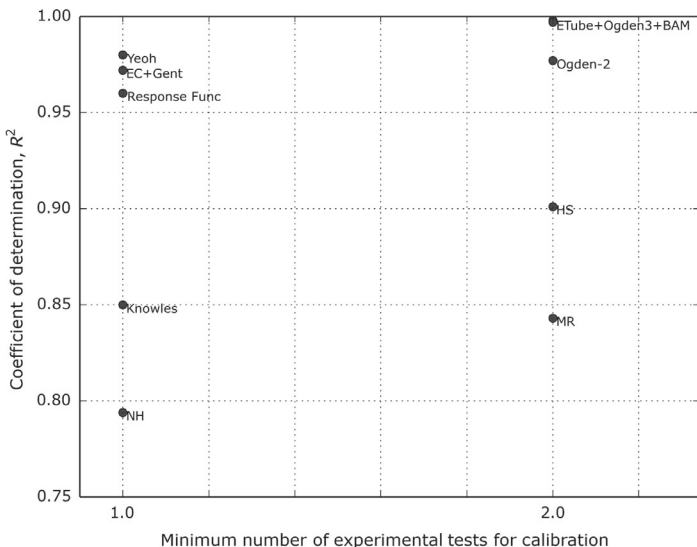


**Figure 5.33** Comparison between the different hyperelastic material model with respect to the accuracy and the number of required experimental tests.

The results presented here are included for illustrational purposes, and are not intended to provide a comprehensive review and evaluation of the various hyperelasticity models. Furthermore, as will be discussed in more detail in [Section 5.8.1](#), the mechanical behavior of elastomers in real-world applications is significantly more advanced than the simple data represented in Treloar's data set.

For example, the response of elastomers in real loading cases is characterized not only by a non-linear hyperelastic response but also non-linear viscoelasticity and damage (Mullins effect) during cyclic loading. These additional non-linearities of the material response will make the reported  $R^2$ -values in [Table 5.4](#) higher than the actual values in many real-world applications. Hence, if a hyperelastic model is chosen to represent the behavior of an elastomer-like material, then there will likely be inaccuracies in the model predictions due to the lack of viscoelastic effect that are more significant than the difference between some of the more advanced hyperelastic model discussed above.

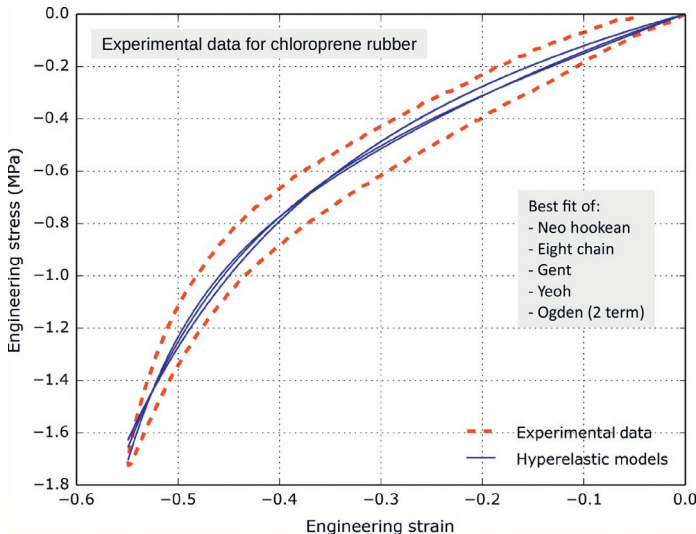


**Figure 5.34** Comparison between experimental data for a chloroprene rubber and calibrated material models for the Neo-Hookean, eight-chain, Yeoh, Gent, and Ogden models.

This behavior is depicted in Figure 5.34. This figure shows that all the different hyperelastic material models provide similar predictions, and that all are unable to predict the loading-unloading response of the material.

## 5.5 Anisotropic Hyperelasticity

Anisotropic hyperelasticity is a relatively new topic that enables many new exciting predictive capabilities, both for biopolymers and other intrinsically anisotropic polymers. Anisotropic hyperelasticity is also a building block for more advanced viscoplastic models as will be discussed in following chapters.

The theory for anisotropic hyperelasticity is covered nicely in the textbook by Holzapfel [13]. If the applied strains are small then it is often sufficient to use an anisotropic elastic model. For larger strains there are two commonly used approaches: strain based [40] and invariant based [41] hyperelasticity. This section summarizes the theory of some commonly used anisotropic hyperelastic models.

### 5.5.1 Generalized Fung Model

The energy function for the generalized Fung anisotropic hyperelastic model [40] can be written:

$$\Psi(c, b_{ijkl}, \kappa) = \frac{c}{2} [\exp(Q) - 1] + \frac{\kappa}{2}(J - 1)^2, \quad (5.144)$$

where  $c$ ,  $b_{ijkl}$ , and  $\kappa$  are material parameters. Note that the parameter  $b_{ijkl}$  is a dimensionless symmetric fourth order tensor of material parameters. The scalar variable  $Q$  is given by:

$$Q = \mathbf{E}^* : \mathbf{b} : \mathbf{E}^* = E_{ijkl}^* b_{ijkl} E_{kl}^*, \quad (5.145)$$

where  $\mathbf{E}^* = [\mathbf{C}^* - \mathbf{I}]/2$  is the Green-Lagrange strain defined in Equation (4.119),  $\mathbf{C}^* = J^{-2/3} \mathbf{F}^\top \mathbf{F}$  is the right Cauchy-Green tensor, and  $J = \det[\mathbf{F}]$ . For a case with cylindrical coordinates, this equation can be written:

$$\begin{aligned} Q = & b_1 E_{\theta\theta}^2 + b_2 E_{zz}^2 + b_3 E_{rr}^2 + 2b_4 E_{\theta\theta} E_{zz} + 2b_5 E_{zz} E_{rr} \\ & + 2b_6 E_{rr} E_{\theta\theta} + b_7 E_{\theta z}^2 + b_8 E_{rz}^2 + b_9 E_{r\theta}^2. \end{aligned} \quad (5.146)$$

The Cauchy stress for the Generalized Fung model is:

$$\boldsymbol{\sigma} = \frac{1}{J} \mathbf{F} \frac{\partial \Psi}{\partial \mathbf{E}^*} \mathbf{F}^\top + \frac{\partial \Psi}{\partial J} \mathbf{I}. \quad (5.147)$$

The Fung anisotropic hyperelastic model is commonly used to model both engineered and native soft tissues used in medical device and surgical applications [42].

### 5.5.2 Invariant Based Anisotropy

Another common approach to incorporate anisotropic effects into a hyperelastic model is to introduce two additional invariants:  $I_4, I_5$  defined by:

$$I_4 = (\mathbf{F} \mathbf{a}_0) \cdot (\mathbf{F} \mathbf{a}_0) = \mathbf{a}_0 \cdot \mathbf{C} \mathbf{a}_0 = \lambda_F^2, \quad (5.148)$$

$$I_5 = \mathbf{a}_0 \cdot \mathbf{C}^2 \mathbf{a}_0, \quad (5.149)$$

where  $I_4$  is the stretch in the provided fiber direction  $\mathbf{a}_0$ , and  $\mathbf{C}$  is the right Cauchy-Green tensor. The total Helmholtz free energy is then given by:

$$\Psi = \Psi_1(I_1^*, I_2^*, J) + \Psi_2(I_4, I_5). \quad (5.150)$$

The Cauchy stress for this type of invariant-based anisotropic hyperelasticity is given by [13]:

$$\begin{aligned} \sigma = & \frac{2}{J} \left[ \frac{\partial \Psi}{\partial I_1^*} + \frac{\partial \Psi}{\partial I_2^*} I_1^* \right] \mathbf{b}^* - \frac{2}{J} \frac{\partial \Psi}{\partial I_2^*} (\mathbf{b}^*)^2 + \left[ \frac{\partial \Psi}{\partial J} - \frac{2I_1^*}{3J} \frac{\partial \Psi}{\partial I_1^*} - \frac{4I_2^*}{3J} \frac{\partial \Psi}{\partial I_2^*} \right] \mathbf{I} \\ & + \frac{2}{J} I_4 \frac{\partial \Psi}{\partial I_4} \mathbf{a} \otimes \mathbf{a} + \frac{2}{J} I_4 \frac{\partial \Psi}{\partial I_5} (\mathbf{a} \otimes \mathbf{b} \mathbf{a} + \mathbf{a} \mathbf{b} \otimes \mathbf{a}). \end{aligned} \quad (5.151)$$

In this equation  $\mathbf{a} = |\mathbf{F}\mathbf{a}_0|$  is the direction of fiber  $\mathbf{a}_0$  in the deformed state.

### Example: Simple Anisotropic Hyperelastic Model.

As an example, consider a NH material with a single family of fibers with the energy function:

$$\Psi_2(I_4) = A \left( I_4^2 - 2I_4 \right) = A \left( \lambda_f^4 - \lambda_f^2 \right). \quad (5.152)$$

For this simple material model the Cauchy stress is given by:

$$\sigma = \frac{\mu}{J} \text{dev}[\mathbf{b}^*] + \kappa(J-1) + \frac{4A}{J} (\lambda_f^2 - 1) (\mathbf{F}\mathbf{a}_0) \otimes (\mathbf{F}\mathbf{a}_0), \quad (5.153)$$

which is plotted in [Figure 5.35](#). This figure shows that adding a single family of fibers can cause a significantly anisotropic response.

### 5.5.3 Bischoff Anisotropic Eight-Chain Model

The Arruda-Boyce EC model (see [Section 5.3.10](#)) is a useful micromechanism inspired model that has been shown to accurately capture the equilibrium response of many isotropic elastomers [43]. Bischoff developed an extension of this model that also works for anisotropic materials [44]. The basic idea of this model framework is that the eight chain unit cell is stretched also its initial unloaded configuration.

The stress predicted by the Bischoff anisotropic EC model is given by:

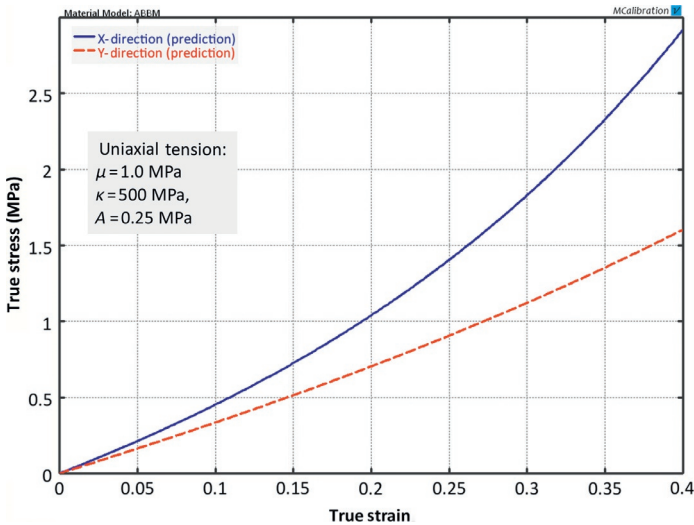


**Figure 5.35** Stress-strain prediction in uniaxial tension of a simple anisotropic Neo-Hookean material model.

$$\sigma = \sum_{f=1}^4 \frac{3\mu}{4J\lambda_f} \frac{\mathcal{L}^{-1}(\lambda_f/\lambda_L)}{\mathcal{L}^{-1}(1/\lambda_L)} (\hat{\mathbf{F}}_f) \otimes (\hat{\mathbf{F}}_f) - \sum_{i=1}^3 3\mu \left( \frac{a_i}{\lambda_L} \right)^2 \mathbf{e}_i \otimes \mathbf{e}_i + \kappa(J-1)\mathbf{I}, \quad (5.154)$$

where  $\mu$  is the shear modulus,  $\kappa$  is the bulk modulus,  $[a_1, a_2, a_3]$  are the side lengths of the unit cell in the undeformed configuration,  $J = \det[\mathbf{F}]$ ,  $\mathcal{L}^{-1}(\cdot)$  is the inverse Langevin function, and where:

$$\lambda_L = \sqrt{a_1^2 + a_2^2 + a_3^2}, \quad (5.155)$$

$$\hat{\mathbf{a}}_1 = [+a_1\mathbf{e}_1 + a_2\mathbf{e}_2 + a_3\mathbf{e}_3]/\lambda_L, \quad (5.156)$$

$$\hat{\mathbf{a}}_2 = [+a_1\mathbf{e}_1 + a_2\mathbf{e}_2 - a_3\mathbf{e}_3]/\lambda_L, \quad (5.157)$$

$$\hat{\mathbf{a}}_3 = [+a_1\mathbf{e}_1 - a_2\mathbf{e}_2 + a_3\mathbf{e}_3]/\lambda_L, \quad (5.158)$$

$$\hat{\mathbf{a}}_4 = [+a_1\mathbf{e}_1 - a_2\mathbf{e}_2 - a_3\mathbf{e}_3]/\lambda_L, \quad (5.159)$$

$$\lambda_f = ||\hat{\mathbf{F}}_f|| = (\hat{\mathbf{a}}_f \cdot \hat{\mathbf{C}}_f \cdot \hat{\mathbf{a}}_f)^{1/2}. \quad (5.160)$$

One example of the Bischoff anisotropic EC model is given in Figure 5.36. This figure shows experimental data for rabbit skin [45] and the stress-strain response from the Bischoff model.

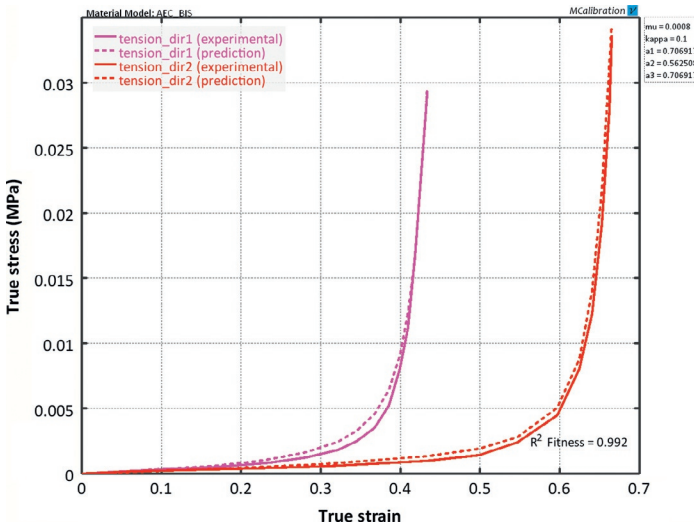


**Figure 5.36** Comparison between experimental data for rabbit skin and predictions from the Bischoff model.

#### 5.5.4 Bergstrom Anisotropic Eight-Chain Model

Another way to create an anisotropic hyperelastic model is to start with the isotropic Arruda-Boyce EC model and then add one or more families of fibers. Using this approach the Cauchy stress can be written [31]:

$$\boldsymbol{\sigma} = \boldsymbol{\sigma}_{8chain}(\mathbf{F}) + \left[ A\lambda_f^2 + B\lambda_f - (A + B) \right] \mathbf{a}_f \otimes \mathbf{a}_f, \quad (5.161)$$

where  $\boldsymbol{\sigma}(\mathbf{F})$ ,  $\mathbf{a}_f = \mathbf{F}\mathbf{a}_0$ ,  $\lambda_f = \|\mathbf{a}_f\|$ . One example of the stress-strain response from this model is shown in Figure 5.35.

#### 5.5.5 Holzapfel-Gasser-Ogden Model

The Holzapfel-Gasser-Ogden (HGO) model [46, 47] is an anisotropic hyperelastic material model that was developed to predict the response of arterial tissue. The HGO model is a versatile model that is a built-in feature in Abaqus.

The model consists of a NH model representation of the matrix response, and up to three different families of fibers. The initial fiber directions are given by the three vectors  $[a_{1x}, a_{1y}, a_{1z}]$ ,

$[a_{2x}, a_{2y}, a_{2z}]$ , and  $[a_{3x}, a_{3y}, a_{3z}]$ . The three fiber directions do not have to be orthogonal.

The strain energy function for the model is given by the following function:

$$\Psi = \frac{\mu}{2}(I_1^* - 3) + \frac{k_1}{2k_2} \sum_{i=1}^3 \left[ e^{k_2 \langle E_i \rangle^2} - 1 \right] + \frac{\kappa}{2}(J - 1)^2, \quad (5.162)$$

where:

- the energy term  $E_i$  is:  $E_i = d(I_1^* - 3) + (1 - 3d)[I_{4i}^* - 1]$ ,
- $d$  is the dispersion,
- $I_{4i}^* = (\mathbf{F}^* \mathbf{a}_i) \cdot (\mathbf{F}^* \mathbf{a}_i)$ ,
- $\langle x \rangle = (x + |x|)/2$  is the ramp function,

If  $d = 0$  then the fibers are perfectly aligned, and if  $d = 1/3$  the fibers are randomly oriented giving an isotropic response.

One example of the stress-strain predictions from the HGO model is presented in Figure 5.37. The prediction is based on the following parameters:  $\mu = 2 \text{ MPa}$ ,  $\kappa = 20 \text{ MPa}$ ,  $k_1 = 1 \text{ MPa}$ ,  $k_2 = 1$ ,  $d = 0.1$  or  $0.2$ , and one family of fibers oriented at  $[1,0,0]$ .

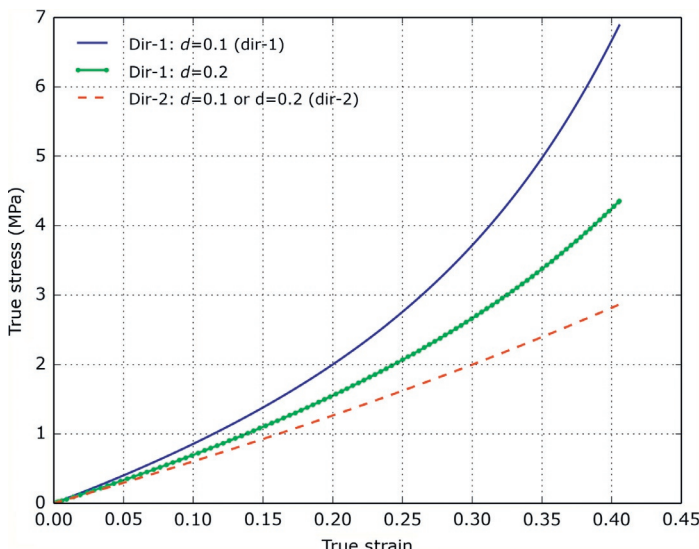


**Figure 5.37** Predicted stress-strain response from the Holzapfel-Gasser-Ogden model.

The figure shows that the stress in the 2-direction is independent of the value of  $d$ . This, of course, is caused by the lack of fibers in the 2-direction. The stress in the 1-direction, however, is dependent on the value of  $d$ .

## 5.6 Hyperelastic Foam Models

The mechanical behavior of compressible polymers, such as foams, can also be approximated using a hyperelastic representation. Since foams can undergo large volume change it is often beneficial to use slightly different forms of the Helmholtz free energy and to use a different set of experimental data when calibrating the hyperelastic model. One of the problems with the common hyperelastic models is illustrated in Figures 5.38 and 5.39.

These figures show the uniaxial tension and compression response of the NH model with a stress function:

$$\boldsymbol{\sigma} = \frac{\mu}{J} \operatorname{dev} [\mathbf{b}^*] + \kappa(J - 1)\mathbf{I}, \quad (5.74\text{-repeat})$$

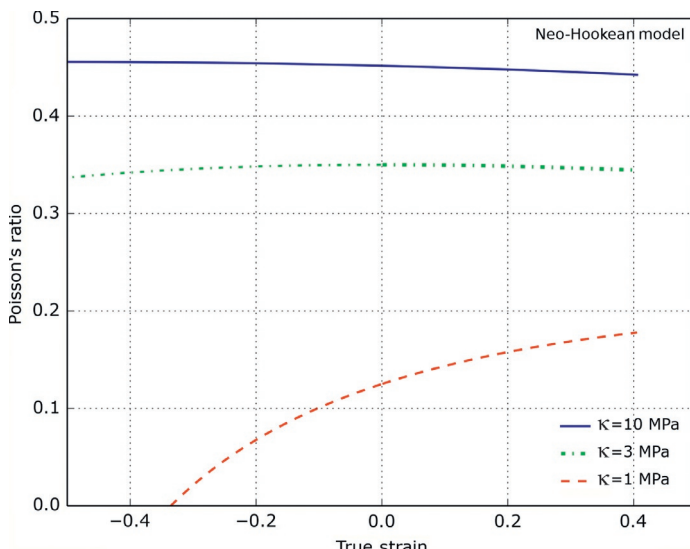


**Figure 5.38** Predicted Poisson's ratio for the (standard) Neo-Hookean model with a shear modulus of 1 MPa.

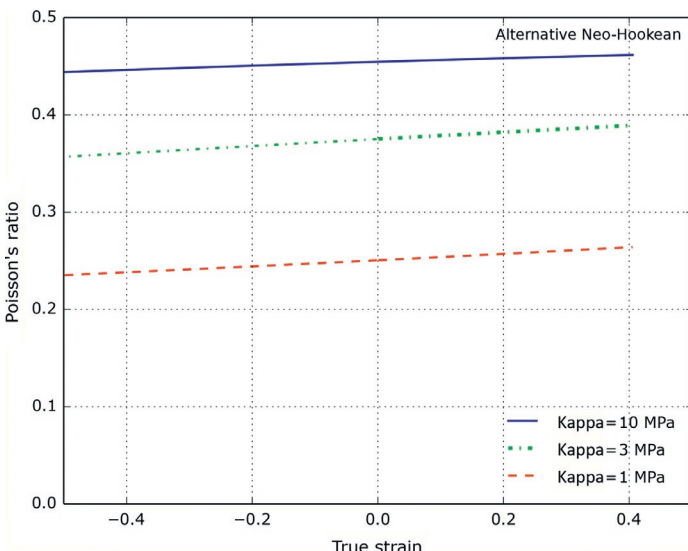


**Figure 5.39** Predicted Poisson's ratio for the alternative Neo-Hookean model where the energy function is not divided into distortional and volumetric parts. The shear modulus is 1 MPa.

and the response of the alternative NH model:

$$\boldsymbol{\sigma} = \frac{\mu}{J} (\mathbf{b} - \mathbf{I}) + \kappa (J - 1) \mathbf{I}. \quad (5.85\text{-repeat})$$

As shown in the figures, the predicted Poisson's ratio from the standard NH material model becomes odd in compressive loading when the bulk modulus is similar in magnitude to the shear modulus. This is a problem when modeling foams since foams often have a small bulk modulus and a corresponding small (but positive) Poisson's ratio.

The alternative NH model avoids this problem by using the total deformation gradient (not only the deviatoric part) in combination with the volumetric response.

Different hyperelastic models have been proposed in order to better predict the non-linear elastic response of foam materials. The following subsections summarize some of the more commonly used the hyperelastic models for foams: the Blatz-Ko model, and the hyperfoam model.

### 5.6.1 Blatz-Ko Foam Model

A commonly used material model for polymer foams is the Blatz-Ko hyperelastic model [48]. This model was developed for porous materials with a known shear modulus, Poisson's ratio, and volume fraction of voids, and is called the *generalized Blatz-Ko* model.

A more commonly used version of the model is obtained by setting the void volume fraction parameter  $f = 0$ , and by setting the Poisson's ratio  $\nu = 0.25$ , giving a model that is typically just called the *Blatz-Ko* model [48, 49], and that has the following strain energy density:

$$\Psi = \frac{\mu}{2} \left( \frac{I_2}{I_3} + 2I_3^{1/2} - 5 \right). \quad (5.163)$$

As shown, this material model only has one material parameter: the shear modulus  $\mu$ .

The Cauchy stress for the Blatz-Ko model is given by:

$$\sigma = \frac{\mu}{J^3} \left[ I_1 \mathbf{b} - \mathbf{b}^2 - (I_2 - J^3) \mathbf{I} \right]. \quad (5.164)$$

The following code example shows one way to implement the Blatz-Ko model for compressible uniaxial loading.

```
Additional Code to "Polymer_Mechanics_Chap05.py":
```

```
def blatzko_3D(stretch, param):
    """Blatz-Ko. 3D loading specified by stretches.
    param[0]=mu"""
    F = array([[stretch[0], 0, 0], [0, stretch[1], 0], [0, 0, stretch[2]]])
    J = det(F)
    b = dot(F, F.T)
    b2 = dot(b, b)
    I1 = trace(b)
    I2 = 0.5 * (I1**2 - trace(b2))
    return param[0]/J**3.0 * (I1*b - b2 - (I2-J**3.0) * eye(3))
```

```
Python Code: "BlatzKo_compressible_uniaxial.py"
```

```
from pylab import *
from Polymer_Mechanics_Chap05 import *

param = [1.0] # mu
trueStrain = linspace(0, 0.4, 100)

trueStress = uniaxial_stress(blatzko_3D, trueStrain, param)
plot(trueStrain, trueStress, 'b-', label='Uniaxial')
xlabel('True Strain')
ylabel('True Stress (MPa)')
grid('on')
show()
```

The predicted stress-strain response in uniaxial, biaxial, and plane strain loading is shown in [Figure 5.40](#).

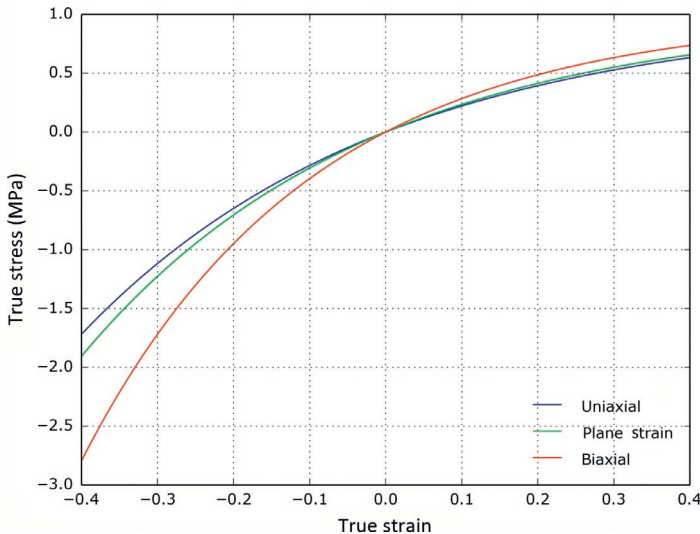


**Figure 5.40** Predicted stress-strain response for the Blatz-Ko model in different loading modes.

### 5.6.2 Hyperfoam Model

One interesting hyperelastic model for polymer foam materials is the hyperfoam model [27, 50]. In this model the Helmholtz free energy is given the following expression:

$$\Psi = \sum_{k=1}^N \frac{2\mu_k}{\alpha_k^2} \left[ (\lambda_1)^{\alpha_k} + (\lambda_2)^{\alpha_k} + (\lambda_3)^{\alpha_k} - 3 + \frac{1}{\beta_k} (J^{-\alpha_k \beta_k} - 1) \right], \quad (5.165)$$

where  $[\mu_i, \alpha_i, \beta_i]$ ,  $i = 1 \dots k$  are material parameters,  $J = \det[\mathbf{F}]$ , and  $\lambda_i$  are the principal stretches. As shown in this equation, the hyperfoam model is very similar to the Ogden model, except that it has a slightly different energy function for the volumetric response. The volumetric response was here selected in order to get a constant Poisson's ratio in uniaxial loading.

The Cauchy stress can be derived from Equation (5.52) giving:

$$\boldsymbol{\sigma} = \sum_{k=1}^N \frac{2\mu_k}{J\alpha_k} \left\{ \sum_{i=1}^3 [(\lambda_i)^{\alpha_k} - J^{-\alpha_k \beta_k}] \hat{\mathbf{n}}_i \otimes \hat{\mathbf{n}}_i \right\}. \quad (5.166)$$

The following code example shows one way to implement the hyperfoam model for uniaxial loading.

Additional Code to "Polymer\_Mechanics\_Chap05.py":

```
def hyperfoam_3D(stretch, param):
    """Hyperfoam model. 3D loading specified by stretches.
    param: [mu1, ..., alpha1, ..., beta1, ...].
    Returns true stress."""
    J = stretch[0] * stretch[1] * stretch[2]
    lam = array(stretch)
    N = int(round(len(param)/3.0))
    mu = param[0:N]
    alpha = param[N:2*N]
    beta = param[2*N:3*N]
    Stress = zeros((3,3))
    for k in range(N):
        fac = 2.0 * mu[k] / (J * alpha[k])
        Stress[0,0] = Stress[0,0] + fac*(lam[0]**alpha[k] - \
            J**(-alpha[k]*beta[k]))
        Stress[1,1] = Stress[1,1] + fac*(lam[1]**alpha[k] - \
            J**(-alpha[k]*beta[k]))
        Stress[2,2] = Stress[2,2] + fac*(lam[2]**alpha[k] - \
            J**(-alpha[k]*beta[k]))
    return Stress
```

Python Code: "hyperfoam\_compressible\_uniaxial.py"

```
from pylab import *
from Polymer_Mechanics_Chap05 import *

# k=1: mu1, alpha1, beta1
param = [1.0, 2.0, 0.2]
trueStrain = linspace(0, 0.4, 40)

trueStress = uniaxial_stress(hyperfoam_3D, trueStrain, param)
plot(trueStrain, trueStress, 'b-', label='uniax')
xlabel('True Strain')
ylabel('True Stress (MPa)')
grid('on')
show()
```

Exemplar stress-strain predictions for the hyperfoam model are shown in [Figure 5.41](#). This figure shows the model predictions when  $\mu = 1 \text{ MPa}$ ,  $\alpha = 2$ , and  $\beta = 0.2$ . The model predictions of the compressive response are in qualitative agreement with many polymer foams, but the tensile predictions are not and may require additional terms in the energy function for proper predictions of an actual material.

It can be shown [\[27\]](#), that the Poisson's ratio for the hyperfoam model is equal to

$$\nu = \frac{\beta}{1 + 2\beta}, \quad (5.167)$$

if all  $\beta_i$  terms are equal. This is a convenient feature of the hyperfoam model that allows all  $\beta$  parameters to be determined from the average Poisson's ratio that can be experimentally measured. The  $\mu_i$  parameters specify the stiffness of the model response, and the  $\alpha_i$  parameters specify the shape of the predicted stress-strain response at larger strains.

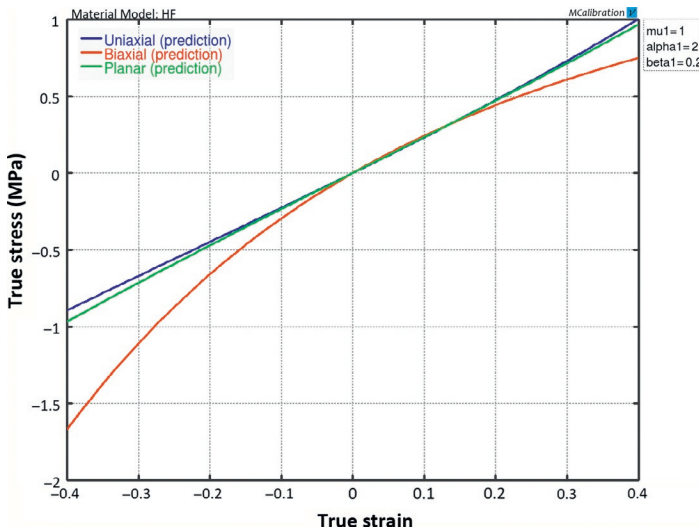


**Figure 5.41** Predicted stress-strain response for the hyperfoam model with  $\mu = 1 \text{ MPa}$ ,  $\alpha = 2$ ,  $\beta = 0.2$ .

## 5.7 Mullins Effect Models

The mechanical stress response of elastomers often undergoes significant softening during the first few load cycles, and after those load cycles the material response becomes repeatable [1, 51–54]. This material softening can be considered a damage accumulation in the material. One example showing experimental data with the Mullins effect is shown in Figure 2.3.

There is still some uncertainty about the details of the mechanisms causing the Mullins effect [54], but the following experimental observations are typically seen in all rubbers that exhibit Mullins damage:

- The extent of Mullins softening increases with filler particle concentration.
- The stress at a given strain is higher in the first load cycle, than in any of the following load cycles.
- The amount of damage that is introduced in the material is the highest in the first load cycle, and then goes down with subsequent load cycles. After about

3 to 5 load cycles (to a given strain level) the material response becomes repeatable.

- The amount of damage is dependent on the max applied strain. If a material is conditioned at, say, 30% strain, then the material will start to exhibit more damage accumulation again if the applied is increased to a larger strain level at a later time.
- The Mullins damage is not permanent, the material often slowly recovers with time. The rate of recovery depends on the temperature.

The most common physical interpretation of the Mullins effect is that it is caused by molecular chain breakage at interface of filler particles, or breakdown of filler particle clusters. Note that the Mullins effect only occurs in elastomers, and elastomer-like materials. Thermoplastic materials can also soften due to damage accumulation, but that behavior is not called the Mullins effect.

The following sections summarize two models for predicting the Mullins effect in a FE simulation.

### 5.7.1 Ogden-Roxburgh Mullins Effect Model

In an attempt to account for the Mullins effect, Ogden and Roxburgh [2] proposed a general extension of hyperelasticity in which the Helmholtz free energy per unit reference volume,  $\Psi$ , is taken to be a function not only of the applied deformation state but also on an internal state variable  $\eta$  that tracks the damage evolution in the material. This model is available as a built-in feature of most FE programs. For incompressible loading, the following form is used:

$$\Psi(\lambda_1, \lambda_2, \lambda_3, \eta) = \eta \Psi(\lambda_1, \lambda_2, \lambda_3), \quad (5.168)$$

where  $\lambda_i$  are the principal stretches. In the Ogden-Roxburgh (OR) model the damage variable  $\eta$  is taken to evolve with the applied deviatoric strain energy as follows<sup>12</sup>:

---

<sup>12</sup>This is an extension of the OR model that is used by the FE program Abaqus. The original OR model had  $\beta = 0$ .

$$\eta = 1 - \frac{1}{r} \operatorname{erf} \left( \frac{\Psi_{\text{dev}}^{\max} - \Psi_{\text{dev}}}{m + \beta \Psi_{\text{dev}}^{\max}} \right), \quad (5.169)$$

where  $r$ ,  $\beta$ , and  $m$  are material parameters,  $\operatorname{erf}(x)$  is the error function,  $\Psi_{\text{dev}}$  is the current deviatoric strain energy density, and  $\Psi_{\text{dev}}^{\max}$  is a state variable for the evolving maximum deviatoric strain energy density for the material point in its deformation history. This simple damage model can be applied to any isotropic hyperelasticity model.

An example of the behavior of the OR model is shown in Figure 5.42. This figure plots stress-strain predictions for a uniaxial tension, and a biaxial load case. In both cases the material was stretched to 30% engineering strain, then unloaded to 10% engineering strain, and then finally loaded to 50% engineering strain. The material model was a NH hyperelastic model with Ogden-Roxburgh Mullins damage parameters:  $\mu = 1 \text{ MPa}$ ,  $r = 2$ ,  $m = 0.2$ , and  $\beta = 0.02$ . The figure shows that the predicted stress-strain behavior is the same during unloading and during the following loading. The model also predicts that all Mullins

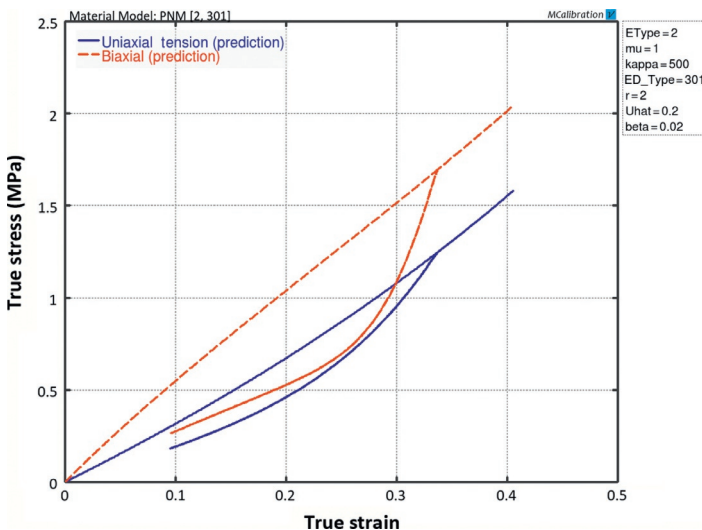


**Figure 5.42** Predicted stress-strain response for a Neo-Hookean hyperelastic model with Mullins damage.

damage occurs in the first load cycle, which is not what is typically not experimentally seen.

### 5.7.2 Qi-Boyce Mullins Effect Model

A different approach to account for the Mullins effect has been developed by Qi and Boyce [3]. In their model the virgin material is considered to consist of two phases: soft domains and hard domains. The Qi-Boyce (QB) model introduces a state variable to track the transformation of hard domains to soft domains with the applied deformation history. For incompressible loading, the following form is used:

$$\Psi = (1 - v_f) \cdot \Psi(I_1). \quad (5.170)$$

The volume fraction of hard domains,  $v_f$ , evolves with the applied chain stretch as follows:

$$v_f = v_{ff} - v_{fi} \exp \left[ \frac{-A \cdot (\Lambda_{\text{chain}}^{\max} - 1)}{\lambda_{\text{lock}} - \Lambda_{\text{chain}}^{\max}} \right], \quad (5.171)$$

where  $v_{ff}$  is the final volume fraction of hard domains,  $v_{fi}$  is the initial volume fraction of hard domains, and  $\Lambda_{\text{chain}}^{\max}$  is the maximum chain stretch the during the deformation history of the material point.

The QB Mullins effect model takes four material parameters:  $v_{ff}$ ,  $v_{fi}$ ,  $A$ ,  $\lambda_{\text{lock}}$ . The QB-model can be applied to any hyperelastic model, but is currently not available in most FE programs.

## 5.8 Use of Hyperelasticity in Polymer Modeling

Hyperelasticity is commonly used to predict the behavior of different elastomer-like materials, primarily due to its ease of use and its availability in virtually all FE programs. Hyperelasticity is also a building block of linear viscoelasticity, and more advanced viscoplasticity models.

Not all hyperelastic models that are presented in this chapter are directly available in all major commercial FE codes. Due

to the simplicity of the hyperelasticity theory, however, it is typically straightforward to implement and use some of the more modern and accurate hyperelastic models if desired. Most FE codes have the capability to augment the built-in material models with user-defined material models, typically coded as external Fortran subroutines that are linked into the FE software during simulations. The use of external user subroutines can provide significant advantages in many circumstances. This topic is discussed in more detail in Chapter 10.

### 5.8.1 Experimental Testing

There are no strict requirements for what experimental tests should be performed in order to accurately calibrate a hyperelasticity model. The minimum set of recommended types of experimental tests is dependent on the hyperelastic model, and performing more experimental testing is always better than running too few experiments.

There is also some confusion in the general literature about the recommended types of experimental tests. Specifically, it is often said that two or preferably three different loading modes are necessary for accurate calibration of a hyperelastic model. It is never bad to perform experiments in three different loading modes (e.g. uniaxial, biaxial, shear), but for many hyperelastic models it is sufficient to use uniaxial loading only.

A general guideline is that hyperelastic models with no dependence on  $I_2$  typically require less experimental tests. The reason for this is that the free energy function in this case becomes a scalar function of only one variable ( $I_1$ ), and that functional dependence can be fully obtained from one experiment. Examples of models that fall into this category are: the NH model, the Gent model, the Arruda-Boyce EC model, and the Yeoh model.

Models with a free energy equation that depend on the principal stretches (such as the Ogden model), and models with  $I_2$  dependence require testing in two or more loading modes such as uniaxial tension, planar tension, simple shear, or biaxial tension.

Note that to verify the accuracy of a hyperelastic model it is sometimes recommended to perform experimental tests in

multiple loading modes. Also note that it is very important to run the experiments to larger strains than what is expected in the real application in order to get a hyperelastic model that is reliable for all strain levels of interest.

### 5.8.2 Drucker Stability

One of the few complications of hyperelasticity models is that some calibrated models are not always stable, i.e. increasing the strain can lead to a reduction in stress (see, for example, [Figure 5.16](#)). One way to examine if a model with a given set of material parameters is stable is to check its Drucker's stability defined by:

$$\Delta(J\sigma) : \Delta(\mathbf{E}_{\ln}) \geq 0, \quad (5.172)$$

where  $J = \det[\mathbf{F}]$ ,  $\sigma$  is the Cauchy stress,  $\mathbf{E}_{\ln}$  is the logarithmic strain.

The challenge is that some hyperelastic models can be Drucker's stable to large strains in tension, but unstable at small strains in a different loading mode such as shear. To ensure that a model is Drucker's stable for all strains of interest it is necessary to examine all loading model or to use a model with known stability behavior.

One common practical approach to examine the Drucker's stability of a hyperelastic material is to examine the stability of the model response in a set of common loading modes, such as uniaxial, biaxial, and simple shear, and apply pre-defined large strain histories. If the model passes these tests then the model may be considered relatively safe to use. This numerical approach to check the Drucker's stability is used by many of the major FE codes.

Also note that not all polymers are Drucker's stable. For example, many thermoplastics soften after yield causing the stress to go down as the strain increases. This is not a problem, it simply means that the Drucker's stability check for those materials is not relevant.

### 5.8.3 Determination of Material Parameters

To specify the complete hyperelastic material model it is necessary to first select a constitutive model, and then find the material parameters by *calibrating* the material parameters to experimental data. Since one or more experimental stress-strain curves are used for the calibration, the mathematical procedure of determining the material parameters involves solving an over constrained set of equations. Hence, it is typically not possible to get a perfect fit of the model to the experimental data. Furthermore, all experimental testing include experimental errors, so the material calibration in practice is limited to finding a set of material parameters that gives a good as possible prediction of the experimental data.

The material calibration, even for a simple material model such as linear elasticity, include selecting a fitness function that express how close a model prediction is to the experimental data, and then using an optimization algorithm to calibrate the material model. Practical aspects of material model calibration are discussed in Chapter 9.

### 5.8.4 Limitations of Hyperelasticity

Hyperelastic models can be quite useful for predicting the behavior of rubber-like polymers. The main strengths of hyperelastic models include:

- Easy to use and calibrate.
- Accessible in major commercial FE codes.
- Computationally efficient.

The main limitations of hyperelasticity models include the following:

- Mainly applicable to rubber-like materials.<sup>13</sup>
- Only accurate for monotonic loading.

---

<sup>13</sup>Hyperelasticity can also be used to predict the small strain behavior of amorphous behavior of amorphous and semicrystalline glassy polymers. For these materials, however, the hyperelasticity models do not provide any significant advantages over linear elasticity.

- Do not capture rate-effects or viscoelasticity.
- Do not capture hysteresis during cyclic loading.

A simple way to extend the hyperelastic models presented in this chapter is to augment the hyperelastic model with linear viscoelasticity as presented in the next chapter.

## 5.9 Hyperelastic Code Examples

The behavior of a number of the hyperelastic models presented in this chapter were examined using short Python functions. In each example, it was listed “Additional Code to Polymer\_Mechanics\_Chap05.py.” This section summarizes the file `Polymer_Mechanics_Chap05.py`. This file can also be downloaded from this web address: [http://PolymerMechanics.com/Polymer\\_Mechanics\\_Chap05.zip](http://PolymerMechanics.com/Polymer_Mechanics_Chap05.zip).

```
from pylab import *
import scipy.optimize

def uniaxial_stress(model, trueStrainVec, params):
    """Compressible uniaxial loading. Returns true stress."""
    stress = zeros(len(trueStrainVec))
    for i in range(len(trueStrainVec)):
        lam1 = exp(trueStrainVec[i])
        calcS22Abs = lambda x: abs(model([lam1,x,x],params)[1,1])
        # search for transverse stretch that gives S22=0
        lam2 = scipy.optimize.fmin(calcS22Abs, x0=1/sqrt(lam1),
                                   xtol=1e-9, ftol=1e-9, disp=False)
        stress[i] = model([lam1, lam2, lam2], params)[0,0]
    return stress

def biaxial_stress(model, trueStrainVec, params):
    """Compressible biaxial loading. Returns true stress."""
    stress = zeros(len(trueStrainVec))
    for i in range(len(trueStrainVec)):
        lam1 = exp(trueStrainVec[i])
        calcS33Abs = lambda x: abs(model([lam1, lam1, x],params)[2,2])
        # search for transverse stretch that gives S33=0
        lam3 = scipy.optimize.fmin(calcS33Abs, x0=1/sqrt(lam1),
                                   xtol=1e-9, ftol=1e-9, disp=False)
        stress[i] = model([lam1, lam1, lam3], params)[0,0]
    return stress

def planar_stress(model, trueStrainVec, params):
    """Compressible planar loading. Returns true stress."""
    stress = zeros(len(trueStrainVec))
    for i in range(len(trueStrainVec)):
        lam1 = exp(trueStrainVec[i])
        calcS33Abs = lambda x: abs(model([lam1, 1.0, x],params)[2,2])
        # search for transverse stretch that gives S33=0
```

```

lam3 = scipy.optimize.fmin(calcS33Abs, x0=1/sqrt(lam1),
                           xtol=1e-9, ftol=1e-9, disp=False)
stress[i] = model([lam1,1.0, lam3], params)[0,0]
return stress

def NH_3D(stretch, param):
    """Neo-Hookean. 3D loading specified by stretches.
    param[0]=mu, param[1]=kappa"""
    F = array([[stretch[0],0,0], [0,stretch[1],0], [0,0,stretch[2]]])
    J = det(F)
    Fstar = J**(-1/3) * F
    bstar = dot(Fstar, Fstar.T)
    dev_bstar = bstar - trace(bstar)/3 * eye(3)
    return param[0]/J * dev_bstar + param[1]*(J-1) * eye(3)

def MR_3D(stretch, param):
    """Mooney-Rivlin. 3D loading specified by stretches.
    param: [C10, C01, kappa]"""
    L1 = stretch[0]
    L2 = stretch[1]
    L3 = stretch[2]
    F = array([[L1,0,0], [0,L2,0], [0,0,L3]])
    J = det(F)
    bstar = J**(-2.0/3.0) * dot(F, F.T)
    bstar2 = dot(bstar, bstar)
    I1s = trace(bstar)
    I2s = 0.5 * (I1s**2 - trace(bstar2))
    C10 = param[0]
    C01 = param[1]
    kappa = param[2]
    return 2/J*(C10+C01*I1s)*bstar - 2*C01/J*bstar2 + \
           (kappa*(J-1) - 2*I1s*C10/(3*J) - 4*I2s*C01/(3*J))*eye(3)

def Yeoh_3D(stretch, param):
    """Yeoh. 3D loading specified by stretches.
    param: [C10, C20, C30, kappa]. Returns true stress."""
    L1 = stretch[0]
    L2 = stretch[1]
    L3 = stretch[2]
    F = array([[L1,0,0], [0,L2,0], [0,0,L3]])
    J = det(F)
    bstar = J**(-2.0/3.0) * dot(F, F.T)
    devbstar = bstar - trace(bstar)/3 * eye(3)
    I1s = trace(bstar)
    return 2/J*(param[0] + 2*param[1]*(I1s-3) + 3*param[2]*(I1s-3)**2) \
           *devbstar + param[3]*(J-1) * eye(3)

def invLangevin(x):
    EPS = spacing(1)
    if type(x) == float or type(x) == float64: # x is a scalar
        if x >= 1-EPS: x = 1 - EPS
        if x <= -1+EPS: x = -1 + EPS
        if abs(x) < 0.839:
            return 1.31435 * tan(1.59*x) + 0.911249*x
        return 1.0 / (sign(x) - x)
    # x is an array
    x[x >= 1-EPS] = 1 - EPS
    x[x <= -1+EPS] = -1 + EPS
    res = zeros(size(x))
    index = abs(x) < 0.839
    res[index] = 1.31435 * tan(1.59*x[index]) + 0.911249*x[index]
    index = abs(x) >= 0.839
    res[index] = 1.0 / (sign(x[index]) - x[index])
    return res

```

```

def EC_3D(stretch, param):
    """Eight-Chain. 3D loading specified by stretches.
    param: [mu, lambdaL, kappa]. Returns true stress."""
    L1 = stretch[0]
    L2 = stretch[1]
    L3 = stretch[2]
    F = array([[L1,0,0], [0,L2,0], [0,0,L3]])
    J = det(F)
    bstar = J**(-2.0/3.0) * dot(F, F.T)
    lamChain = sqrt(trace(bstar)/3)
    devbstar = bstar - trace(bstar)/3 * eye(3)
    return param[0]/(J*lamChain) * invLangevin(lamChain/param[1]) / \
           invLangevin(1/param[1]) * devbstar + param[2]*(J-1) * eye(3)

def Gent_3D(stretch, param):
    """Gent. 3D loading specified by stretches.
    param: [mu, Jm, kappa]. Returns true stress."""
    L1 = stretch[0]
    L2 = stretch[1]
    L3 = stretch[2]
    F = array([[L1,0,0], [0,L2,0], [0,0,L3]])
    J = det(F)
    bstar = J**(-2.0/3.0) * dot(F, F.T)
    I1s = trace(bstar)
    devbstar = bstar - trace(bstar)/3 * eye(3)
    return param[0]/J / (1 - (I1s-3)/param[1]) * devbstar + \
           param[2]*(J-1) * eye(3)

def HS_3D(stretch, param):
    """Horgan-Saccomandi. 3D loading specified by stretches.
    param: mu, lamMax, kappa. Returns true stress."""
    L1 = stretch[0]
    L2 = stretch[1]
    L3 = stretch[2]
    F = array([[L1,0,0], [0,L2,0], [0,0,L3]])
    J = det(F)
    bstar = J**(-2.0/3.0) * dot(F, F.T)
    bstar2 = dot(bstar, bstar)
    I1s = trace(bstar)
    I2s = 0.5 * (I1s**2 - trace(bstar2))
    mu = param[0]
    lamM = param[1]
    kappa = param[2]
    fac = mu * lamM**4 / J
    den = lamM**6 - lamM**4 * I1s + lamM**2 * I2s - 1
    return fac/den * ((lamM**2 - I1s)*bstar + bstar2 - (lamM**2*I1s-2*I2s)/
            3*eye(3)) \ + kappa*(J-1) * eye(3)

def Ogden_3D(stretch, param):
    """Ogden model. 3D loading specified by stretches.
    param: [mu1, mu2, ..., alpha1, alpha2, kappa]. Returns true stress."""
    J = stretch[0] * stretch[1] * stretch[2]
    lam = J**(-1/3) * stretch
    N = round((len(param)-1)/2)
    mu = param[0:N]
    alpha = param[N:2*N]
    kappa = param[-1]
    Stress = kappa*(J-1)*eye(3)
    for i in range(N):
        fac = (2/J) * mu[i] / alpha[i]
        tmp = (lam[0]**alpha[i] + lam[1]**alpha[i] + lam[2]**alpha[i]) / 3
        Stress[0,0] = Stress[0,0] + fac * (lam[0]**alpha[i] - tmp)
        Stress[1,1] = Stress[1,1] + fac * (lam[1]**alpha[i] - tmp)
        Stress[2,2] = Stress[2,2] + fac * (lam[2]**alpha[i] - tmp)
    return Stress

```

```

def ETube_3D(stretch, param):
    """Extended Tube model. 3D loading specified by stretches.
    Param: Ge, Gc, delta, beta, kappa"""
    Ge = param[0]
    Gc = param[1]
    delta = param[2]
    beta = param[3]
    kappa = param[4]
    L1 = stretch[0]
    L2 = stretch[1]
    L3 = stretch[2]
    F = array([[L1,0,0], [0,L2,0], [0,0,L3]])
    J = det(F)
    bstar = J**(-2.0/3.0) * dot(F, F.T)
    devbstar = bstar - trace(bstar)/3 * eye(3)
    lam = J**(-1/3) * array(stretch)
    I1s = trace(bstar)
    fac1 = (1+(1+I1s**2-4*I1s)*delta**2 + (5*I1s-I1s**2-6)*delta**4) / \
        (1 - (I1s-3)*delta**2)**2
    stressC = Gc/J * fac1 * devbstar
    fac2 = -2*Ge/(J*beta)
    tmp = (lam[0]**(-beta) + lam[1]**(-beta) + lam[2]**(-beta)) / 3
    stressE = zeros((3,3))
    stressE[0,0] = fac2 * (lam[0]**(-beta) - tmp)
    stressE[1,1] = fac2 * (lam[1]**(-beta) - tmp)
    stressE[2,2] = fac2 * (lam[2]**(-beta) - tmp)
    stressV = kappa*(J-1)*eye(3)
    return stressC + stressE + stressV

def Knowles_3D(stretch, param):
    """Knowles. 3D loading specified by stretches.
    param: mu, n, b, kappa. Returns true stress."""
    L1 = stretch[0]
    L2 = stretch[1]
    L3 = stretch[2]
    F = array([[L1,0,0], [0,L2,0], [0,0,L3]])
    J = det(F)
    bstar = J**(-2.0/3.0) * dot(F, F.T)
    I1s = trace(bstar)
    devbstar = bstar - trace(bstar)/3 * eye(3)
    return param[0]/J * (1+param[2]/param[1]*(I1s-3))**((param[1]-1) * \
        devbstar \ + param[3]*(J-1) * eye(3))

def blatzko_3D(stretch, param):
    """Blatz-Ko. 3D loading specified by stretches.
    param[0]=mu"""
    F = array([[stretch[0],0,0], [0,stretch[1],0], [0,0,stretch[2]]])
    J = det(F)
    b = dot(F, F.T)
    b2 = dot(b, b)
    I1 = trace(b)
    I2 = 0.5 * (I1**2 - trace(b2))
    return param[0]/J**3.0 * (I1*b - b2 - (I2-J**3.0) * eye(3))

def hyperfoam_3D(stretch, param):
    """Hyperfoam model. 3D loading specified by stretches.
    param: [mu1, mu2, ..., alpha1, alpha2, ..., beta1, beta2, ...].
    Returns true stress."""
    J = stretch[0] * stretch[1] * stretch[2]
    lam = array(stretch)
    N = int(round(len(param)/3.0))
    mu = param[0:N]
    alpha = param[N:2*N]
    beta = param[2*N:3*N]
    Stress = zeros((3,3))
    for k in range(N):

```

```

fac = 2.0 * mu[k] / (J * alpha[k])
Stress[0,0] = Stress[0,0] + fac*(lam[0]**alpha[k]
- J**(-alpha[k]*beta[k]))
Stress[1,1] = Stress[1,1] + fac*(lam[1]**alpha[k]
- J**(-alpha[k]*beta[k]))
Stress[2,2] = Stress[2,2] + fac*(lam[2]**alpha[k]
- J**(-alpha[k]*beta[k]))
return Stress

```

## 5.10 Exercises

1. In what applications or situations can linear elasticity be a suitable material model for FE modeling of a polymer?
2. What are the definitions of the three invariants  $I_1$ ,  $I_2$ , and  $I_3$ ?
3. Derive the expression for true stress as a function of the applied stretch for incompressible uniaxial loading of a NH material model.
4. Why cannot the NH material model accurately predict the large strain response of most elastomers?
5. What is the difference between the NH and the Mooney-Rivlin hyperelastic models? Why is it more difficult to properly use the Mooney-Rivlin model?
6. Under what conditions is the Yeoh model unstable? What can be done to improve the stability of the Yeoh model?
7. Show that the Cauchy stress for the Arruda-Boyce EC model given in Equation (5.98) can be directly derived from Equation (5.99).
8. What is the definition of the molecular chain stretch that is defined in the Arruda-Boyce EC model?
9. In what ways are the Ogden model different than the  $I_1$ ,  $I_2$ ,  $I_3$  based hyperelastic models? Is the Ogden model always stable?
10. How many experimental tests are required to calibrate the Gent model?
11. What is the foundation of the extended tube model? What is the reason the extended tube model so accurately predicts experimental hyperelastic behaviors.

12. Which hyperelastic model is your favorite? Why?
13. What are the two most common ways to formulate anisotropic hyperelasticity?
14. What is the difference between traditional hyperelasticity and hyperelastic models for foams?
15. Can a Mullins effect model be used to predict hysteresis of a material exposed to cyclic loading?
16. What is Drucker stability and why is it important?
17. What are the strengths and limitations of hyperelasticity?

## References

- [1] L. Mullins, N.R. Tobin. Stress softening in rubber vulcanizates. Part I. Use of a strain amplification factor to describe the elastic behavior of filler-reinforced vulcanized rubber. *J. Appl. Polym. Sci.*, 9 1965 2993-3009.
- [2] R.W. Ogden, D.G. Roxburgh. A pseudo-elastic model for the Mullins effect in filled rubber. *Proc. R. Soc. Lond. A*, 455 1999 2861-2877.
- [3] H.J. Qi, M.C. Boyce. Constitutive model for stretch-induced softening of the stress-strain behavior of elastomeric materials. *J. Mech. Phys. Solids*, 52 2004 2187-2205.
- [4] S.H. Crandall, T.J. Lardner, N.C. Dahl. *An Introduction to the Mechanics of Solids*. McGraw Hill, New York, 1999.
- [5] J.M. Gere, S.P. Timoshenko. *Mechanics of Materials*. PWS Publishing Company, Boston, 1997.
- [6] M.F. Ashby, D.R. Jones. *Engineering Materials: An introduction to Their Properties and Applications*. Pergamon, New York, 1980.
- [7] J.E. Marsden, T.J.R. Hughes. *Mathematical Foundations of Elasticity*. Dover Publications, New York, 1994.
- [8] A.E. Love. *Treatise on the Mathematical Theory of Elasticity*. Dover Publications, New York, 1927.
- [9] S.P. Timoshenko. *Theory of Elasticity*. McGraw-Hill, New York, 1970.
- [10] I. Sokolnikoff. *Mathematical Theory of Elasticity*. McGraw-Hill, New York, 1956.
- [11] A.E. Green, W. Zerna. *Theoretical Elasticity*. Dover Publications, New York, 1968.

- [12] R.W. Ogden. Non-linear Elastic Deformations. Dover Publications, New York, 1997.
- [13] G.A. Holzapfel. Nonlinear Solid Mechanics: A Continuum Approach for Engineering. John Wiley & Sons, Chichester, 2000.
- [14] P. Chadwick. Continuum Mechanics: Concise Theory and Problems. Dover Publications, New York, 1999.
- [15] L.R.G. Treloar. Stress-strain data for vulcanized rubber under various types of deformation. *Trans. Faraday Soc.*, 40 1944 59-70.
- [16] L.R. Treloar. The Physics of Rubber Elasticity. Oxford University Press, Oxford, 1975.
- [17] O. Kratky, G. Porod. Röntgenuntersuchung gelöster fadenmoleküle. *Recl. Trav. Chim. Pays-Bas.*, 68 1949 1106-1122.
- [18] M. Fixman, J. Kovac. Polymer conformational statistics. III. Modified Gaussian models of stiff chains. *J. Chem. Phys.*, 58 1973 1564-1568.
- [19] J.F. Marko, E.D. Siggia. Stretching DNA. *Macromolecules*, 28 1995 8759-8770.
- [20] F. Reif. Fundamentals of Statistical and Thermal Physics. McGraw-Hill, New York, 1965.
- [21] P.J. Flory. Statistical Mechanics of Chain Molecules. Oxford University Press, Oxford, 1988.
- [22] W. Kuhn, F. Grün. Beziehungen zwischen elastischen Konstanten und Dehnungsdoppelbrechung hochelastischer Stoffe. *Kolloid Z.*, 101 1942 248.
- [23] J.S. Bergström, M.C. Boyce. Mechanical behavior of particle filled elastomers. *Rubber Chem. Technol.*, 72 1999 633-656.
- [24] O.H. Yeoh. Some forms of the strain energy function for rubber. *Rubber Chem. Technol.*, 66 (5) 1993 754-771.
- [25] M. Kaliske, H. Rothert. On the finite element implementation of rubber-like materials at finite strains. *Eng. Comput.*, 14 (2) 1997 216-232.
- [26] S. Kawabata, Y. Yamashita, S. Yoshida. Mechanism of carbon-black reinforcement of rubber vulcanizate. *Rubber Chem. Technol.*, 68 1995 311-329.
- [27] HKS, Inc.. ABAQUS, Pawtucket, RI, ver. 6.14, 2014.
- [28] E.M. Arruda, M.C. Boyce. A three-dimensional constitutive model for the large stretch behavior of rubber elastic materials. *J. Mech. Phys. Solids*, 41 (2) 1993 389-412.
- [29] M.C. Boyce. Direct comparison of the Gent and the Arruda-Boyce constitutive models of rubber elasticity. *Rubber Chem. Technol.*, 69 1997 781-785.

- [30] A. Cohen. A Pade approximant to the inverse Langevin function. *Rheol. Acta*, 30 1991 270-273.
- [31] PolyUMod. <http://PolyUMod.com/>.
- [32] A.N. Gent. A new constitutive relation for rubber. *Rubber Chem. Technol.*, 69 1996 59.
- [33] C.O. Horgan, G. Saccomandi. Constitutive modeling of rubber-like and biological materials with limiting chain extensibility. *Math. Mech. Solids*, 7 2002 353-371.
- [34] C.O. Horgan, J.G. Schwartz. Constitutive modeling and the trousers test for fracture of rubber-like materials. *J. Mech. Phys. Solids*, 53 2005 545-564.
- [35] J.K. Knowles. The finite anti-plane shear field near the tip of a crack for a class of incompressible elastic solids. *Int. J. Fracture*, 13 1977 611-639.
- [36] C. Suhocki. A finite element implementation of knowles stored-energy function: theory, coding and applications. *Arch. Mech. Eng.*, LVIII (3) 2011 319-346.
- [37] D. Hayman, C. Bergerson, S. Miller, M. Moreno, J.E. Moore. The effect of static and dynamic loading on degradation of PLLA stent fibers. *J. Biomech. Eng.*, 136 2014.
- [38] T. Sussman, K.J. Bathe. A model of incompressible isotropic hyperelastic material behavior using spline interpolations of tension-compression data. *Commun. Numer. Methods Eng.*, 25 2009 53-63.
- [39] M. Kaliske, G. Heinrich. An extended tube-model for rubber elasticity: statistical-mechanical theory and finite element implementation. *Rubber Chem. Technol.*, 72 1999 602-632.
- [40] Y. Fung. *Biomechanics: Mechanical Properties of Living Tissues*. Springer, New York, 1993.
- [41] A.J.M. Spencer. Constitutive Theory for Strongly Anisotropic Solids. *Continuum Theory and the Mechanics of Fiber-Reinforced Composites*, CISM Courses and Lectures No. 282, 1984 1-32.
- [42] W. Sun, M.S. Sacks. Finite element implementation of a generalized Fung-elastic constitutive model for planar soft tissues. *Biomech. Model Mechanobiol.*, 4 2005 190-199.
- [43] J.S. Bergström. Large Strain Time-Dependent Behavior of Elastomeric Materials. Ph.D. thesis, MIT 1999.
- [44] J.E. Bischoff, E.A. Arruda, K. Grosh. A Microstructurally Based Orthotropic Hyperelastic Constitutive Law. *Trans. ASME* 2002 570-579.

- [45] Y. Lanir, Y.C. Fung. Two-dimensional mechanical properties of rabbit skin. II. Experimental results. *Journal of Biomechanics*, 7 1974 171-182.
- [46] G.A. Holzapfel, T.C. Gasser, R.W. Ogden. A new constitutive framework for arterial wall mechanics and a comparative study of material models. *J. Elasticity*, 61 2000 1-48.
- [47] T.C. Gasser, R.W. Ogden, G.A. Holzapfel. Hyperelastic modelling of arterial layers with distributed collagen fibre orientations. *J. Royal Society Interface*, 3 2006 15-35.
- [48] P.J. Blatz, W.L. Ko. Application of finite elastic theory to the deformation of rubber materials. *Transactions of the Society of Rheology*, 1962 223-251.
- [49] C.O. Horgan. Material instabilities for large deformations of the generalized Blatz-Ko material. *Applied Mechanics Review*, 50 S93-S96.
- [50] B. Storåkers. On material representation and constitutive branching in finite compressible elasticity. *J. Mech. Phys. Solids*, 34 (2) 1986 125-145.
- [51] J.A.C. Harwood, L. Mullins, A.R. Payne. Stress softening in natural rubber vulcanizates. Part II. Stress softening in pure gum and filler loaded rubbers. *J. Applied Polym. Sci.*, 9 1965 3011-3021.
- [52] J.A.C. Harwood, A.R. Payne. Stress softening in natural rubber vulcanizates. Part III. Carbon black-filled vulcanizates. *J. Applied Polym. Sci.*, 10 1966 315-324.
- [53] J.A.C. Harwood, A.R. Payne. Stress softening in natural rubber vulcanizates. Part IV. Unfilled vulcanizates. *J. Applied Polym. Sci.*, 10 1966 1203-1211.
- [54] J. Diani, B. Fayolle, P. Gilormini. A review of Mullins effect. *Eur. Polym. J.*, 45 2009 601-612.